LOW PRESSURE PLASMAS FOR HIGH POWER MICROWAVE SOURCES

Peter Frank Hirst

A Thesis Submitted for the Degree of PhD
at the
University of St Andrews

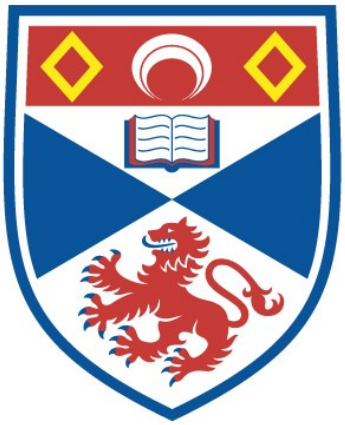

1992

LOW PRESSURE PLASMAS

FOR

HIGH POWER MICROWAVE SOURCES

A thesis presented by

Peter Frank Hirst, BSc. (Hons)

to the

University of St Andrews

in application for the degree of

Doctor of Philosophy

May 1992

RESTRICTED

In submitting this thesis to the University of St Andrews I wish access to it to be subject to the following conditions:

for a period of 5 years from the date of submission, the thesis shall be made available for use only with the written consent of Dr Arthur Maitland.

I understand, however, that the title and abstract of the thesis will be published during the period of this restricted access; and that after the expiry of this period the thesis will be made available for use in accordance with the regulations of the University Library for the time being in force, subject to any copyright in the work not being affected thereby, and a copy of the work may be supplied to any *bona fide* library or research worker.

RESTRICTED

DECLARATION

I, Peter Frank Hirst, hereby certify that this thesis has been composed by myself, that it is a record of my own work, and that it has not been accepted in partial or complete fulfilment of any other degree or professional qualification.

Signed

CERTIFICATE

I hereby certify that the candidate has fulfilled the conditions of the Resolution and Regulations appropriate to the Degree of Ph.D.

Signed.....

ACKNOWLEDGEMENTS

I would like to thank my supervisor, Dr Arthur Maitland, for his invaluable advice and friendship during the course of this work; also everyone in Laser One, particularly Natalie Ridge, Brian Condon, Bill Dawber and Ewan Livingstone for many useful discussions. Thanks also to the gentlemen of the Departmental Workshop for their expertise, and to Frits for his skillful glass-blowing.

I am particularly grateful to Dave Parkes and his colleagues at DRA Electronics Division for supporting this work and for asking stimulating and challenging questions.

Finally, thank you to Chris, Simon, Alex and all my friends at St Andrews who have made life so interesting.

DEDICATION

I dedicate this thesis to my grandmother, Mrs H. A. Amos.

ABSTRACT

This thesis describes an investigation of the use of low pressure plasmas for the generation of high power microwaves. Previous research has shown that the efficiency of a high power microwave ("HPM") source such as a BWO is enhanced by the introduction of a low pressure plasma into the oscillator cavity. The principle aim of this thesis is to extend the use of low pressure plasmas to the whole HPM system.

Electron beams with current densities of the order of 20 A cm^{-2} can be generated in a cold cathode glow discharge at low gas pressures. Results are presented which show the effects of magnetic fields and electrode spacing on the I-V characteristics of a DC glow discharge electron gun. A glow discharge electron gun with an operating voltage of 350 kV has been designed and tested.

A new kind of RF plasma cathode is proposed in which electrons are drawn from an RF discharge in a low pressure gas. An analysis of the production of an annular RF plasma cathode using a microwave-excited helical slow-wave structure is presented. Experimental results show that the RF plasma cathode yields electron current densities an order of magnitude higher than does a solid cathode. Examples of the implementation of the RF plasma cathode in a number of components of an HPM system are given.

The propagation of electromagnetic waves in plasma-loaded waveguides of circular cross-section has been modelled. Numerical solutions are presented for the case of slow-waves in a longitudinally-magnetised plasma waveguide. Propagation below the

cut-off frequency of the waveguide is generally possible and, according to the configuration, the propagating waves may be used for plasma generation or for RF power transmission. A new kind of high power microwave waveguide switch, based on the properties of plasma waveguides, is proposed.

The design of new kind of magnetron, the "Glow Discharge Inverted Magnetron" ("GDIM"), is presented. The GDIM is an inverted magnetron with the resonant structure located on the cathode. The resonant cavities are used as a source of glow discharge electron beams, which gives high power operation without requiring relativistic voltages.

I: INTRODUCTION 1
I.1 A Brief History of High Power Microwave Sources 1
I.2 Recent Applications of High Power Microwaves 3
I.3 Recent Advances in HPM Sources 5
I.4 Low Pressure Plasmas for HPM Sources 6
I.5 Outline of Thesis 7
I.6 References 9
II: GASEOUS ELECTRONICS: CATHODES, PLASMAS AND ELECTRON BEAMS 11
II.1 Introduction 11
II.2 Glow Discharge Electron Beams 15
II.2.1 Overview of Gas Breakdown 15
II.2.2 The Glow Discharge 17
II.2.3 High Voltage Glow Discharges 18
II.2.4 Electron Beams 19
II.2.5 Simple Glow Discharge Electron Gun 23
II.2.6 Electron Gun with Variable Electrode Spacing 25
II.2.7 High Voltage High Frequency Electron Guns 28
II.2.8 Conclusions: High Voltage Electron Gun Design 30
II.3 The RF Plasma Cathode 31
II.3.1 Introduction 31
II.3.2 Conditions at the Cathode Grid 33
II.3.3 Conditions at the Earth Grid 34
II.3.4 The Anode-Cathode Gap 34
II.3.5 Surface Wave Plasmas 35
II.3.6 Plasma Waveguides 36
II.3.7 Plasma Production Using Helical Structures 36
II.3.8 Experimental Results 47
II.3.9 Analysis of Experimental Results and Discussion 49
II.3.10 Example Designs 50
II.3.11 Simple Electron Gun 50
II.3.12 Pierce Electron Gun 51
II.3.13 Magnetron 52
II.3.14 Thyratron 53
II.3.15 High Power Electron Gun 53
II.3.16 Conclusions 54
II.4 References 55
III: PLASMA WAVEGUIDES 57
III.1 Introduction 57
III.2 Maxwell's Equations in a Plasma with Uniformity in One Dimension 59
III.2.1 General Formulation 59
III.2.2 Free-space Waveguide 63
III.2.3 Homogeneous, Isotropic Plasma Waveguides 65
III.2.4 Inhomogeneous, Isotropic Plasma Waveguides 65
III.2.5 Waveguide Partially Filled with Homogeneous Plasma 67
III.2.6 Longitudinally Magnetised, Homogeneous Plasma Waveguides 70
III.3 Slow-wave Solutions 72
III.3.1 Introduction 72
III.3.2 Finite Longitudinal Magnetic Field 74

III.3.3 Conclusions 83
III.4 Summary 84
III.5 References 85
IV: PLASMA SWITCHING AND PULSE COMPRESSION IN PLASMA WAVEGUIDES 86
IV.1 Introduction 86
IV.1.1 Background 86
IV.1.2 Cavity Dumping 87
IV.1.3 Dispersive Compression 91
IV.2 Novel Plasma Waveguide Closing Switch 94
IV.2.1 Introduction 94
IV.2.2 Waveguide Eqivalent of an Optical Saturable Absorber 95
IV.2.3 Triggered Waveguide Switch 98
IV.3 Conclusions 100
IV.4 References 102
V: THE GLOW DISCHARGE INVERTED MAGNETRON 103
V.1 Introduction 103
V.2 Formation of Electron Beam 105
V.3 Magnetron Geometry 107
V.4 RF Signal Coupling 108
V.5 Design of a Strapped GDIM 112
V.6 Conclusions 116
V.7 References 118
VI: SUMMARY 120
VI.1 Glow Discharge Electron Guns 120
VI.2 The RF Plasma Cathode 122
VI.3 Plasma Waveguides 123
VI.4 Plasma Switching and Pulse Compression 124
VI.5 The Gas Discharge Inverted Magnetron 125
VI.6 Concluding Remarks 126

CHAPTER I

INTRODUCTION

I.1 A Brief History of High Power Microwave Sources

The origins of electromagnetic theory can be traced back to the work of James Clark Maxwell in the late nineteenth century[1]: from mathematical considerations, Maxwell hypothesized the electromagnetic wave nature of light. In the period 1887-1891 Maxwell's theory was verified experimentally by Heinrich Hertz. Hertz used a high voltage spark gap to excite a half wave dipole antenna at a frequency of about 60 MHz and a receiver which consisted of an adjustable loop connected in series with another spark gap[2]. Following the death of Hertz (aged 36) in 1894 major effort was directed towards the commercial realisation of radio.

Probably the most famous pioneer of radio is Signor Marconi who on March 27, 1899 successfully transmitted radio messages across the English Channel[3]. Building on his early successes Marconi went on to earn a reputation as the grandfather of wireless telegraphy. Meanwhile, however, in the USA the foundations of pulse power for high power radio transmission were being laid down by a Serbian engineer named Nikola Tesla. Tesla's achievements include the invention of the polyphase system of electricity generation and transmission and the discovery of the rotating magnetic field that led to the invention of the induction motor. In the belief that undamped oscillations would be of great importance to radio transmission, Tesla experimented extensively with high frequency alternators (generating at 20 kHz).

Tesla's investigations seem to have led him to the belief that some new mechanism of radio transmission would result only if the input power were large enough. Other researchers were content with powers of a few watts which only produce extremely weak signals at a distance. In order to obtain higher powers Tesla required much higher voltages and frequencies than were possible with the rotating generator and began experimenting with impulse induction circuits. His research led to the development of the high frequency transformer, with which he believed he could cause the whole earth to resonate and transmit electrical power. In an experiment at Colorado Springs in 1899, the same year as Marconi's cross channel radio link, Tesla used a high frequency transformer coupled to an elevated antenna to transmit enough power to light a lamp at a distance of 30 km and to produce detectable signals at 1000 km[4,5].

High frequency transformers formed the basis of early radio transmitters until, around the year 1910, the need for undamped excitations in radio transmitters became acute. Rotating generators were systematically developed and successfully deployed in some high power transatlantic stations. The need for such alternators passed away with the development of the high power triode valve about 1922.

In 1921 Hull invented the magnetron[6], but it remained nothing more than an interesting laboratory device until about 1940. The magnetron represents the family of generators known as M-type tubes in which operation relies on the interaction of a rotating electron space charge with crossed electric and magnetic fields. During World War II, an urgent need for high power microwave generators for radar transmitters led to a very rapid development of the magnetron to its present state. By the end of the War magnetrons operating at wavelengths down to 3 cm were available, with peak powers up to 1 MW at 10 cm. At the present state of the art, a magnetron can deliver a peak power output of up to 40 MW with a driving voltage of the order of 50 kV at a frequency of 10 GHz and with an efficiency ranging from 40 to 70%. The magnetron was the first reliable source of microwave power at centimetre wavelengths.

Linear beam tubes started with the Heil oscillators in 1935[7] and the Varian brothers' klystron amplifiers in 1939[8]. The work was advanced by the space-charge wave propagation theory of Hahn and Ramo in 1939[9] and continued with the invention of the helix -type travelling-wave tube (TWT) by R. Kompfner in 1944[9]. These tubes are representative of linear-beam, O-type tubes in which the electrons receive their energy from the DC beam voltage before they arrive in the microwave interaction region where their energy is converted into electromagnetic energy. From the early 1950s the low powers of linear-beam tubes have been increased to levels which now surpass the magnetron.

A wide range of variations of the basic M-type and O-type tubes have been developed, including hybrids such as the twystron amplifiers[10] which is a TWT/klystron hybrid. The maximum power levels which could be obtained from conventional high power microwave sources was limited by volume considerations and cathode performance. The transition to higher peak powers was achieved by increasing the beam energies to relativistic levels. Thus began the development of relativistic high power microwave generators.

I.2 Recent Applications of High Power Microwaves

Before reviewing the recent research on high power microwave (HPM) sources it is instructive to consider some of their application areas. Fifty years on, radar is still one of the most important applications of HPM and the state-of-the-art is ultrawideband radar (UWR). UWR requires very short microwave pulses at very high powers. The most basic reason for decreasing the pulse length (increasing the bandwidth) of a radar signal is that the resolution is thereby increased. Higher resolution assists in target recognition and allows smaller objects and features to be detected. Higher transmitter powers improve the noise immunity of a radar system and may also increase the range, particularly in unfavourable propagation conditions. Microwave detectors generally

have a minimum activation energy, and as the pulse length is reduced the peak power must be increased in order to maintain sensitivity.

Wideband radar is encompassed by the wider application area of electronic warfare (EW). One aspect of EW is that of electronic countermeasures (ECM) which, in "defence-speak", degenerates into a recursion of counter-countermeasures (EC^2M, EC^3M and so on). Broadly speaking, the application of HPM to EC^nM is in signal disruption or jamming. Clearly, very high powers are desirable to swamp the target signal. More subtly, the interests of the electronic aggressor are often best served by very short, high power pulses which make it more difficult for the target to identify the source of attack. Also, the wide bandwidth of ultrashort microwave pulses increases the probability of successful deployment against frequency agile systems.

The above considerations highlight another advantage of ultrawideband radar for military applications, namely the possibility of having an "undetectable" radar system which gives the target no information that it is under surveillance. The field of "udetectability" has been given the name "stealth technology". One aspect of stealth technology is the reduction of the radar cross section of an object by careful design of the geometry to avoid retroreflecting surfaces and the application of microwave absorbing coatings to vulnerable surfaces. The consequent reduction in the radar footprint of a stealthy target can, to some extent, be combated by increasing the power of the interrogating radar.

The primary non-military application for very high power microwave generators is in the field of high energy particle physics. Particle accelerators of very high energy often use the interaction between a charged particle beam and a high power microwave signal to accelerate the particle beam to velocities close to the speed of light. The particle beams are used in high energy physics experiments, including investigations relating to controlled nuclear fusion. Other applications of high power microwaves include power beaming, industrial processing and satellite and deep space communications systems.

I.3 Recent Advances in HPM Sources

In the study of microwave generation by intense, relativistic electron beams, a useful figure of merit is the peak power divided by the square of the wavelength. This metric allows a useful comparison to be made between sources which inherently operate at different wavelengths. In several recent experiments a figure of merit of more than 1 GW cm^{-2} has been reported over a wavelength range from 2 mm to 3 cm. For wavelengths over 1 cm, the highest powers and efficiencies have been achieved in multi-wave Cerenkov generators[11], and at millimetre wavelengths the most impressive results have been obtained with free electron lasers which employ a tapered wiggler[12]. Most of the HPM research has been conducted in the USA and the USSR. The maximum achieved performance of HPM sources as of 1989 are shown in Figure I.3.1.

As HPM sources have been pushed through the 1 GW cm^{-2} limit, increasing attention has focussed on the effects of plasma liners on the efficiency. Plasma filled waveguides were first investigated in the 1950s but the lack of technology required to implement efficient plasma sources inhibited further research. In 1982 Kuzelev reported the operation of a 100 MW, S-band plasma Cerenkov maser (PCM)[13]. Numerical modelling of a proposed 1 GW PCM was undertaken by de Groot *et al* in 1988[14]. At the University of Maryland, high efficiency X-band operation has been achieved with a plasma-filled backward wave oscillator (BWO)[15].

The mechanism by which efficiency is improved in some plasma filled HPM sources is not entirely understood. It seems likely, however, that the efficiency enhancement can be explained in terms of the effect of the plasma on the waveguide dispersion relation. In general, gain occurs when a waveguide mode has the same phase velocity as the electron beam (the so-called "synchronism" condition) and the microwave fields grow at the expense of the beam kinetic energy. Thus, as the microwave fields increase in magnitude, the phase velocity of the electron beam decreases until the synchronism condition fails (amplification ceases). The presence of the plasma modifies the

waveguide dispersion relation in such a way that some modes have a constant frequency over a range of phase velocities. The synchronism condition for these modes holds true even as the electron beam gives up its energy to the microwave fields. Thus a higher proportion of the total kinetic energy of the electron beam is available for amplification and the efficiency of the source is enhanced.

The complexity of the interactions which occur in plasma-filled relativistic microwave sources has led some eminent researchers to dismiss these devices as untenable[16]. The efficiency improvements, however, cannot be denied and research on relativistic HPM sources containing plasmas is growing.

I.4 Low Pressure Plasmas for HPM Sources

Up until the last decade the presence of low pressure residual gases in high power microwave tubes was considered to be a constant cause for concern. Sophisticated manufacturing processes were developed to minimise the concentrations of residual gases over the lifetime of a tube. Recent advances in super power microwave sources, however, have shown that a controlled low pressure gas forms a plasma which in some circumstances can improve the efficiency of the source. The advantages of having some sections of a HPM source filled with a low pressure gas are gaining recognition with researchers.

The original aim of the research which forms the basis of this thesis is simply stated thus:

Having accepted that it is often desirable for some components of a HPM system to contain a plasma, to investigate the possibility of producing integrated HPM systems in which the entire system is filled with the same low pressure gas.

There are several potential advantages for HPM systems which are integrated in this way. The elimination of pressure seals between components is beneficial for both production and operational reasons. From the point of view of manufacture, the simplification of design is generally desirable and the high vacuum requirements may be relaxed. In operation, pressure seals can introduce tracking problems at high power levels and have a tendency to degrade under electrical stress.

The performance of individual components may be enhanced when they are implemented in a low pressure gas environment. For instance, the efficiency of the BWO is increased by the introduction of a plasma into the interaction region. It is known that cathodes in gas discharges generally yield higher current densities than cathodes which operate in vacuo. There may be some related beneficial effects for the operation of a low pressure HPM system.

New plasma-based microwave components may arise from the investigation of the effects of plasmas on HPM systems. In particular, there is often some difficulty involved in coupling the microwave power out of a HPM generator. The presence of a plasma offers extra degrees of freedom for the purposes of matching the source to the load.

I.5 Outline of Thesis

In this thesis results from a research programme in the field of plasma-filled high power microwave sources are presented. The principal aim is to investigate the possibility of producing integrated HPM systems in which the entire system is filled with the same low pressure gas.

Chapter II deals with the production of electrons in low pressure gases. Conventional cathode technology is reviewed, both for electron beam production and switching purposes. Glow discharges are discussed with particular reference to the conditions for

the production of high energy electrons and the advantageous effects of slotted cathode geometries and space-charge neutralisation. Experiments in which glow discharges are used to produce electron beams with energies up to 350 keV are described.

A new kind of cathode - the electrodeless RF cathode in which electrons are extracted from an electrodeless RF discharge plasma is proposed. An analysis of the operation of the device is given. Experimental results show that the RF plasma cathode yields a current density an order of magnitude greater than does the solid cathode of a DC glow discharge cathode in similar conditions of geometry and pressure. Designs are given for a number of electron tubes which utilise the RF plasma cathode.

Chapter III is a theoretical treatment of the propagation of electromagnetic waves in plasma-loaded waveguides. Maxwell's equations are reduced to a general formulation in cylindrical coordinates which is applicable to systems with uniformity in the longitudinal direction. The wave equations are derived for a number of situations, including magnetised plasmas and solved for the specific instance of slow-wave propagation. The solutions are used to calculate the fields and the power flow in plasma-loaded waveguides. A summary of the propagating modes of plasma-loaded waveguides is given.

In Chapter IV the results of Chapter III are used in a design study for a new kind of microwave waveguide switch ("MWS"). The switch is a *closing* switch which is activated by the generation of a plasma in a section of waveguide. This is to be compared with a conventional TR cell - a waveguide *opening* switch which is activated by the generation of a plasma. We then draw upon the experimental results of Chapter II to develop both self triggering and externally triggered implementations of the MWS, drawing on the experimental results of Chapter II. The application of the MWS to cavity dumping schemes for microwave pulse compression is described. A mechanism for spatio-temporal dispersive pulse compression in plasma-loaded waveguides is discussed.

Chapter V is a design study for a novel magnetron: the Glow Discharge Inverted Magnetron ("GDIM"). The high electron current density of an obstructed glow discharge allows high power operation without resorting to relativistic electron energies. The magnetron geometry is inverted and the resonant cavities are used to enhance electron production using the slotted cathode effect. Unlike conventional inverted magnetrons, the resonant cavities are located so that they surround the interaction region, thereby simplifying extraction of the microwaves.

I.6 References

[1] A Treatise on Electricity and Magnetism, J. C. Maxwell, Dover, N. Y., 1954.

[2] Electric Waves, being researches on the propagation of electric action with finite velocity through space, D. E. Jones translation. Macmillan, N. Y., 1893 and Dover, 1962.

[3] Letter, J. A. Fleming, The Times, London, April 3 1899. Reproduced in The Principles of Electric Wave Telegraphy, J. A. Fleming, Longmans, London, 1906.

[4] Nikola Tesla, A Commemorative Lecture given by A. P. M. Fleming at the IEE, 25 Nov 1943.

[5] Colorado Springs Notes, 1899-1900 Nikola Tesla, Belgrade, Yugoslavia. (Published by the Nikola Tesla Museum).

[6] Beam and Wave Electrons in Microwave Tubes, R. G. E.Hutter, Van Nostrand, 1960.

[7] Velocity Modulated Tubes, R. R. Warnecke, in Advances in Electronics, vol. 3, Academic Press, New York, 1951.

[8] A High Frequency Oscillator and Amplifier, R. H. Varian and S. F. Varian, J. Appl. Phys., **10** p401, 1939.

[9] Microwave Electronic Tube Devices, Liao, Prentice-Hall, 1988, ISBN 0-13-582073-1

[10] Multi-Megawatt Hybrid TWTs at S-band and C-band, A. D. La Rue and R. R. Rubert, Presented to the IEEE Electron Devices Meeting, Washington D. C., 1964.

[11] S. P. Bugayev, Proc. 6th Int. Conf. on High Power Particle Beams, Kobe, Japan, 9-12 June 1986.

[12] See, for example, Guided Radiation Beams in Free Electron Lasers, P. Sprangle *et al*, Nucl. Instr. & Meth.. in Phys. Res. **A272**(1-2) pp536-542, 1988.

[13] Relativistic plasma microwave oscillators, M. V. Kuzelev, F. Kh. Mukhametzyanov, M. S. Rabinovich, A. A. Rukhadze, P. S. Strelkov and A. G. Shkvarunets, Sov. Phys. JETP **56**(4) p780, 1982.

[14] High Power and Superpower Cerenkov Masers, J. S. de Groot, R. A. Stone, K. Mizuno, J. H. Rogers and T. D. Pointon, IEEE Trans. Plas. Sci., **16**(2) pp206-216, 1988.

[15] Demonstration of Efficiency Enhancement in a High Power Backward -Wave Oscillator by Plasma Injection, Y. Carmel, Phys. Rev. Lett. **62** pp2389-2392, 1989.

[16] G. Bekefi, Workshop on Intense Microwave and Particle Beams II at SPIE OE-LASE, Los Angeles, USA, 1991.

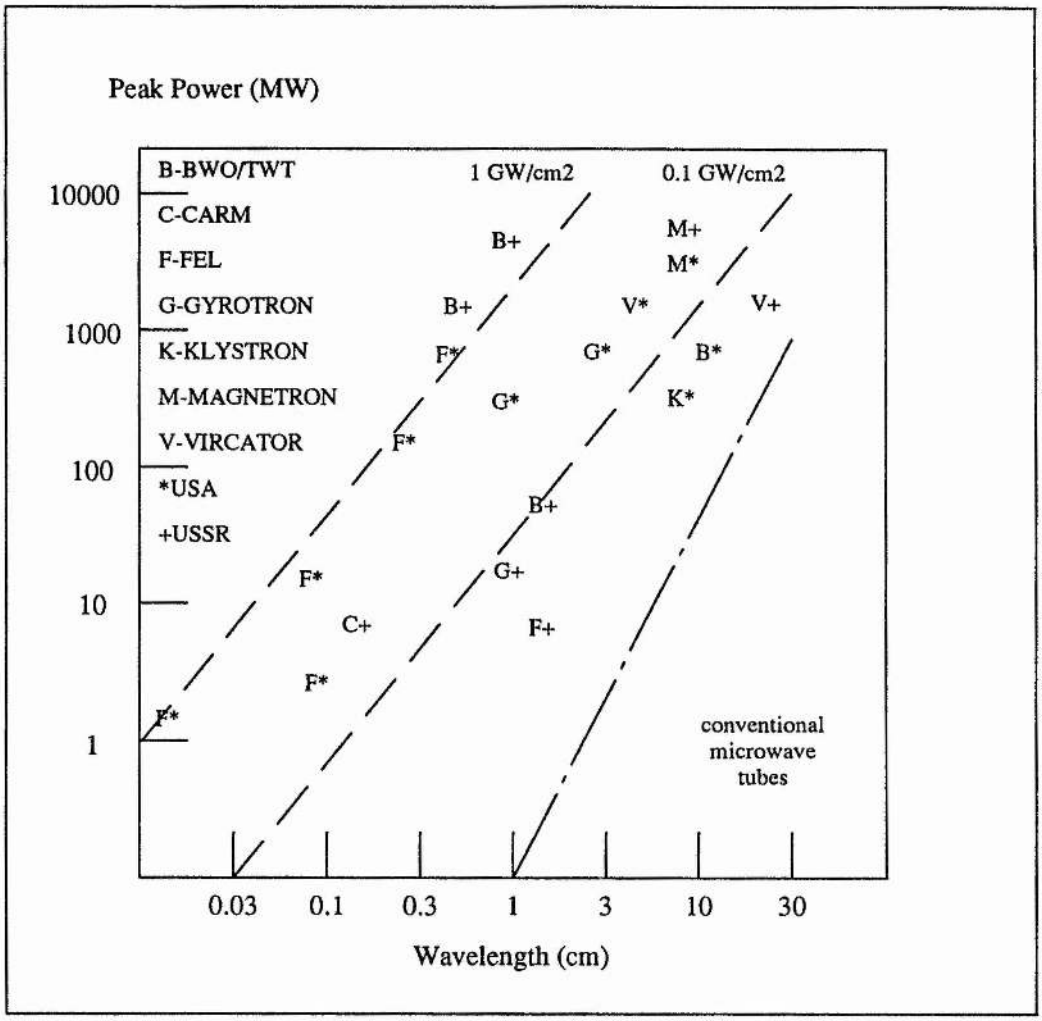

Figure I.3.1: High Power Microwave Generation in 1989

CHAPTER II

GASEOUS ELECTRONICS: CATHODES, PLASMAS AND ELECTRON BEAMS

II.1 Introduction

Cathodes which are capable of producing high current densities uniformly over large areas are required for many devices including thyratrons, electron beam pumped lasers, microwave tubes and accelerators. Several cathode technologies are available for these applications, but each has its limitations. Thermionic cathodes, for instance, have a maximum current density given in the weak field case by the Richardson-Dushman equation for the current density:

$$j = A\,(1-r)\,T^2 \exp\left[\frac{-e\phi}{kT}\right] \qquad \text{(II.1.1)}$$

where A is a universal constant,

$$A = 4\pi \frac{mk^2 e}{h^3} = 120\ \text{A cm}^{-2}\,\text{K}^{-2} \qquad \text{(II.1.2)}$$

and ϕ is the work function of the surface. The electron reflection coefficient, r, of the cathode surface for zero applied field is usually small for clean metallic surfaces and may be as large as 0.99 for common cathode materials. A thermionic cathode may

normally be operated at any temperature up to the melting point of the cathode material. In practice, as the temperature is increased the behaviour departs from that predicted by the Richardson-Dushman equation and the current density saturates. The most extensively used thermionic emitting surface is a mixture of barium and strontium oxides applied as a coating either to an indirectly heated cathode surface or directly to a filament. Such an oxide coating has an effective work function of 1.0 to 1.5 and an emission constant A $(1-r^2)$ of 1.2 and may be operated at temperatures of the order of 1000 K, thus giving a saturated emission current density of the order of 100 mA cm^{-2} with a heater efficiency of 20 mA W^{-1}.[1]

The operation of a thermionic cathode in a hydrogen thyratron is modified by the presence of the gas. Ion bombardment and space charge neutralisation increase the maximum current densities by two orders of magnitude.[2] The ion bombardment also leads to degradation of the cathode emission with time. Thermionic cathode materials are highly susceptible to contamination and cannot, in general, be exposed to the atmosphere. The operating temperature of the order of 1500K introduces a warm up time of several minutes. Furthermore, the implementation of large area thermionic cathodes introduces a thermal management problem which often limits the maximum current.

Cold cathode sources may be divided into three categories according to the processes which lead to electron production: field emission, photoelectric emission and secondary emission. Field emission relies on electric field enhancement around a sharp point or edge (large area cathodes can be made of velvet). During the liberation of electrons at high current densities the cathode surface is vaporised and the resulting plasma drifts across the anode-cathode gap. When the plasma reaches the anode the diode is short circuited and electron production ceases until the gap clears. Thus high current density field emission cathodes are inherently pulsed devices which suffer from gap closure with consequent pulse shortening and low repetition rate operation. Furthermore,

nonuniformities in the plasma production lead to poor emissivities and the drift of the plasma across the gap leads to a time varying impedance through the pulse.

Photoelectric cathodes exploit the photon-electron interaction of an incident illumination to enable electrons to overcome the work function of the cathode surface. A simple analysis yields the electron current density per watt of uniform illumination. The photon flux is given by

$$\phi = \frac{I}{h\nu} \qquad \text{(II.1.3)}$$

where the incident radiation has intensity I, frequency ν and h is Planck's constant. Let us assume that each absorbed photon yields a single electron. Then the current density is

$$j = (1-R)(1-r)\frac{e}{h\nu} I = \kappa I \qquad \text{(II.1.4)}$$

where R is the optical reflection coefficient of the cathode surface. For typical values of ν = 0.4 PHz, (1–R) = 0.1 we obtain $\kappa \cong 50$ mA W^{-1} cm^{-2}. This number is comparable to the efficiency of a typical thermionic cathode (from equation II.1.1) which requires much less technology. High power pulsed laser sources generally have pulse durations which are too short for practical cathode applications. Photoemissive cathodes are particularly useful when several electron beam geometries may be required from a cathode since the emittance area of the cathode can be controlled by focussing the incident radiation into an image of the required cathode shape.

Secondary emission cold cathode sources utilise bombardment of the cathode by primary particles to expel electrons from the cathode. In a glow discharge the field distribution is such that positive ions are accelerated onto the cathode from the discharge plasma. The impact of the positive ions releases secondary electrons from the cathode which are accelerated in the same high field region and produce further ionisation. Typically (for a molybdenum cathode in a helium discharge) the secondary

electron yield ranges from one electron per ion for ions with an energy of 1 keV to ten electrons per ion for 100 keV ions. Secondary emission at the cathode also occurs due to ultraviolet radiation from the discharge. The discharge is maintained by the current flowing in the diode which may operate either in the normal glow or the abnormal glow regimes. At low currents and voltages, the normal glow covers part of the cathode surface. As the discharge current is increased, the glow spreads over the cathode to keep the current density and voltage constant. Once the discharge covers the entire cathode surface, any further increase in current causes the discharge voltage to rise and high energy electron beams may be produced. This is the abnormal glow. A further increase in current leads to a sudden fall in voltage as the discharge forms a low impedance arc.

Secondary emission cold cathode discharges can operate in pulsed or continuous mode. In the continuous mode cathode current densities of the order of 1 A cm^{-2} are possible[3] and for pulsed operation this value rises to as much as 20 A cm^{-2} [4]. These values are for cathodes optimised for maximum current density operating in helium at pressures of the order of 1 mbar. The main disadvantage of cold cathode glow discharges for electron beam production is that the extreme conditions at the cathode lead to cathode sputtering which damages the cathode and poisons the discharge.

Most electron guns operate in the space-charge limited regime, and the simplest case is for plane, parallel electrodes in vacuum. The current in this case is given by[2]

$$I = \frac{4}{9}\varepsilon_0 \left(\frac{2e}{m}\right)^{\frac{1}{2}} \frac{A}{d^2} V^{\frac{3}{2}} \qquad \text{(I.1.5)}$$

where A is the area of the electrodes, d is their separation and the other symbols have their usual meaning. This is the well known Child-Langmuir equation which states that the diode voltage,V, and current, I, are related by a constant which is a function of the geometry. This constant is given the name "perveance" and is usually denoted by the

letter K. In fact, the 3/2 voltage law holds for any diode geometry[2]. Thus, in any diode system, the perveance is defined as

$$K \equiv \frac{I}{V^{\frac{3}{2}}} \qquad (I.1.5)$$

The perveance is an important parameter as it defines the characteristics of an electron beam and is controllable to some extent. The beam voltage is set by the diode voltage and the beam current is then set by the perveance. Low power microwave tubes require beam perveances of the order of 10^{-6} A $V^{-3/2}$ with current densities of the order of 1 A cm^{-2}. High power microwave tubes, which are of particular interest in this thesis, require beam perveances of the order of 10^{-6} A $V^{-3/2}$ with beam current densities of the order of 50 A cm^{-2}.

II.2 Glow Discharge Electron Beams

II.2.1. Overview of Gas Breakdown

The glow discharge has been investigated and analysed by a large number of researchers. Full descriptions and derivations are not given in this account as they are readily available in the references. There is, however, some value in reviewing such work and developing the terminology as is relevant to this thesis.

When a potential difference is applied between two electrodes in a low pressure gas a current flows between the electrodes. A typical voltage-current characteristic is shown in Figure II.2.1.1 and several regimes of operation are indicated. In Region I the current flows in sporadic bursts caused by ionisation of the gas by external background radiation. This is the dark current.

The electrons produced by random ionisations are accelerated in the electric field and, as the discharge current is increased, the potential difference between the electrodes increases asymptotically to a constant value. In passing through the gas under the influence of the applied field, the electrons undergo collisions with neutral species. A collision may result in the attachment of the electron or, if the field is high enough, the ionisation of the neutral to produce additional electrons. These secondary electrons are, in turn, accelerated in the electric field and produce further ionisation. As the potential difference between the electrodes attains a critical value (the Townsend breakdown voltage) the electron multiplication results in the generation of an electron avalanche. This corresponds to Region II in Figure II.2.1 and the discharge voltage falls sharply as there is a transition into the higher current regime.

Region III is the normal glow discharge. The discharge is self sustaining and is characterised by a constant voltage and cathode current density. The "sustaining voltage" of a glow discharge is typically of the order of 500 V. The discharge is visible because of excitation of the gas by the high electron current As the discharge current is increased the glow spreads over the cathode to keep the current density and voltage constant. Once the discharge covers the whole cathode surface further increases in current result in an increase in the discharge voltage. This is shown in Region IV. (the "abnormal glow"). When the potential across the abnormal glow discharge increases to a critical value the current rises rapidly and a low pressure arc discharge is formed (Region V). The potential across the arc discharge is of the order of 10V.

The Townsend breakdown voltage V_s is, in general, determined by the nature and pressure of the gas, the material and state of the electrodes and the degree of pre-existing ionisation. Experiment shows, however, that for a wide range of conditions (with plane parallel electrodes) the breakdown voltage obeys the similarity law known as Paschen's law:

$$V_s = f(pd)_s \qquad \text{(II.2.1)}$$

where p is the pressure, d is the length of the discharge path and f is usually called the "Paschen curve". The Paschen curves for a number of gases are shown in Figure II.2.1.2. All of the curves have a similar shape, with a minimum breakdown voltage $V_{s\ min}$ occurring at $(pd)_{min}$, a right hand branch with increasing breakdown voltage with increasing (pd) and a left hand branch for which the breakdown voltage increases rapidly with decreasing (pd). The existence of a high breakdown voltage for small values of (pd) is central to the operation of many practical gas discharge devices.

II.2.2 The Glow Discharge

Observation of a normal glow discharge reveals a number of regions distinguished by their different appearances. These are shown diagrammatically in Figure II.2.2.1. The cathode dark space (CDS) is a region of net positive space charge which produces a high electric field and across which most of the total discharge potential appears (the "cathode fall"). The glow discharge is sustained by the release of secondary electrons from the cathode through bombardment by ions which have been accelerated by the cathode fall and photons.

The CDS can be subdivided into three regions: the Aston dark space, the cathode glow and the Crookes dark space. In the Aston dark space the electrons have not yet obtained enough energy to excite the gas into a radiative state. Excitation occurs in the cathode glow and by the time the electrons have reached the Crookes dark space they have a reduced collision cross-section for inelastic collisions (by virtue of their energy).

The negative glow (NG) is a narrow, intensly luminous region which is ionised by the high energy electrons from the CDS. It is the main source of the ions and photons

which produce secondary emission at the cathode. For moderate values of the cathode fall (normal glow) the electrons lose all of their energy in inelastic collisions in the NG.

In the Faraday dark space the electrons once more gain the energy they lost in the NG and when they again reach the ionisation energy they cause the positive column. The positive column is a passive region the primary function of which is to connect the anode to the active discharge region. The anode glow is produced by electrons that may have gained enough energy in their last few mean free paths to produce a slight excess of ionisation because of the space charge field disturbance by the positive ions that are forced from the anode. The anode dark space is a region of space charge, which may be either positive or negative, and has a thickness of the same order of magnitude as the electron mean free path.

II.2.3 High Voltage Glow Discharges

In the abnormal glow discharge an increase in the discharge current is accompanied by an increase in the cathode fall. An abnormal glow discharge may have a cathode fall of several kilovolts before the transition to an arc discharge occurs. In this case the electrons are accelerated through the cathode fall to a high energy for which the electron collision cross-section is small and the mean free path is correspondingly long. The discharge may then be said to be generating an electron beam in the CDS. Two other ways of increasing the discharge voltage to produce electron beams are the use of obstructed and constricted glow discharges.

The presence of the regions between the negative glow and the anode is not required in order to sustain a glow discharge. If the anode is moved through the positive column (for fixed discharge current) the discharge voltage drops slightly. As the anode penetrates the negative glow, however, the production of ions and photons is impaired and the discharge can only be maintained by a rise in the sustaining voltage - the

discharge is said to be obstructed. (This emphasises the importance of the negative glow in the normal discharge). Thus high energy electrons are produced and if the anode contains a hole then an electron beam may be injected into the space beyond the anode.

The radius of the discharge tube has hardly any effect on the cathode fall of a glow discharge without a positive column, provided that the tube radius is larger than the electron mean free path. When, however, the pressure (or radius) is such that the electron mean free path is comparable to the radius the discharge the voltage rises steeply and highly energetic electron beams may be produced. This is the constricted glow discharge.

II.2.4 Electron Beams

Glow discharge electron guns have been developed for applications such as welding, laser pumping and switching. These devices usually employ an obstructed discharge with a perforated anode for extraction of the beam. Rocca *et al*[4] report electron current densities of 20 A cm^{-2} in a constricted pulsed discharge at beam energies up to 100 keV.

The current density in the electron beam mode can be increased by an order of magnitude by using a cathode which has a slot of appropriate dimensions (Maitland and Carman, 1986[3]). The function of the cathode slot appears to be twofold. Firstly (Figure II.2.4.1) the slot perturbs the potential near the cathode to produce an electron focussing effect. Secondly, the electric field inside the slot directs the ions onto the sides of the slot which gives both a larger surface area and a higher yield (because of the glancing angle of impact) for secondary emission of electrons. Current densities of the order of 1 A cm^{-2} (DC) can be obtained with slotted cathode electron guns.

The generation of electron beams in a gaseous medium introduces a focussing effect due to "space charge neutralisation". Electrons from the electron beam undergo inelastic colisions with the gas molecules with a collision cross section which is charactistic of the electron energy, the gas species and the pressure. Ionising collisions result in the generation of a plasma in the beam track. The negative space charge of the electron beam repels plasma electrons, and because the plasma ion mobility is relatively low, a positive ion space charge sheath forms around the electron beam. The positive sheath electrostatically neutralises the space charge of the electron beam and reduces its divergence. Thus the action of space charge neutralisation allows a higher electron beam current density to propagate in an (ionised) gas than in vacuum.

The magnitude of the space charge neutralisation of an electron beam in a low pressure gas can be estimated using the Thomson classical electron ionisation cross section:

$$\sigma_i = 4\,n\,\frac{E_H^2}{E_i^2}\,\frac{E_i}{E}\left[1-\frac{E_i}{E}\right]\pi\,a_0^2 \qquad \text{(II.2.4.1)}$$

where n is the number of electrons in the outer shell, E_H is the ionisation potential of hydrogen, E_i is the ionisation potential of the gas, a_0 is the Bohr radius and E is the energy of the electron stream. For low electron energies equation II.2.4.1 overestimates σ_i by a factor of five and, for high electron energies, σ_i varies as the natural logarithm of the electron energy. Values of σ_i for various gases and electron energies are shown in Table II.2.4.1.

Energy	H	H_2	He	He^+	O_2	N_2	N	N^{2+}
$2.0\ 10^1$	$2.68\ 10^{-1}$	$2.70\ 10^{-1}$			$3.12\ 10^{-1}$	$3.19\ 10^{-1}$		
$4.0\ 10^1$	$6.38\ 10^{-1}$	$8.59\ 10^{-1}$	$1.71\ 10^{-1}$		$1.50\ 10^0$	$1.55\ 10^0$	$9.40\ 10^{-1}$	
$6.0\ 10^1$	$6.78\ 10^{-1}$	$9.80\ 10^{-1}$	$2.99\ 10^{-1}$	$1.2\ 10^{-2}$	$2.32\ 10^0$	$2.34\ 10^0$	$1.36\ 10^0$	$7.80\ 10^{-2}$

$8.0\ 10^{1}$	$6.38\ 10^{-1}$	$.70\ 10^{-1}$	$3.41\ 10^{-1}$	$2.3\ 10^{-2}$	$2.62\ 10^{0}$	$2.61\ 10^{0}$	$1.50\ 10^{0}$	$1.41\ 10^{-1}$
$1.0\ 10^{2}$	$5.98\ 10^{-1}$	$9.23\ 10^{-1}$	$3.60\ 10^{-1}$	$3.6\ 10^{-2}$	$2.77\ 10^{0}$	$2.69\ 10^{0}$	$1.53\ 10^{0}$	$1.67\ 10^{-1}$
$2.0\ 10^{2}$	$4.22\ 10^{-1}$	$7.21\ 10^{-1}$	$3.38\ 10^{-1}$	$4.5\ 10^{-2}$	$2.59\ 10^{0}$	$2.40\ 10^{0}$	$1.30\ 10^{0}$	$1.69\ 10^{-1}$
$4.0\ 10^{2}$	$2.55\ 10^{-1}$	$4.71\ 10^{-1}$	$2.44\ 10^{-1}$	$3.9\ 10^{-2}$	$1.85\ 10^{0}$	$1.72\ 10^{0}$	$8.93\ 10^{-1}$	$1.26\ 10^{-1}$
$6.0\ 10^{2}$	$1.68\ 10^{-1}$	$2.74\ 10^{-1}$	$1.87\ 10^{-1}$	$3.1\ 10^{-2}$	$1.42\ 10^{0}$	$1.34\ 10^{0}$	$6.10\ 10^{-1}$	$9.70\ 10^{-2}$
$7.5\ 10^{2}$	$1.4\ 10^{-1}$	$2.9\ 10^{-1}$	$1.58\ 10^{-1}$	$2.7\ 10^{-2}$	$1.21\ 10^{0}$	$1.15\ 10^{0}$	$4.60\ 10^{-1}$	$8.2\ 10^{-2}$
$1.0\ 10^{3}$	$1.2\ 10^{-1}$	$2.24\ 10^{-1}$	$1.22\ 10^{-1}$	$2.2\ 10^{-2}$	$9.76\ 10^{-1}$	$9.36\ 10^{-1}$		
$5.0\ 10^{3}$	$2.8\ 10^{-2}$	$5.00\ 10^{-2}$	$3.60\ 10^{-2}$	$6.3\ 10^{-3}$	$2.60\ 10^{-1}$	$2.44\ 10^{-1}$		
$1.0\ 10^{4}$	$1.5\ 10^{-2}$	$2.82\ 10^{-2}$		$3.2\ 10^{-3}$	$1.40\ 10^{-1}$	$1.23\ 10^{-1}$		

Table II.2.4.1: Electron ionization cross sections[13]. Energy in eV, cross sections in 10^{-16} cm^2

The ionisation rate per unit length for a monoenergetic electron beam propagating through a gaseous medium is given by:

$$N = \frac{J_0}{e}[1 - \exp(-n_g \sigma_i)] \qquad \text{(II.2.4.2)}$$

where J_0 is the electron beam current density and n_g is the gas number density. In order to calculate the plasma density profile produced by the electron beam we assume that J_0 is uniform across the beam and that equilibrium is maintained by ambipolar diffusion to the walls. Consider an elemental volume of unit length, radius r and width dr, centred on the electron beam. The rate R_i at which ions enter the volume is:

$$R_i = -2\pi\, r\, D_a \left(\frac{dn}{dr}\right)_r \qquad \text{(II.2.4.3)}$$

where D_a is the coefficient of diffusion. The rate at which particles leave the volume is:

$$R_o = -2\pi\,(r+dr)\, D_a \left(\frac{dn}{dr}\right)_{r+dr}$$

$$\cong -2\pi\,(r+dr)\,D_a\left[\frac{dn}{dr} + dr\,\frac{d}{dr}\left(\frac{dn}{dr}\right)\right] \qquad \text{(II.2.4.4)}$$

and the rate of particle generation in the volume is:

$$R_g = N\,2\pi\,r\,dr \qquad \text{(II.2.4.5)}$$

In equilibrium we require:

$$R_g + R_i = R_o \qquad \text{(II.2.4.5)}$$

and substituting from equations II.2.4.3–5 we obtain the equation which relates the plasma density profile to the ionisation rate in the beam:

$$\frac{d^2n}{dr^2} + \frac{1}{r}\,\frac{dn}{dr} + \frac{N}{D_a} = 0 \qquad \text{(II.2.4.6)}$$

For a uniform electron beam of radius b in a cylindrical tube of radius a the boundary conditions are that n(r=0) is finite, n(r=b) = 0 and n and dn/dr are continuous functions at r=a. The solution of equation II.2.4.6 subject to these conditions is

$$n(r) = \begin{cases} \dfrac{-N}{D_a}\left[\dfrac{r^2}{2} + b^2 \ln\dfrac{b}{a} - \dfrac{1}{2}\right] & 0<r<b \\ \dfrac{-Nb^2}{2\,D_a}\ln\dfrac{r}{a} & b<r<a \end{cases} \qquad \text{(II.2.4.7)}$$

The number density profile is shown in Figure II.2.4.2.; the vertical marker indicates the beam radius. Now for a non relativistic electron beam the current density is:

$$J_0 = n_b\,e\sqrt{\frac{2eV}{m}} \qquad \text{(II.2.4.8)}$$

where n_b is the electron density in the beam and eV is the beam energy. From equations II.2.4.2, 7 and 8 we obtain an equation for the plasma density, n, which is of the form:

$$n = K\, n_b \qquad \text{(II.2.4.9)}$$

If we have K >> 1, then the electron beam space charge can be completely neutralised by a small perturbation of the plasma and the ambipolar diffusion assumption is valid.

In the case $K \cong 1$, it is not clear whether or not ambipolar diffusion occurs. The ion mobility, μ_i, is generally lower than the electron mobility, μ_e and so one ion can neutralise the charge of several beam electrons. Thus, if we have $n<n_b$ the electron beam can be totally space charge neutralised if

$$\frac{n}{n_b} \cong \frac{\mu_i}{\mu_e} \qquad \text{(II.2.4.10).}$$

For values of K such that $1 > K > \mu_i/\mu_e$, equation (II.2.4.7) overestimates the plasma density because electrons can diffuse freely to the walls. This effect can be approximated by replacing the ambipolar diffusion coefficient D_a with the electron free diffusion coefficient D_e ($>D_a$). When we have $K < \mu_i/\mu_e$, electrons diffuse to the wall under the influence of the residual field from the beam space charge and an even larger diffusion coefficient is required for equation II.2..4.7 to hold.

II.2.5 Simple Glow Discharge Electron Gun

Initial experiments were conducted using a gas insulated, single anode glow discharge electron gun made by EEV Ltd. The design of the electron gun and the experimental arrangement are shown in Figures II.2.5.1-2. The electron gun is mounted in a quartz tube with a radius 3.5 cm and length of 65 cm. The tube is supported inside a solenoid

which produces a longitudinal magnetic field strength of up to 200 gauss. Measurements were made in residual air in the pressure range 0.15 mbar to 1 mbar.

The characteristics of the glow discharge electron gun and the effects of the applied magnetic field are shown in Figures II.2.5.3-4.. At the higher pressures the track of the electron beam can be seen as a white glow caused by electron excitation and ionisation of the gas. At lower pressures the glow is too faint to be visible but the presence of fast electrons causes a green fluorescence in the quartz walls. The electron beam is deflected by a small permanent magnet.

With no applied magnetic field the penetration and shape of the electron beam varies with the pressure. At 1 mbar the electron beam appears to diverge rapidly and fill the quartz tube after 5 cm. As the pressure is reduced at constant voltage the divergence of the beam decreases and its penetration increases. The results obtained by substituting the experimental parameters into equation II.2.4.7 suggests that total space-charge neutralisation should always occur. The conclusion is that the beam divergence occurs as a result of collisions (not necessarily inelastic) with the gas molecules and the beam divergence is characteristic of the scattering angle function.

When a longitudinal magnetic field is applied, the electron beam is confined and propagates the length of the solenoid without diverging. This is because the longitudinal magnetic field reduces the value of the maximum scattering angle. As the strength of the magnetic field is increased, the intensity of the glow and the discharge current increase. The increased intensity of the glow can be understood in terms of the increased discharge current and the effect of the transverse ambipolar diffusion coefficient, D_s, in a longitudinal magnetic field, B[14]:

$$D_s = \frac{D_a}{1+\mu_i\mu_e B^2} \qquad \text{(II.2.5.1).}$$

Decreasing the value of the diffusion coefficient in equation II.2.4.7 clearly increases the number density in the plasma. The increase in the discharge current with increasing magnetic field occurs because the magnetic field causes the electrons to propagate in a helical path with a radius which is a function of the applied field and the electron energy. The helical path increases the number of collisions experienced by an electron travelling between the electrodes. Thus, the effective mean free path is decreased by the magnetic field and this effectively represents an increase in the pressure of the gas.

Because the electron gun is not aligned with the central axis of the solenoid the magnetic field at the end of the solenoid deflects the beam onto the quartz wall. Fluorescence is visible at the point of impact and rapid local heating occurs – the quartz becomes red hot in a few seconds. If the electron gun is inclined at an angle to the magnetic field then the beam follows a helical path. The radius of the helical path is just the gyromagnetic radius for the transverse velocity component of the electrons in the applied field:

$$r_e = \frac{1}{B}\sqrt{\frac{2mV}{e}}\cos\theta \qquad \text{(II.2.5.2)}$$

where B is the applied magnetic field, V is the beam voltage and θ is the angle that the axis of the electron gun makes with the direction of the magnetic field. These values are shown graphically in Figure II.2.5.5.

II.2.6 Electron Gun with Variable Electrode Spacing

The electron gun described in Section II.2.5 has an anode which is fixed with respect to the cathode. Scaling to higher voltages was achieved using the similarity relationship between the pressure and electrode spacing. In this section an experiment with variable electrode spacings and geometry is described. Also, the possibility of employing an auxilliary electrode for beam focussing is investigated.

The experimental tube is shown in Figure II.2.6.1. The position of the anodes A1 and A2 are fixed by their connecting pins which seal on the outside of the tube. The cathode is mounted inside a threaded nylon bushing which allows the position of the cathode to be adjusted in the longitudinal direction. All of the connection pins are threaded so that they can be removed and the electrodes can be interchanged. The cathode is made of brass and has a 4 mm wide, 15 mm deep central slot. There is a choice of two anodes A1, one made from a washer (A1a) and the other made from a Swage-Lock collar (A1b). The anodes are mounted in nylon discs which electrically insulate the connecting pins.

The charcateristics of the electron gun with anode A1a are shown in Figure II.2.6.2. These results are for air at 0.4 mbar and anode-cathode spacings of 1 mm, 3 mm and 8 mm. The characteristics are all of the form:

$$I = K V^n \qquad \text{(II.2.6.1)}$$

and from the logarithmic plots we obtain the numerical values of K and n for each electrode spacing, d:

d (mm)	K (A cm^{-2} V $^{-n}$)	n
1	2.3×10^{-9}	2.0
3	1.9×10^{-10}	2.0
8	7.4×10^{-12}	2.0

Table II.2.6.1: Electron gun characteristics for different values of the anode-cathode gap.

The value of n=2 differs form the value of 3/2 predicted by the Child Langmuir equation. The V^2 dependence can be explained if the current is mobility limited rather than space-charge limited. The constant, K, is not the perveance usually quoted for an electron gun because of the parabolic form of the characteristics. A simple analysis of the mobility limited current between parallel electrodes gives the current proportional to V^2/d^3 where d is the electrode separation[2]. We find, however, that the experimentally determined value of K varies as $d^{-3.3}$ between d=3 mm and d= 8 mm and as $d^{-2.3}$ between d=1 mm and d=3 mm. These results expose the inadequacy of the simple parallel electrode model for high voltage glow discharge electron guns in which the electrode structures are of comparable size to the electrode spacing.

The conditions in which the simple parallel electrode model fails can be estimated by considering the fringe fields at the anode hole. If there is no anode hole, and assuming that the discharge is obstructed, there is a constant field between the electrodes, given by

$$E = \frac{V}{d} \qquad \text{(II.2.6.2)}$$

For the case where the anode contains an aperture we assume that the edge of the aperture has a radius of curvature, R. Then it is easy to show that the fringing field is given approximately by

$$E_f \cong \frac{RV}{r^2} \qquad \text{(II.2.6.3)}$$

where r is the distance from the anode. The parallel electrode model fails when the fringing field at the cathode is of the same order as the field given by equation II.2.6.2., that is, when we have $d \cong R$. For the results given in Table II.2.6.1 the value of R is of the order of 1 mm and the behaviour does indeed depart from that predicted by the parallel electrode model for values of d which are of this order.

The electron beam formed using anode A1a diverges and fills the tube after a few centimetres. The insertion of a floating electrode (A1b) after A1a produces a beam which is well collimated with a diameter equal to the exit aperture of the collimating electrode. The focussing can be explained if the collimating electrode is charged to a negative potential by the electron beam. The main anode is earthed so the field between A1a and A1b produces a constricting force on the electrons in the beam. The details of the focussing effect are complicated by space charge neutralisation, collisions and the formation of sheaths at the electrodes.

II.2.7 High Voltage High Frequency Electron Guns

In order to identify some of the problems associated with the construction of glow discharge electron guns at voltages over 100 kV a simple glass envelope low pressure tube was fabricated. The low pressure tube is shown in Figure II.2.7.1. The cathode is aluminium and contains a 1 mm diameter central slot which is 15 mm deep. The tube is evacuated to 10^{-6} mbar using a diffusion pump and sealed off. The high voltage power supply is a 350 kV Tesla generator operating at a resonant frequency of 300 kHz and a repitition rate of 100 pps. The high frequency nature of the signal generated by a Tesla coil allows an unusual electrode configuration in which the anode is earthed only by its parasitic capacitance.

In operation, a discharge fills the region between the cathode and the anode. A large coronal discharge forms at the external anode connection. This occurs because the discharge current charges the parasitic capacitance of the anode until the anode field causes atmospheric breakdown. The sides of the tube surrounding the cathode fluoresce and are heated very quickly until the glass is red hot after a few seconds. The localised fluorescence and heating are evidence that a radial electron beam is formed at the cathode. Cathodic sputtering causes a gradual discoloration of the tube. The sputtering and heating causes the release of gases into the tube and the pressure rises

over a period of several minutes. As the pressure rises the discharge radius decreases to form an unstable ribbon-like discharge. This behaviour is typical of the transition from the positive column of a glow discharge to a low pressure arc.

The results obtained from the sealed-off tube were used in the design of an improved high voltage electron gun for the Tesla generator (Figure II.2.7.2). The original tube was a sealed envelope device in order to avoid electrical breakdown in the pumping line. The out-gassing caused by the discharge conditions, however, limits the sealed tube lifetime to a few minutes. In order to extend the lifetime of a tube, operational conditioning is required, that is, the tube needs to be actively pumped with the discharge running until the adsorbed gases have been released and evacuated.

The required fast pumping rate and high absolute vacuum is achieved using a zeolite cryopump. Despite the length of the pumping line (3 m) the presence of metallic components in the rotary pump used to reduce the getter to its operating pressure leads to breakdown in the line. The resulting discharge disrupts the cryopump by raising its temperature. The cryopump is, therefore, isolated from the discharge by a capacitively coupled earth connection and a strong (greater than 1000 gauss), transverse magnetic field between the pump and the main discharge chamber. Once tube conditioning has been completed, the main chamber is sealed off and the pumping line removed. A tube which has been conditioned for a period of eight hours has a lifetime of over twenty hours before a noticable change in pressure occurs.

The closely spaced quartz cathode shield prevents breakdown and electron beam formation on the cylindrical surface of the cathode. The glass-to-metal gap provides gas insulation by having a high ratio of surface area (for recombination) to volume. The formation of corona at the anode is controlled by two methods. Firstly, the anode is a large area silver coating applied to the inside surface of the spherical envelope. The large anode area increases its capacitance and reduces the fields around the anode. Secondly, no external connection is made to the anode so there is no metal at anode

potential which is exposed to atmospheric pressure. The anode is coupled to earth by its parasitic capacitance – a technique which relies on the high frequency components of the signal from the Tesla generator.

In operation, an electron beam is formed perpendicular to the surface of the cathode. Fluorescence occurs in the glass envelope, intense at the point of impact of the electron beam and diffuse over the remainder of the envelope, the latter effect suggesting the presence of energetic x-rays. The shape of the electron beam can be inferred from the pattern of fluoresecence which consists of a highly intense central spot (which causes rapid heating in the glass) surrounded by a less intense annular region.

The voltage generated by the Tesla coil is approximately a sinusoidal signal at 300 kHz which is modulated at 100 Hz. The effect of this modulation on the electron beam is not known. Two obvious possibilites are that the beam is modulated at 300 kHz or that the tube operates as an amplitude modulation detector and produces an electron beam modulated at 100 Hz. It is known, however, that a high voltage constricted discharge can be used to generate pulsed electron beams with a duration of the the order of 1 μs at low repitition rates. It is therefore plausible that the electron beam may be modulated at 300 kHz. A possible method of confirming the modulation frequency of the electron beam would be to monitor the intensity of the fluorescent spot using a photodiode. Unfortunately the Tesla generator produces large amounts of electrical noise at 300 kHz which interferes with the measurement. A future experiment should incorporate an optical fibre coupled to a remote photodetector to measure the elecron beam modulation.

II.2.8 Conclusions: High Voltage Electron Gun Design

Glow discharge electron guns are robust, instant-start devices. Electron beams with current densities of the order of 20 A cm^{-2} and electron energies up to 350 keV have

been produced. The effects of space charge neutralisation and mobility current-limitation generally lead to glow discharge electron guns having higher perveances than equivalent vacuum devices.

The maximum operating voltage of a glow discharge electron gun scales with electrode spacing and pressure according to Paschen's law V = f(pd). The perveance is inversely proportional to some power (of the order of 2.5) of the electrode separation. Simple theoretical models provide order-of-magnitude estimates of the perveance but the experimental evidence does not always agree with the theoretical predictions. The discrepancy is attributed to departures from the parallel electrode approximation when the electrode separation is similar to the dimensions of any apertures in the electrodes.

II.3 The RF Plasma Cathode

II.3.1 Introduction

The problems associated with cathode surfaces can be circumvented by the use of a plasma cathode: a dense plasma is formed in the cathode region and electrons are drawn from the plasma, in a manner similar to field emission. The plasma boundary is, however, controlled and gap closure can be prevented. A number of schemes to produce a plasma cathode have reported, notably electrical glow discharges[5], low pressure arcs[6] and plasma jets. Glow discharge plasma cathodes use either the negative glow or the positive column of a discharge to form the plasma from which the electrons are extracted. The degree of ionisation in these plasmas is usually relatively low. Low pressure arcs and plasma jets have higher electron densities but may suffer from poor temporal stability and spatial uniformity. In all of the above plasma sources, the cathode which produces the plasma forms part of the main circuit.

In this section a new kind of plasma cathode in which a plasma is generated by an RF field is described. Relative to DC discharges, RF discharges (in particular microwave

ones) are generally less expensive, easier to handle, more efficient and more reliable sources of particles. They may be maintained between metal electrodes or in a variety of electrodeless configurations. The use of a pulsed RF source can provide extremely high peak power densities at relatively low average powers, offering both start-up time and thermal management advantages over thermionic cathodes. Designs for RF plasma cathodes based on the propagation of electromagnetic surface waves, plasma waveguide waves and slow waves on helical structures are presented. These RF plasma sources are known to operate from pressures of 10^{-5} mbar to several atmospheres and produce plasma densities of the order of 10^{13} cm^{-3} with RF powers of the order of 1 kW[7,8]. The excitation conditions employed also serve electrically to isolate the plasma source from the main cathode current. This allows an extra degree of freedom of control over the plasma and offers the possibility of forming a uniform, stable cathode.

A schematic diagram of a simple plasma cathode is shown in Figure II.3.1.1. The plasma is unconfined in the longitudinal direction and will tend to diffuse towards the anode. This diffusion is clearly undesirable and is prevented in the case of a plasma jet cathode by the supersonic flow of the plasma across the cathode region. In the RF plasma cathode, however, the plasma must be confined by other means. In fact the plasma may conveniently be confined by using a grid mesh electrode which has a potential which is positive with respect to the plasma (Figure II.3.1.2). The cathode grid has a further effect which is extremely advantageous to the cathode operation. Figure II.3.1.3 shows a notional variation of potential with longitudinal distance. The positive control grid is expected to cause the formation of a double space charge sheath with a negative space charge cloud around the grid. This negative space charge cloud can be compared to the space charge cloud at the surface of a thermionic cathode and is the effective electron source of the cathode. The positive control grid thus defines the position of the effective cathode and will henceforth be referred to as the cathode grid (Fig II.3.1.2).

II.3.2 Conditions at the Cathode Grid

The cathode sheath width, s, for "cold", incoming electrons is given by the standard relation[6]:

$$s = 1.5\text{x}10^{-3}\, j_e^{0.5}\, V_{gc}^{0.75} \qquad \text{(II.3.2.1)}$$

where s is in cm, j in A cm^{-2} and V is the cathode grid potential with respect to earth in volts. A plot of sheath width against bias voltage (Equation II.3.2.1) is shown in Figure II.3.2.1. In order for electrons to be extracted from the cathode region, the sheath thickness must be at least as great as the thickness of the cathode mesh. This condition defines the minimum bias voltage for the grid. In order to minimise the current in the bias circuit, the cathode grid must have a high electron transparency factor. The bias potential accelerates electrons through the cathode grid where they form a space charge cloud. In the absence of an accelerating field from the anode these electrons are prevented from crossing the gap to the anode by their own space charge. When the anode potential is applied a space charge limited current can flow.

A negative space charge cloud can only form at the cathode grid if the grid has a positive bias with respect to the plasma between the cathode-grid and earth. In fact, by applying a negative bias to the grid, a positive space charge sheath can be formed provided that the magnitude of the grid voltage V_g satisfies:

$$V_g^2 > \left[\frac{k\,T_e}{e}\right]^2 \qquad \text{(II.3.2.2)}$$

Thus, there is the possibility that the cathode can be controlled and even switched on and off by the application of appropriate potentials.

II.3.3 Conditions at the Earth Grid

The earth grid is the surface at which ion neutralisation maintains the plasma at a negative potential with respect to the cathode grid. An important factor in the maintenance of the electron current which can be drawn from the plasma is the ion neutralisation rate at the earth grid. For large electron currents, large ion currents flow to the earth grid. Unlike the case of a glow discharge, however, the ion current to earth is not accelerated through a cathode fall potential. The grid surface is not damaged by ion bombardment and sputtering does not occur. The RF plasma generators allow large areas of metal to be inserted into the plasma thereby allowing for a large surface area for ion neutralisation.

II.3.4 The Anode-Cathode Gap

If the plasma cathode is to be incorporated into an electron gun then it is essential that breakdown does not occur in the anode-cathode gap. The gap will not breakdown provide that the electron mean free path in the gap is longer than the dimensions of the gap. This condition is met on the left hand branch of the Paschen curve (Figure II.2.1.2). If the cathode has a parallel electrode geometry and is operating in the Child-Langmuir space charge limited regime, then the perveance of the cathode is given by:

$$K = \frac{4}{9}\varepsilon_0 \frac{A}{d^2}\sqrt{\frac{2e}{m}} \qquad \text{(II.3.4.1)}$$

where A is the area of each electrode and d is their separation. Thus, the use of a small anode-cathode gap to prevent breakdown also leads to a high perveance for the electron beam.

An RF discharge can produce twenty percent ionisation at pressures as low as 10^{-5} mbar (see section II.3.7). At these pressures even moderately sized gaps of the

order of a centimetre hold off tens of kilovolts. In this case shaped electrode geometries such as the one due to Pierce can be employed to increase the perveance of the electron beam.

Two other solutions to the anode-cathode breakdown problem are differential pumping and the use of a "gas puff" in the cathode region. Differential pumping involves engineering the vacuum system in such a way that the pressure in the anode-cathode gap is maintained at a value considerably lower than that within the plasma cathode region. "Gas puff" technology can be used independently of, or in conjunction with, differential pumping. "Puff valves" are available which can deliver precise quantities of gas on a trigger signal[15]. If the anode-cathode gap has been reduced to a reasonably hard vacuum then large electrode spacings can be used. Cathode formation is initiated by the introduction of a "gas puff" into the plasma cathode so as to produce an increase in local pressure sufficient for a dense plasma to be produced. The anode-cathode gap cannot break down until the gas has diffused through the cathode mesh and filled the gap. This may take several microseconds and magnetic insulation can extend this time by an order of magnitude.

II.3.5 Surface Wave Plasmas

The fact that a surface wave can propagate along the interface between a plasma column and a dielectric tube has been known since the 1960s.[9] In the 1970s attention focussed on the use of such surface waves for the generation of plasma columns. In 1974 Moisan developed the surfatron[10] which was the first simple, compact and efficient surface wave launcher for the generation of long plasma columns at microwave frequencies. More recent work has extended the frequency range at which surface wave launchers operate from less than 1 MHz to 10 GHz with a variety of launchers including ro-box (LC), ro-box (stub), surfatron, waveguide-surfatron and surfaguide. Plasmas with densities of the order of 10^{13} cm^{-3} can be obtained in the

pressure range 10^{-5} mbar up to a few atmospheres. The plasmas are stable, reproducible and quiescent, the level of electron fluctuations being low. A comprehensive treatment of plasma sources based on the propagation of electromagnetic waves is given in the review article by Moisan and Zakrzewski[7].

II.3.6 Plasma Waveguides

Plasma waveguide modes were first analysed by Trivelpiece and Gould for use in plasma diagnostics (see section III.3). One important result is that a plasma-filled waveguide can actually propagate an electromagnetic wave which has a frequency below both the plasma frequency and the empty waveguide cut-off frequency provided that there is an externally applied magnetic field of the correct configuration. In particular, for waveguides of small radius the propagating wave impedance can be sufficiently high that the RF fields are high enough for the plasma to be sustained by the RF. If the waveguide is formed into a resonant cavity at the RF frequency then plasma densities of the order of 10^{14} cm^{-3} can be achieved with high efficiency[7]. The range of operating parameters is similar to the surface wave sustained plasma sources.

II.3.7 Plasma Production Using Helical Structures

It is well known that slow wave structures can be used for high density plasma production. The usual techniques employ a helix-loaded waveguide or an interdigital line excited by an appropriate antenna (for example a radial dipole or an axial monopole)[8]. These methods of plasma generation generally require the application of a profiled magnetic field and the plasma is excited by electron cyclotron resonance (ECR). Care must be taken to ensure that the source, antenna and plasma loaded helical guide are well matched and that the appropriate slow wave mode is excited in the

helical guide. High degrees of ionisation (about 20 per cent) have been reported at pressures as low as 10^{-5} mbar.

Many of the problems associated with matching, slow-wave excitation and the generation of magnetic fields can be overcome by driving the slow-wave helical source directly[11]. Following the method of Pierce, the fields generated by an RF signal on a wire helix can be approximated (in the absence of breakdown) by solving Maxwell's equations with a solid sheath with the same dimensions replacing the helix. The sheath is assumed to be perfectly conducting at an angle ψ corresponding to the pitch angle of the helix and nonconducting in the orthogonal direction. For the zeroth order circularly symmetric wave propagating in the z direction we obtain the electric fields:

$$E_z = B\, I_0(\gamma r) \exp j(\omega t - \beta z) \qquad \text{(II.3.7.1)}$$

$$E_r = jB \frac{\beta}{\gamma} I_1(\gamma r) \exp j(\omega t - \beta z) \qquad \text{(II.3.7.2)}$$

$$E_\phi = -B \frac{I_0(\gamma a)}{I_1(\gamma a)} \frac{1}{\cot \psi} I_1(\gamma r) \exp j(\omega t - \beta z) \qquad \text{(II.3.7.3)}$$

inside the helix and

$$E_z = B \frac{I_0(\gamma a)}{K_0(\gamma a)} K_0(\gamma r) \exp j(\omega t - \beta z) \qquad \text{(II.3.7.4)}$$

$$E_r = -jB \frac{\beta}{\gamma} \frac{I_0(\gamma a)}{K_1(\gamma a)} K_0(\gamma r) \exp j(\omega t - \beta z) \qquad \text{(II.3.7.5)}$$

$$E_\phi = -B \frac{I_0(\gamma a)}{K_1(\gamma a)} \frac{1}{\cot \psi} K_1(\gamma r) \exp j(\omega t - \beta z) \qquad \text{(II.3.7.6)}$$

outside the helix where we have

$$\psi = \tan^{-1} \frac{p}{2\pi a} \qquad \text{(II.3.6.7)}$$

$$\gamma^2 = \beta^2 - \beta_0^2 \qquad \text{(II.3.6.8)}$$

In equations II.3.6.1-8 the helix has radius a and pitch p, and β, β_0 are the axial and free space phase constants and B is a constant determined by the RF power. Application of the boundary conditions at r=a (involving the assumptions regarding the conductivity) to equations III.3.6.1-3 yields the equation for γ:

$$(\gamma a)^2 \frac{I_0(\gamma a)\, K_0(\gamma a)}{I_1(\gamma a)\, K_1(\gamma a)} = (\beta_0 a \cot \psi)^2 \qquad \text{(II.3.7.9)}$$

Following the practice of travelling wave tube theory, a coupling parameter κ is introduced, where

$$\kappa = \frac{E_z^2(0)}{2\beta^2 P} \qquad \text{(II.3.7.10)}$$

and P is the RF power. By integrating the Poynting vector ($E \times H^*$), the value of κ is found to be

$$\kappa = \frac{1}{2} \frac{\beta}{\beta_0} \left[\frac{\gamma}{\beta}\right]^4 F(\gamma a)^3 \qquad \text{(II.3.7.11)}$$

where we have

$$F^3 = \frac{1}{\frac{\gamma a}{240}\frac{I_0(\gamma a)}{K_0(\gamma a)}\left[\frac{I_1(\gamma a)}{I_0(\gamma a)} - \frac{I_0(\gamma a)}{I_1(\gamma a)} + \frac{K_0(\gamma a)}{K_1(\gamma a)} - \frac{I_1(\gamma a)}{I_0(\gamma a)} + \frac{4}{\gamma a}\right]} \qquad \text{(II.3.7.12)}$$

From equations II.3.7.10-12 the axial electric field is

$$E_z(0) = \sqrt{\frac{\gamma^4}{\beta\beta_0} F(\gamma a)^3 P} \qquad \text{(II.3.7.13)}$$

Equating (II.3.7.13) to (II.3.7.12) with r=0 gives the value of the constant B:

$$B = \sqrt{\frac{\gamma^4}{\beta\beta_0} F(\gamma a)^3 P} \qquad \text{(II.3.7.14)}$$

An example of the radial profile of the longitudinal electric field is shown in Figure II.3.7.1 where a typical breakdown field for a low pressure gas is indicated. The above analysis suggests that a plasma may be generated in an annular region around the helix. An important implicit assumption in the derivation of equations II.3.7.1-6 is that the plasma density is low enough that the plasma frequency is much smaller than the frequency of the applied field. In cases where this assumption is not valid the effects of the plasma must be included in the model.

A full solution for the plasma loaded microwave helix involves the simultaneous solution of Maxwell's equations and the plasma equilibrium equations. The ionisation rate is inferred from the RF attenuation constant and the plasma density profile is derived from the flux balance equations. Clearly the full solution requires a complicated iterative computation. Given the number of factors which enter into the computational solution and are difficult to quantify (for example ionisation cross sections, temperatures, etc.) it is difficult to improve on the accuracy of simpler, order

of magnitude calculations. In order to obtain an insight into the form and magnitude of the plasma density we solve the flux continuity equation for a number of cases.

The simplest case of interest is for a uniform ionisation rate, N per unit volume per second, in an annular region a<r<b where b is the radius of a the cylindrical tube. Assuming that equilibrium is maintained by recombination at the wall equation II.2.4.6 gives:

$$\frac{d^2n}{dr^2} + \frac{1}{r}\frac{dn}{dr} + \frac{N}{D_a} = 0 \qquad \text{(II.3.7.15).}$$

The boundary conditions are that n(r=0) is finite, n(r=b)=0, n(r) and dn/dr are continuous at r=a. The solution of equation II.3.7.15 subject to these boundary conditions is :

$$n(r) = \begin{cases} \dfrac{-N}{4D_a}\left[r^2 - b^2 + 2a^2 \ln\dfrac{b}{r}\right] & a<r<b \\ \dfrac{-N}{4D_a}\left[a^2 - b^2 + 2a^2 \ln\dfrac{b}{a}\right] & 0<r<a \end{cases} \qquad \text{(II.3.7.16)}$$

A graph of the radial density profile is shown in Figure II.3.7.2: The density is constant in the centre of the tube and decays parabolically to zero at the walls. Figure II.3.7.1 shows the magnitude of the electric field varying approximately linearly from a maximum at the tube radius b to the breakdown field at some radius a. The model may therefore be refined by assuming that the plasma generation rate N is a linear function of r:

$$N(r) = \frac{2N_0}{b-a}(r-1) \qquad \text{(II.3.7.17)}$$

where N_0 is the mean value of N. Now (II.2.4.6) becomes:

$$r\frac{d^2n}{dr^2}+\frac{dn}{dr}+\frac{r}{D_a}\frac{2N_0}{b-a}(r-1)=0 \qquad \text{(II.3.7.18).}$$

The boundary conditions are the same as for the case N=constant and the solution for the plasma density is:

$$n(r) = \begin{cases} \dfrac{-2N_0}{D_a(b-a)}\left[\dfrac{r^3-b^3}{6}+\dfrac{r^2-b^2}{4}+a^2\left(\dfrac{1}{2}-\dfrac{a}{3}\right)\ln\dfrac{b}{r}\right] & a<r<b \\ \dfrac{-2N_0}{D_a(b-a)}\left[\dfrac{a^3-b^3}{6}+\dfrac{a^2-b^2}{4}+a^2\left(\dfrac{1}{2}-\dfrac{a}{3}\right)\ln\dfrac{b}{a}\right] & 0<r<a \end{cases}$$

(II.3.7.19)

A graph of equation II.3.7.19 is shown in Figure II.3.7.3. Again the plasma density is constant in the central region and decays to zero at the wall. This agrees with experimental observation at low pressures where the discharge appears to fill the tube. As the pressure is increased, however, the discharge clearly becomes annular. In order to establish if the current model is valid in the higher pressure regime, where an annular discharge is observed, we consider what form of plasma generation profile N(r) is required to give an annular plasma density n(r). We assume that plasma generation occurs in an annular region defined by N(r) where r>a and N(r) is independent of n. The general flux continuity equation is:

$$\frac{d^2n}{dr^2}+\frac{1}{r}\frac{dn}{dr}+\frac{N(r)}{D_a}=0 \qquad \text{(II.3.7.20)}$$

Equation II.3.7.20 can be integrated to give:

$$r\frac{dn}{dr} = \frac{-1}{D_a}\int N(r)\,dr + C \qquad \text{(II.3.7.21)}$$

The boundary condition at r=a gives

$$\left.\frac{dn}{dr}\right|_{r=a} = 0 \qquad \text{(II.3.7.22)}$$

and the value of the constant C is

$$\left.\int N(r)\,dr\right|_{r=a} = C \qquad \text{(II.3.7.23)}$$

Now, in order to obtain an annular plasma, we require a local maximum of n(r) at $r=r_0>a$ (recalling that n(r=b)=0 where $b>r_0$). That is, we have

$$\left.\frac{dn}{dr}\right|_{r=r_0} = 0 \qquad \text{(II.3.7.24)}$$

and from equations II.3.7.21 and 23 we obtain

$$\left.\int N(r)\,dr\right|_{r=a} = \left.\int N(r)\,dr\right|_{r=r_0} \qquad \text{(II.3.7.25)}$$

Differentiation with respect to r gives

$$N(a) = N(r_0) \qquad \text{(II.3.7.26)}$$

A necessary condition for equation II.3.7.26 to hold is that the inverse function (N^{-1}) is not single-valued. Thus N(r) cannot be a constant or a linear function. Furthermore, there must be some radius r_0 in the interval (a,b) for which $N(r_0)=0$. It is possible to envisage circumstances in which these conditions are true. For instance, the conditions hold if breakdown occurs in an annular region with maximum radius smaller than the tube radius. These considerations, however, bring into question the validity of one of the assumptions underlying equation II.3.7.20, namely that N(r) is independent of n(r).

A more general assumption is that the plasma generation rate is a function of the radius and the number density. We then have to solve the equation

$$r^2 \frac{d^2 n}{dr^2} + r \frac{dn}{dr} + \frac{r^2}{D_a} N(r,n) = 0 \qquad \text{(II.3.7.27).}$$

There is, in general, no analytic solution for equations of this form. For some functions N(r), however, equation II.3.2.27 reduces to a form which is solvable in terms of Bessel functions. The form of the electric field solution (equations II.3.7.11-14) suggests that it is reasonable to expect N(r) to vary quadratically with r. In order to approximate the n-dependence of N we consider briefly the physical processes involved in the breakdown. Essentially electrons are accelerated in the RF field and produce further ionisation when they collide with neutrals. It seems reasonable, then, as a first order approximation to assume that N varies linearly with n. Then, e may write

$$N(r,n) = \begin{cases} 2\,p\,r^2\,n & a<r<b \\ 0 & 0<r<a \end{cases} \qquad \text{(II.3.7.28)}$$

The general solution of equation II.3.7.27 with N(r,n) given by (II.3.7.28) is

$$n(r) = \begin{cases} A\,J_0(qr^2) + B\,Y_0(qr^2) & a<r<b \\ C & 0<r<a \end{cases} \qquad \text{(II.3.7.29)}$$

where we have $q=p/D_a$. Application of the usual boundary conditions then gives the following solution for n(r),

$$n(r) = \begin{cases} A\left[J_0\left(qr^2\right) - \dfrac{J_0\left(qb^2\right)}{Y_0\left(qb^2\right)} Y_0\left(qr^2\right) \right] & a<r<b \\ A\left[J_0\left(qa^2\right) - \dfrac{J_0\left(qb^2\right)}{Y_0\left(qb^2\right)} Y_0\left(qa^2\right) \right] & 0<r<a \end{cases}$$

(II.3.7.30)

where q must satisfy the equation

$$\begin{vmatrix} J_0\left(qb^2\right) & Y_0\left(qb^2\right) \\ -2qaJ_1\left(qa^2\right) & 2qaY_1\left(qa^2\right) \end{vmatrix} = 0 \qquad \text{(II.3.7.31)}$$

The plasma density profile given by equation II.3.7.20 is shown in Figure II.3.7.4. For some values of the parameter q, the density has an annular form with a constant value in the central region. It is possible, therefore, to model the production of an annular number density profile in a discharge controlled by diffusion to the walls.

Whilst the diffusion controlled discharge model gives an annular number density profile it also predicts that there will also be a central region of constant, nonzero plasma density. This is still not in full agreement with the experimental observations in which there is no plasma in the central region at higher pressures. The high pressure regime requires a new model in which free recombination plays a role. Recombination effects are extremely difficult to analyse because of the variety of mechanisms (ion-ion, electron attachment, etc.) and the complicated nature of the parameters. The values of recombination constants have, however, been determined experimentally from measurements of the decay constants in the afterglow of a plasma.

For a neutral plasma the decay rate due to recombination is given by

$$N_\alpha = \alpha n^2 \qquad \text{(II.3.7.32)}$$

where α is the coefficient of recombination. For the typical values $\alpha \cong 10^{-6}$ cm^3 s^{-1} and $n \cong 10^{12}$ cm^{-3}, we have $N_\alpha \cong 10^{18}$ cm^{-3} s^{-1}. Now the plasma generation rate N in a typical microwave helical discharge has been determined experimentally (see section II.3.8) to be of the order of 10^{19} cm^{-3} s^{-1} so it is reasonable to assume that recombination loss plays some role in the stabilisation of the discharge. The recombination loss term N_α can be incorporated into the flux continuity equation

$$r^2 \frac{d^2 n}{dr^2} + r \frac{dn}{dr} + \frac{1}{D_a}\left[N(r,n) - \alpha n^2\right] = 0 \qquad \text{(II.3.7.33)}$$

There is no known analytic solution for non-linear second order differential equations of this form. The usual method of handling non-linearities is to make a linear approximation. In order to obtain a crude analytic solution we approximate the third term of equation II.3.7.33 as follows

$$\frac{1}{D_a}\left[N(r,n) - \alpha n^2\right] \cong \frac{\chi - \alpha'}{D_a} n \qquad \text{(II.3.7.34)}$$

where χ is the plasma generation rate per unit volume per second in the region $a<r<b$ ($\chi=0$ for $R<a$) and α' is an effective recombination constant. Clearly this approximation is only reasonable for small values of n in which case χ and α' are small and approximately equal. The general form of the solutions obtained with tbis approximation may be assumed to give an indication of the form of the full non-linear solution. (This is generally true between non-linear systems and their linear approximations, provided that the non-linear system is stable). The linearised solution, subject to the usual boundary conditions, is

$$n(r) = \begin{cases} A\left[J_0(Xr) - \dfrac{J_0(Xb)}{Y_0(Xb)} Y_0(Xr) \right] & a<r<b \\ A\left[\dfrac{J_0(Xa)\, Y_0(Xb) - J_0(Xb)\, Y_0(Xa)}{Y_0(Xb)\, I_0(Ya)} \right] I_0(Yr) & 0<r<a \end{cases}$$

(II.3.7.35)

where X,Y satisfy the equation

$$\begin{vmatrix} J_0(Xb) & Y_0(Xb) & 0 \\ J_0(Xa) & Y_0(Xa) & -I_0(Ya) \\ -XJ_1(Xa) & -XY_1(Xa) & -YI_1(Ya) \end{vmatrix} = 0 \qquad \text{(II.3.7.36)}$$

and we have used

$$X = \sqrt{\frac{\chi - \alpha'}{D_a}}$$

$$Y = \sqrt{\frac{\alpha'}{D_a}} \qquad \text{(II.3.7.37)}$$

A graph of the solution of this set of equations is shown in Figure II.3.7.5. The range of values of α' and χ for which the model approximates to physical reality corresponds to the solution being positive for r in the range (0,b). The plasma density is strongly annular and zero in the central region of the tube. This result is in broad agreement with the experimental observations.

II.3.8 Experimental Results

In this section we describe a proof of principle experiment for the RF plasma cathode. Figure II.3.8.1 shows the experimental configuration of the glass envelope tube on which measurements were made. The tube design and drive circuitry were not optimised for plasma cathode operation but was kept simple to allow a number of experiments to be performed on various configurations without changing too many parameters.

The discharge tube has a radius of 3 cm and contains two grids, G1 and G2, which are 16 cm apart. The length of the tube is 65 cm and an additional electrode is provided at each end of the tube. The microwave helix has an axial length of 27 cm and extends beyond G1 and G2. The tube is evacuated to 10^{-3} mbar and measurements are made in hydrogen at pressures from 0.1 mbar to 2.5 mbar. The microwave source is a radar set operating at 3.05 GHz with peak powers up to 13 kW. The RF pulse has a rise time of 20 ns and a pulse duration which can be switched between 250 ns (medium pulse) and 1 μs (long pulse). Simultaneous time-resolved measurements of the cathode current, anode current and anode voltage are made using fast probes, and the mean discharge current and voltage are also monitored. The radiated fields are measured using a small biconic antenna connected to an RF spectrum analyser.

The experiment proceeds by first establishing a stable DC glow discharge between two electrodes and measuring the discharge voltage and current. The RF signal is applied with a pulse repetition rate of 1 kHz and measurements are made of the mean and time resolved values of the discharge voltage and current.

The results obtained with G1 as an earthed cathode and E1 as an anode are shown in Figures II.3.8.2-12. Figures II.3.8.2 to 5 show the discharge characteristics at various pressures, with and without the applied RF field. These results are shown in a different format in Figures II.3.3.6 to 9, where the effect of the RF field on the mean discharge current is highlighted. The peak currents shown in Figures II.3.8.10-11 are a simple

measure of the peak current enhancement and were obtained by multiplying the increase in mean current by the duty cycle of the RF source. They show a current enhancement of two orders of magnitude over the DC glow discharge current.

Figure II.3.8.12 shows the discharge characteristics as a function of time. The bottom two traces show the anode and cathode currents (100 mA/div) and the top trace shows the anode voltage (1 kV/div); the time scale is 1 μs/div. There are a number of features of interest shown in Figure II.3.8.12. The anode voltage initially falls rapidly for a few tens of nanoseconds and then more gradually for the remainder of the RF pulse. This change of gradient is a consistent feature over the whole pressure range examined. During the first few tens of nanoseconds, the anode and cathode currents rise rapidly to several hundred milliamps. When the RF pulse ends, the voltages and currents decay exponentially corresponding to the decay of the afterglow in the plasma.

A very striking feature in Figure II.3.8.12 is the large oscillation in the cathode current at a frequency of the order of 1 MHz. Paradoxically this current oscillation is not present at the anode and we can offer no satisfactory explanation of the phenomenon. It may be, however, that the cathode current oscillation is a relaxation oscillation associated with a large negative dynamic impedance of the discharge during the formation of the plasma cathode. The presence of a large negative impedance is indicated by the magnitude of the currents during the RF pulse which are larger than might be expected from the values of the external ballast resistor and parasitic circuit capacitance. The absence of the large current oscillations at the anode is presumably connected with the presence of a plasma source in the cathode region.

II.3.9 Analysis of Experimental Results and Discussion

The experimental data from the RF plasma cathode experiment can be used to estimate the plasma parameters. The DC conductivity for a partially ionized plasma is given approximately by

$$\sigma = \frac{n e^2}{m \nu_{eff}} \qquad \text{(II.3.9.1)}$$

where the effective collision frequency, ν_{eff}, is given by

$$\nu_{eff} = \nu_m (1-f) + \frac{N e^2 f}{2x10^3 (kT/e)^{3/2}} \qquad \text{(II.3.9.2)}$$

and n, N are the electron and neutral number densities, f = n/N is the degree of ionisation and ν_m is the electron-neutral momentum collision frequency. From equations II.3.9.1-2 we see that for a weakly ionised plasma for small perturbations in n we can approximate the relationship between the discharge current and number density by

$$I = \kappa n \qquad \text{(II.3.9.3)}$$

In order to estimate the ionisation rate in the RF field we can equate it to the ionisation loss rate immediately after the end of the RF pulse. Using equation II.3.9.3 we obtain

$$\frac{dn}{dt} = \frac{dI}{dt}\frac{n}{I} \qquad \text{(II.3.9.4).}$$

The value of n can be calculated from the DC conductivity if a value for the discharge area is assumed. Using these approximations we estimate the electron density of the RF plasma to be of the order of 10^{12} cm^{-3} and the ionisation rate to be 10^{19} cm^{-3} s^{-1}. Furthermore, for an H_2 ionisation energy of 15 eV, this ionisation rate corresponds to a power of the order of 7 kW being absorbed from the RF field.

Experiments conducted with the plasma source located in the anode region of the discharge result in no increase in the discharge current. This shows that the RF plasma has a major effect on the cathode processes to produce the very high current densities which are observed.

II.3.10 Example Designs

In the following sections and accompanying figures some examples of implementations of RF plasma cathodes are described. In each, for the sake of example, a particular method of RF excitation, has been chosen but other RF excitation methods may also be appropriate. The configuration of the electrode connections to the external circuitry may also be varied. The choice, for instance, of which electrode is connected to earth may affect the performance of the device. The versatility offered by the various configurations of a single tube is a desirable property (*cf* different trigger modes of a triggered spark gap).

II.3.11 Simple Electron Gun

An annular electron gun employing a wire helix plasma cathode is shown in Figure II.3.11.1. The electron gun is a triode with the electrode connections labelled as "earth", "cathode grid" and "anode". In this configuration the electron beam current flows through the high density (and high conductivity) plasma behind the cathode grid. This current is controlled by the potential applied to the cathode grid and the conductivity of the plasma. With no anode potential applied, a very large current would flow in the cathode grid circuit. This can be avoided by the use of a large series resistor. Although the potential divider formed by the external resistance and the plasma reduces the voltage on the cathode grid, the current drawn is small. When an anode potential is applied, a large electron current is drawn from the negative space

charge cloud which surrounds the cathode grid. Thus, the majority of the plasma cathode current flows in the anode circuit through the electron beam.

In another configuration no electrical connection is made to the cathode grid. In this case the grid floats to a positive potential when the anode voltage is applied. Operation is then similar to the previous case, except that there is no external grid current. In a variation of this configuration the cathode grid is maintained at a small negative potential by a small capacitor which is charged through a large inductance. The negative bias helps to confine the plasma. When the anode voltage pulse is applied, the capacitive divider formed by the electrodes and the cathode capacitor generates the required positive potential on the grid.

In a fourth configuration of the annular electron gun shown in Figure II.3.11.1 the cathode grid is connected to earth and a negative bias is applied to the electrode which was formerly connected to earth. Again a negative space charge cloud forms around the cathode grid. In this arrangement, however, the operation is slightly modified when an anode potential is applied. A space charge limited electron current is drawn from the cathode region and is maintained through the neutralisation of ions at the cathode grid. The electron beam current is not required to flow through the main body of the plasma to the third electrode.

II.3.12 Pierce Electron Gun

One way to increase the perveance of an electron beam is to shape an electrode so that it produces a field which compensates for the missing positive space charge which would be required to neutralise the electron beam. Pierce showed that a surface at cathode potential should be inclined at 67.5 degrees to the electron beam[12] between the anode and cathode. For low pressure gaseous applications, however, this electrode structure introduces a longer breakdown path which reduces the maximum operating

voltage of the device. The increased breakdown path can be compensated by an appropriate reduction in the operating pressure. For a cold cathode device this reduced pressure would severely limit the current and cancel the benefits of the Pierce cathode. In the case of the RF plasma cathode, however, high plasma densities can be obtained at the required lower pressures.

The RF plasma generator shown in Figure II.3.12.1 is of the surface wave type. The surface wave launcher is driven by the coaxial feed from the waveguide-to-coaxial transition. For high RF power densities, the waveguide regions would normally consist of pressurised components. The plasma is formed in the low pressure region between the cathode grid and the control grid and is confined by the dielectric walls. A number of configurations for operation of the electron gun are possible, as for the simple electron gun described in section II.3.11.

II.3.13 Magnetron

In Figure II.3.13.1 the main features of the design for a magnetron are shown in which the usual thermionic cathode has been replaced with an RF plasma cathode. As in the case of the electron guns described above, this device is a triode and a similar choice of configurations applies. The plasma cathode is formed by a helical line which is fed through the external magnet in a coaxial transmission line. In the design shown provision has been made to set the central magnetic field to a cyclotron resonance of the helix drive frequency independently of the main magnetron field magnets. This ensures that dense plasmas can be formed at very low pressures.

The anode-cathode gap is more susceptible to breakdown in the RF plasma cathode magnetron than in the electron guns because of the presence of RF fields in the gap and because of the extended electron trajectories in a magnetic field. The capability of the plasma source to operate at very low pressures helps to alleviate this breakdown and

careful engineering of the magnetron RF circuit is also required. The use of a gas puff system combined with the strong fixed magnetic field which is intrinsic to the magnetron would provide still better protection against breakdown and allow the magnetron to operate at higher power levels. This would necessitate continuous pumping, but the start-up time would still be fast.

II.3.14 Thyratron

There are many varieties of thyratron available today and there is a corresponding variety of applications of the RF plasma cathode. Figure II.3.14.1 shows how an RF plasma cathode might simply replace the thermionic cathode in an otherwise conventional metal-ceramic hydrogen thyratron. In this case a surface wave maintained plasma source is shown, driven by a coaxial feed. In another configuration the control grid extracts the electrons radially from a cylindrical plasma cathode to produce an annular space-charge cloud, analogous to a dispenser thermionic cathode in a conventional thyratron. An RF plasma cathode with this end-on annular geometry is used in the high power electron gun which is described in section II.3.15.

II.3.15 High Power Electron Gun

The design for a high power annular electron gun which incorporates several of the features discussed in previous sections is shown in Figure II.3.15.1. The plasma source is a helical line immersed in a DC magnetic field. This magnetic field serves to provide the cyclotron resonance for plasma generation and also, together with the auxiliary grid 3, acts to confine a high density negative space charge cloud in the cathode region. This cloud has an annular form which is extended in the longitudinal direction and has a large volume. For appropriate values of the cathode magnetic field and positive bias of grid 3 with respect to grid 1 a boundary layer of electrons is established at the

cathode surface, extending some distance into the inter-grid gap (*cf* magnetron operation). Thus, there is a large cross-sectional electron density available for beam formation.

The cathode is profiled for high perveance and also includes an element of magnetic focussing (from the increasing magnetic field gradient between the anode and cathode) and magnetic confinement (in the large magnetic field in the anode and drift space). Again there is some choice concerning the external connections of the electrodes which affects the operation of the electron gun.

II.3.16 Conclusions

A new family of plasma cathodes in which an electron beam is extracted from an RF generated plasma has been proposed. The conditions in the RF plasma cathode have been investigated theoretically and experimentally and the results used in the design of a number of electron devices. RF discharge plasma cathodes are instant start, high current density cathodes which offer an alternative to thermionic and glow discharge cathodes. They are also gateable and may be capable of operation at high repetition rates.

The detailed physics of RF plasma cathodes is a complex area. An understanding of some of the processes involved has been developed, but experimental results reveal a number of aspects which warrant further investigation. According to the electrode configuration the electron current may be limited either by the positive ion mobility in the cathode sheath or by the bulk conductivity of the RF plasma. Due to the complicated nature of these processes, the comparison of various electrode configurations will require extensive experimental data.

II.4 References

[1] Microwave Electronic Tube Devices, Liao, Prentice-Hall, 1988. ISBN 0-13-582073-1

[2] New Low Pressure Gas Switches, C. R. Weatherup, 1991, PhD Thesis (St And).

[3] DC Glow Discharge Electron Guns for the Excitation of Rare Gases, R. J. Carman, 1986, PhD Thesis (St And).

[4] Study of Intense Electron Beams Produced by High-Voltage Pulsed Glow Discharges, H. F. Ranae-Sandoval, N. Reesor, B. T. Szapiro, C. Murray, J. J. Rocca, IEEE Trans. Plas. Sci. **PS-15**(4) pp361-374, 1987.

[5] Technological Sources of Charged Particles With Plasma Emitters, S. P. Bugaev, IEEE Trans. Plas. Sci., **19**(5) pp743-745, 1991.

[6] Grid-controlled plasma cathodes, S. Humphries, Jr., S. Coffey, M. Savage, L. K. Len, G.W. Cooper, D. M Woodall, J. Appl. Phys. **57**(3) pp709-713, 1985.

[7] Plasma sources based on the propagation of electromagnetic surface waves, M. Moisan, Z. Zakrzewski, J. Phys. D, **24** pp1025-1048, 1991.

[8] Studies on Microwave-Induced Plasma Production Using Helical Slow-Wave Structures, A. Ganguli, P. Appala, D. P. Tewari, IEEE Trans. Plas. Sci., **19**(2) pp433-444, 1991.

[9] Slow Wave Propagation in Plasma Waveguides, A. W. Trivelpiece and A. W. Gould, San Fransisco Press 1967.

[10] M. Moisan,P. Leprince, C. Beaudry, E. Bloyet, Phys. Lett. **50 A** p125, 1974.

[11] Microwave-Triggered Annular Switching, I. Park, A. Maitland, D. M. Parkes, Proc 6th IEEE Pulsed Power Conference, Arlington Va, USA, 1987.

[12] Theory and Design of Electron Beams, J. R. Pierce, Van Nostrand 1954.

[13] C. E. Moore, A Multiplet Table of Astrophysical Interest, Revised Edition, Natl. Stand. Ref. Data ser. Natl. Bur. Stand. **40** (1972)

[14] Introduction to Electrical Discharges in Gases, S. C. Brown, Wiley 1966.

[15] Balanced Puff Valve for Imploding Gas Puff Experiments, S. Wong, P. Smiley, T. Sheridan, J. Levine, V. Buck, Rev. Sci. Inst **57**(8), pp 1684-1686, 1986.

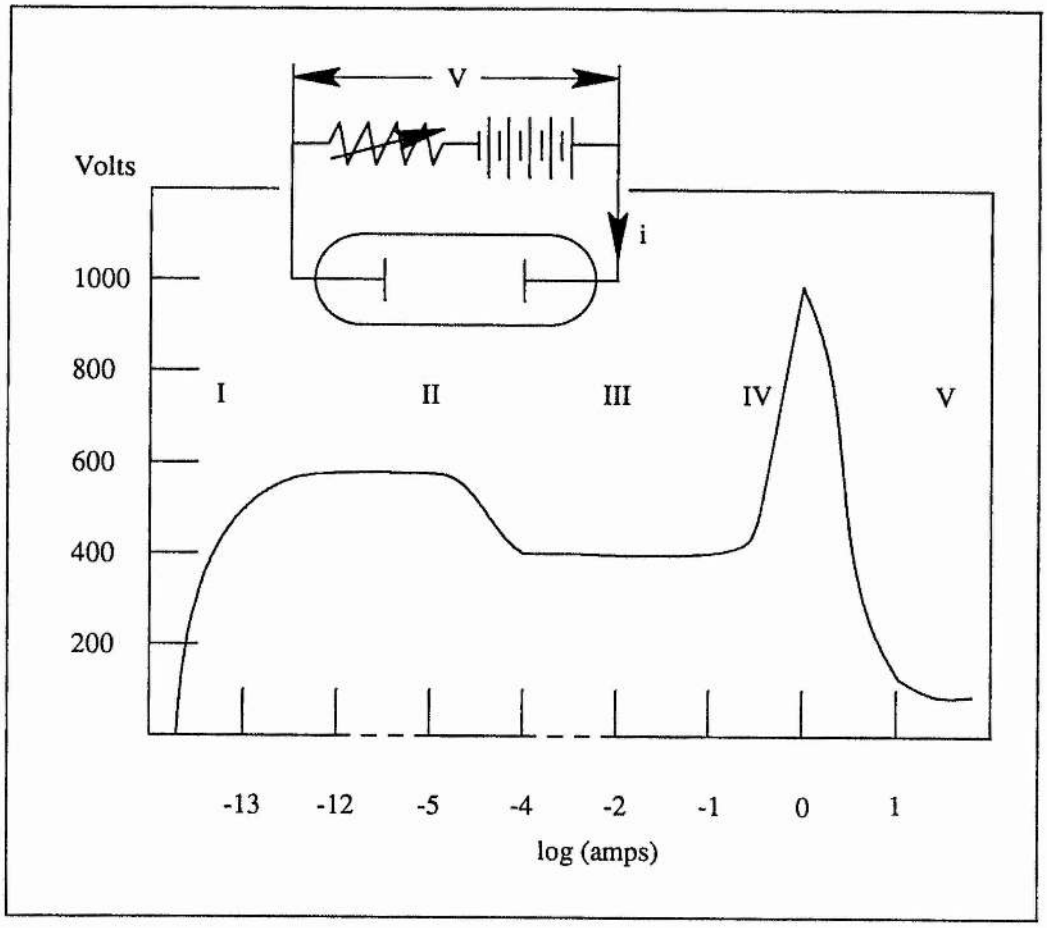

Figure II.2.1.1: Characteristics of a Gas Discharge Tube

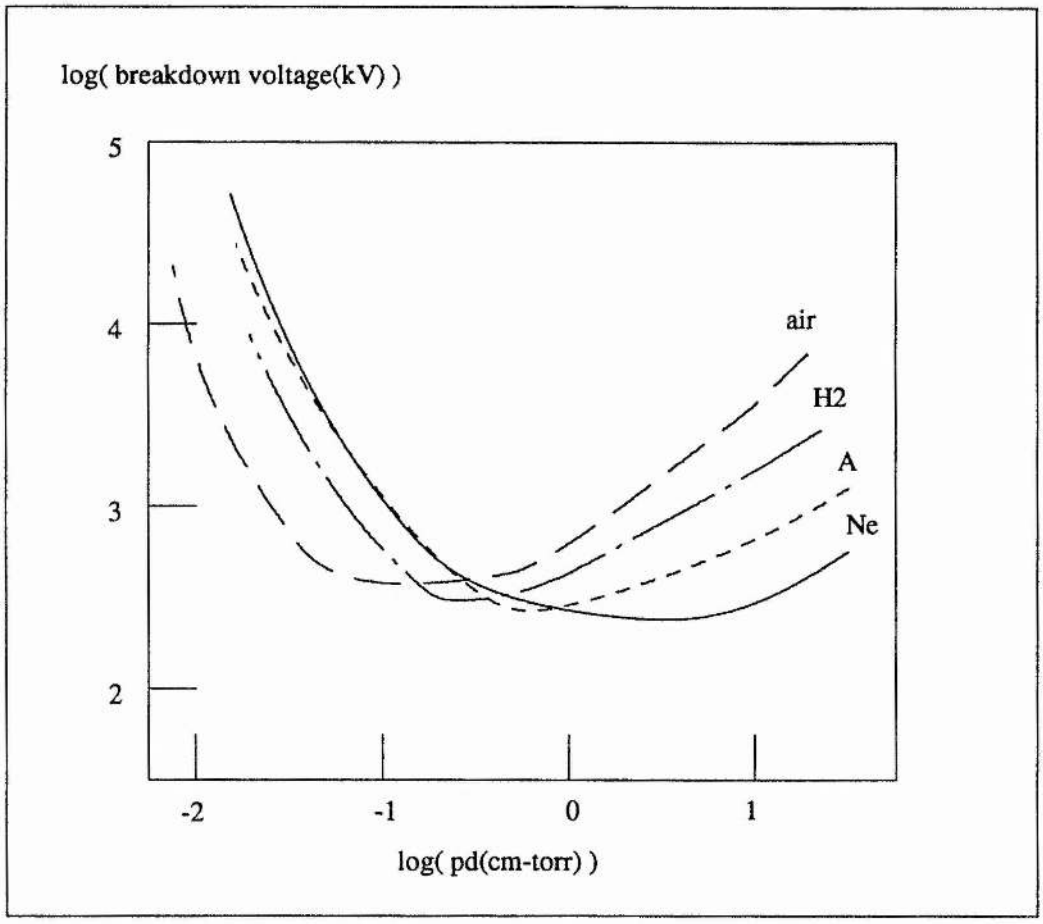

Figure II.2.1.2: The Paschen Curve for Several Gases

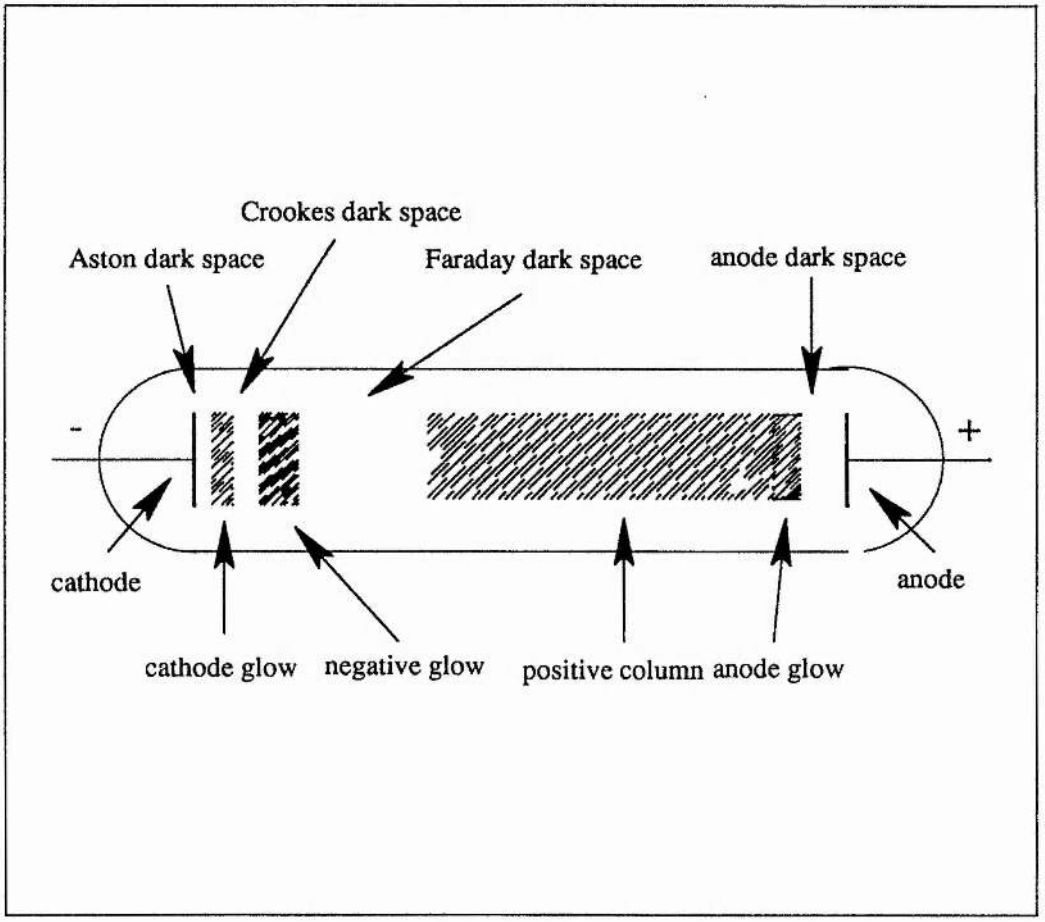

Figure II.2.2.1: The Regions of a Glow Discharge

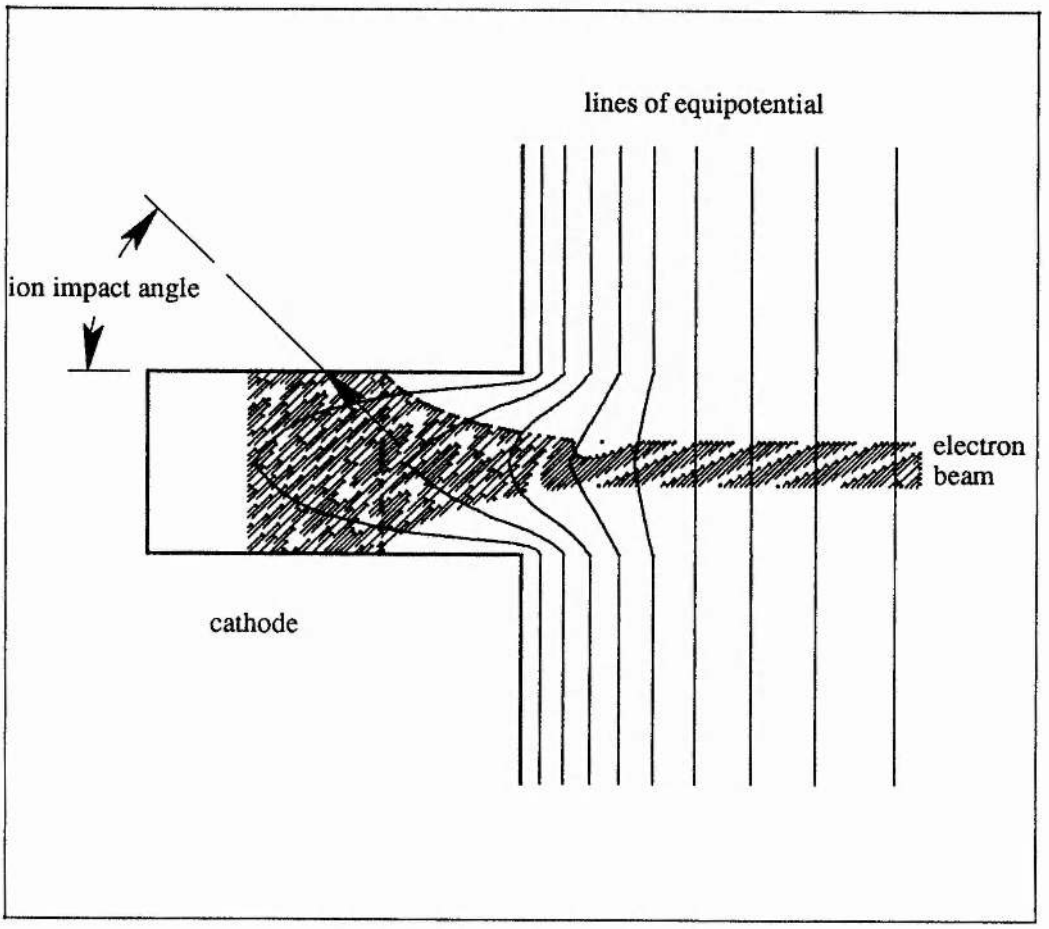

Figure II.2.4.1: The Formation of an Electron Beam in a Slotted Cathode

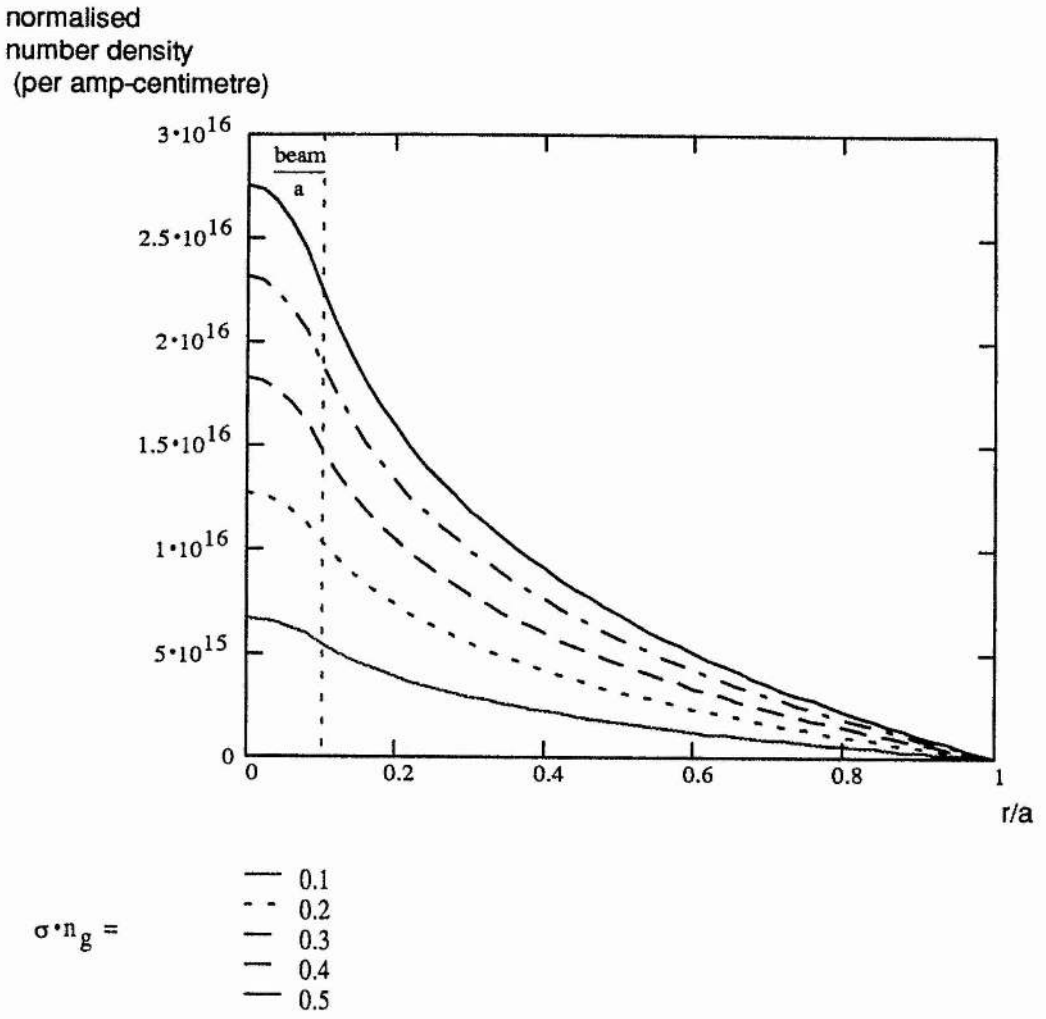

Figure II.2.4.2: The Plasma Density Profile Produced by an Electron Beam in a Low Pressure Gas

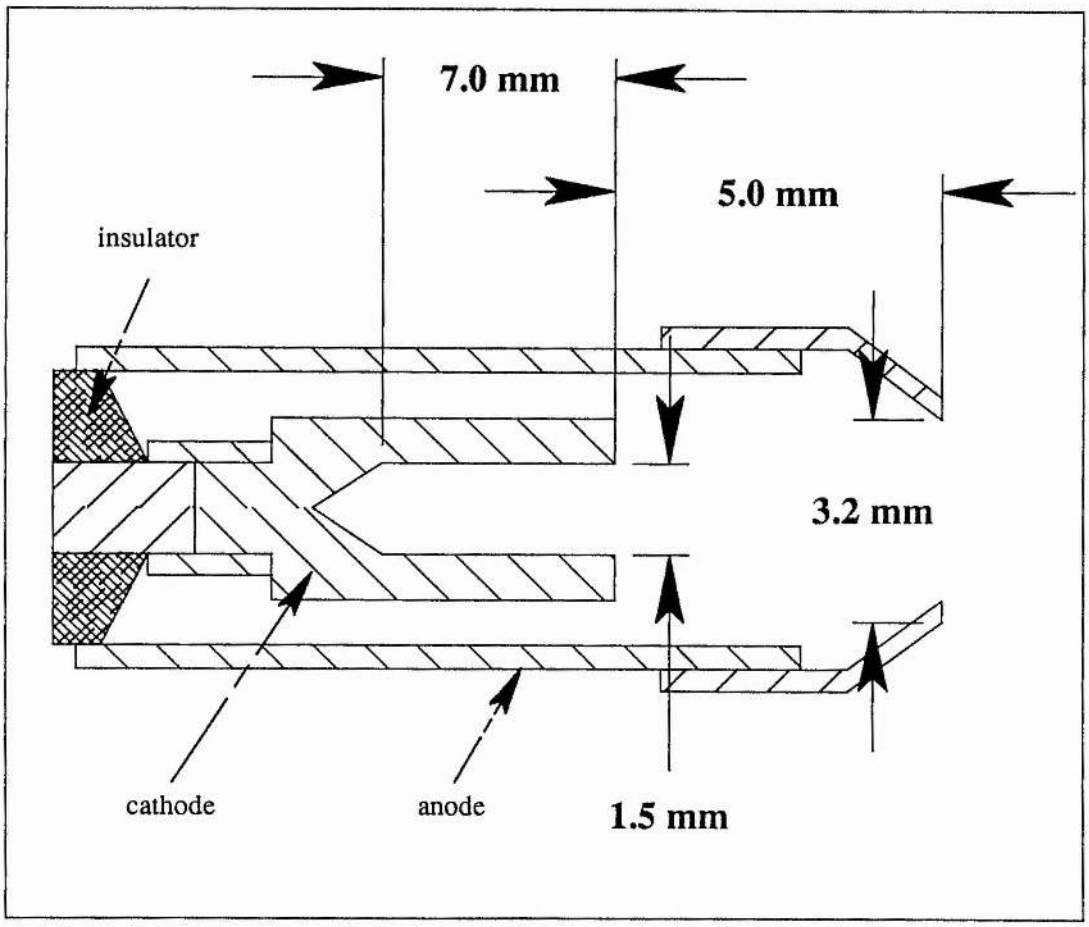

Figure II.2.5.1: Details of the EEV Electron Gun

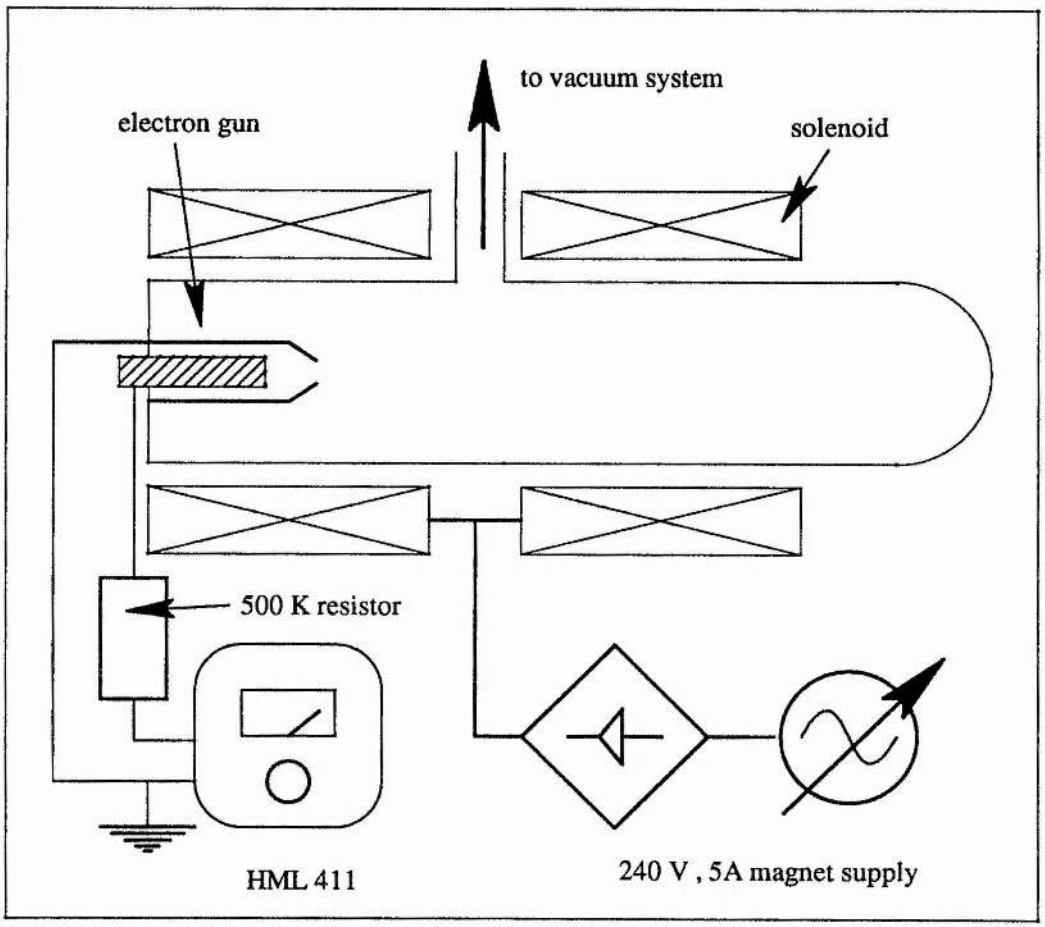

Figure II.2.5.2: Experimental Configuration of the EEV Electron Gun and Focussing Magnets

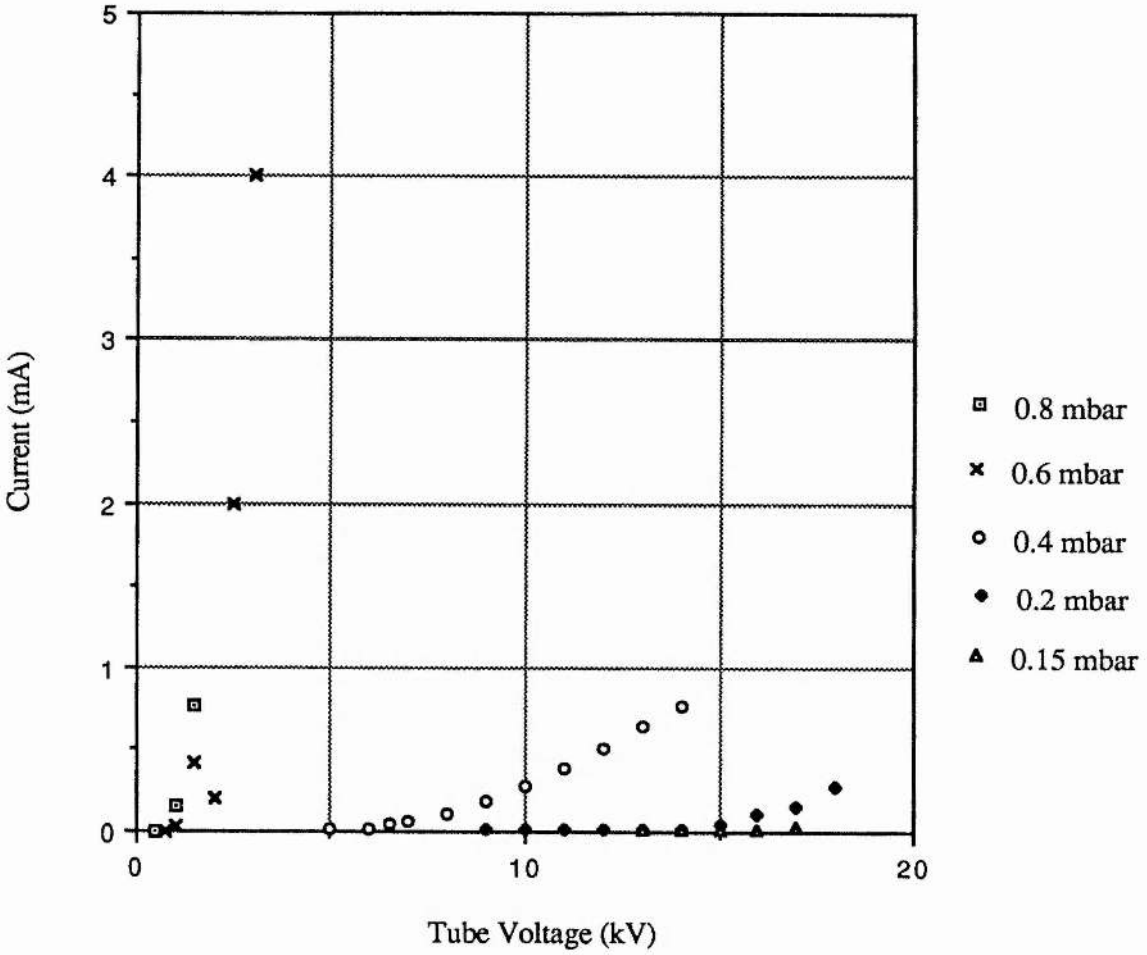

Figure II.2.5.3: The Characteristics of the EEV Electron Gun as a Function of Pressure

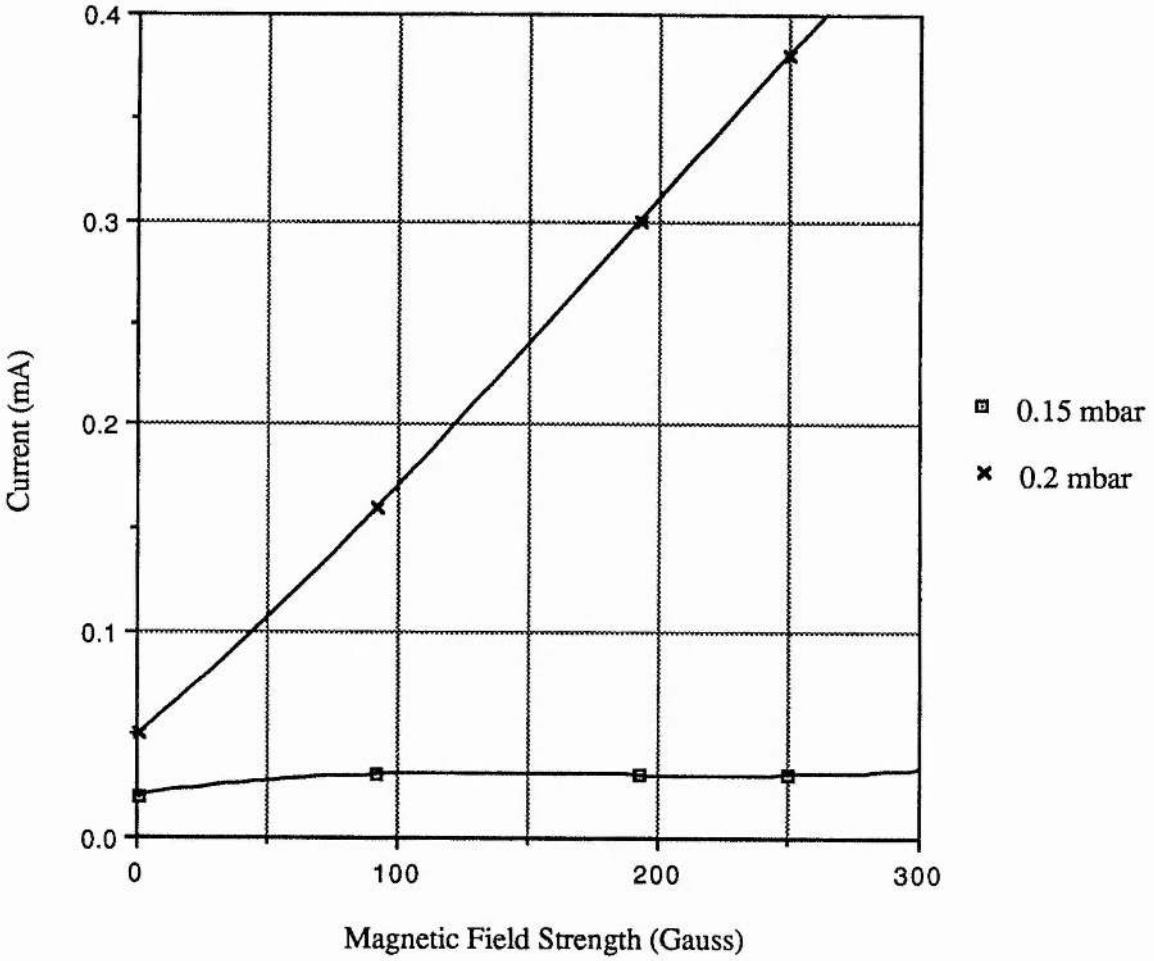

Figure II.2.5.4: The Effect of the Longitudinal Magnetic Field on the Electron Current as a Function of Pressure

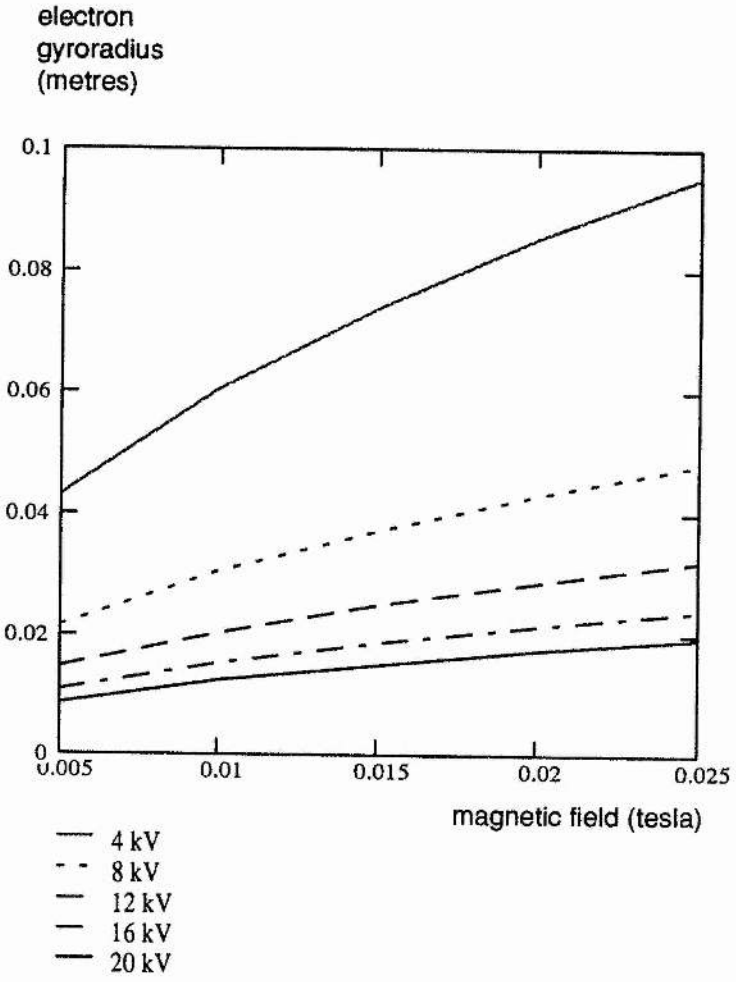

Figure II.2.5.5: The Radius of Gyration for Electrons in a Magnetic Field

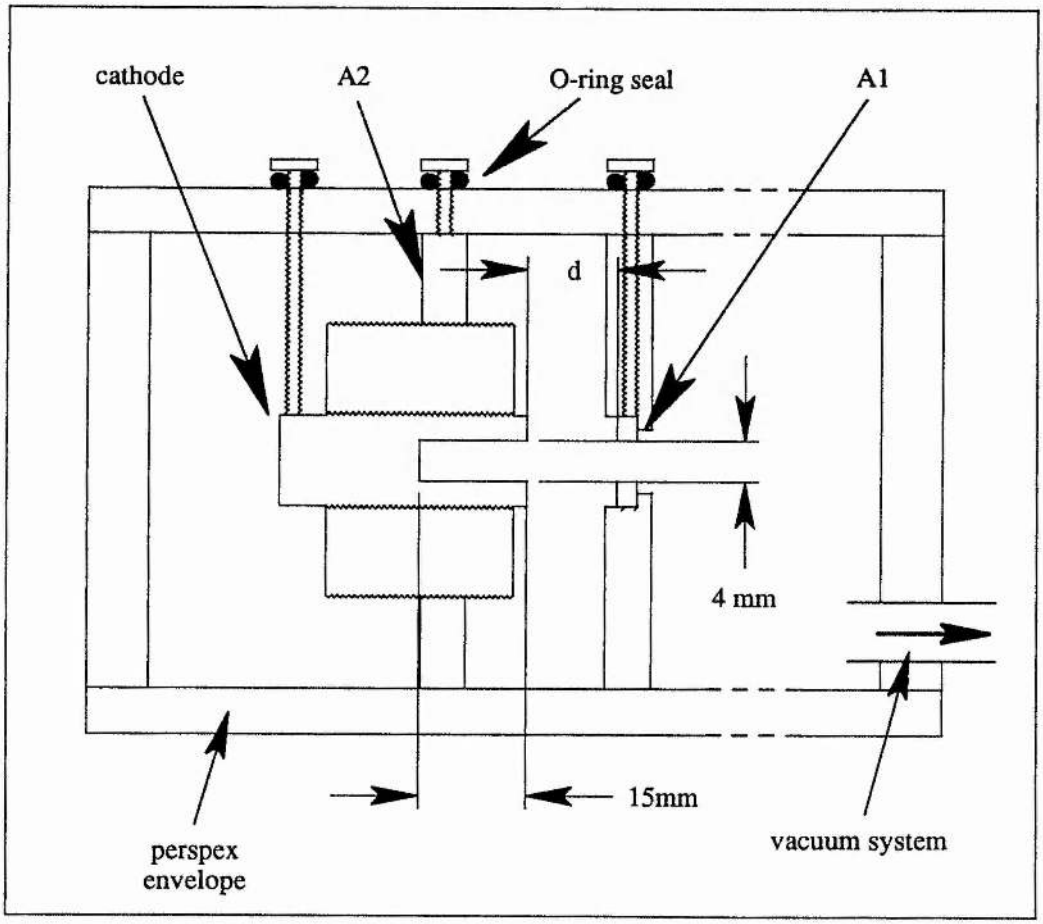

Figure II.2.6.1: The Electron Gun with Variable Electrode Spacing

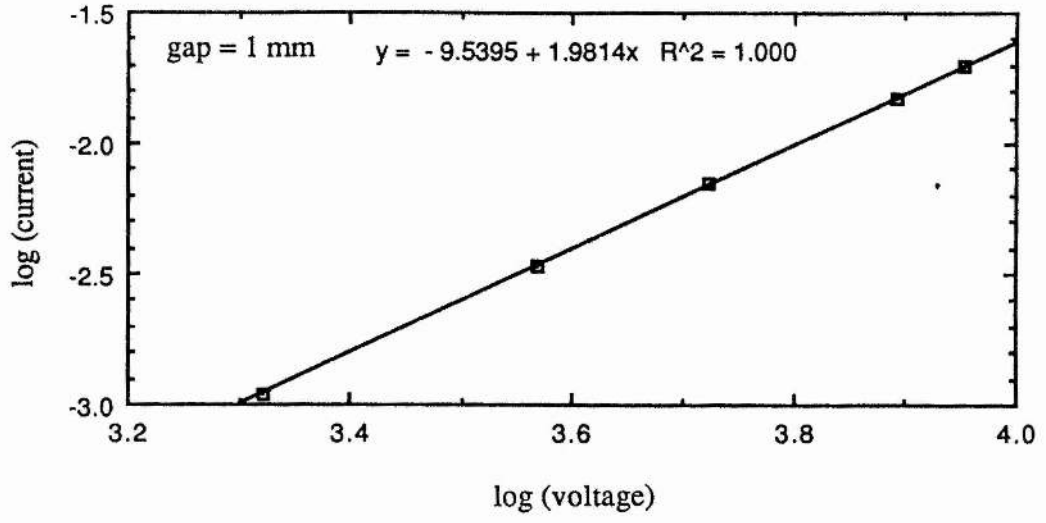

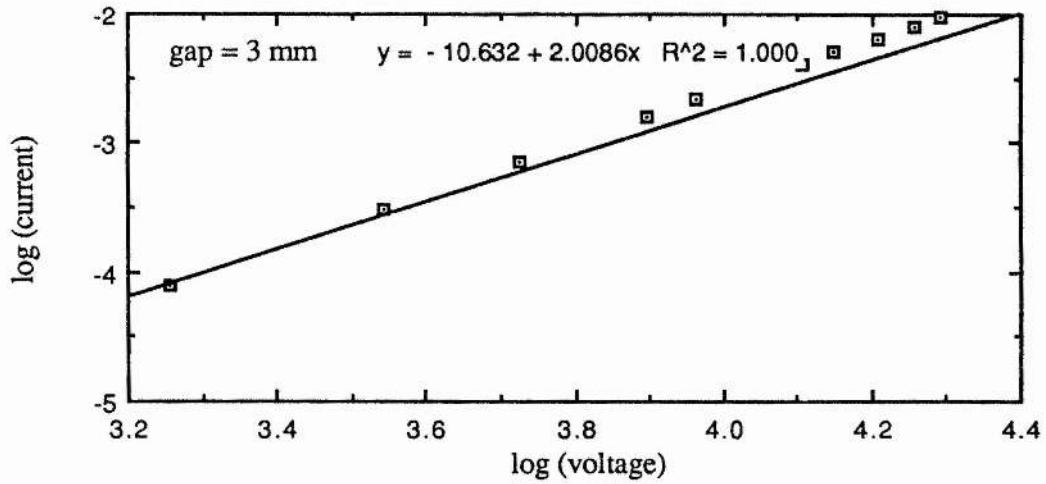

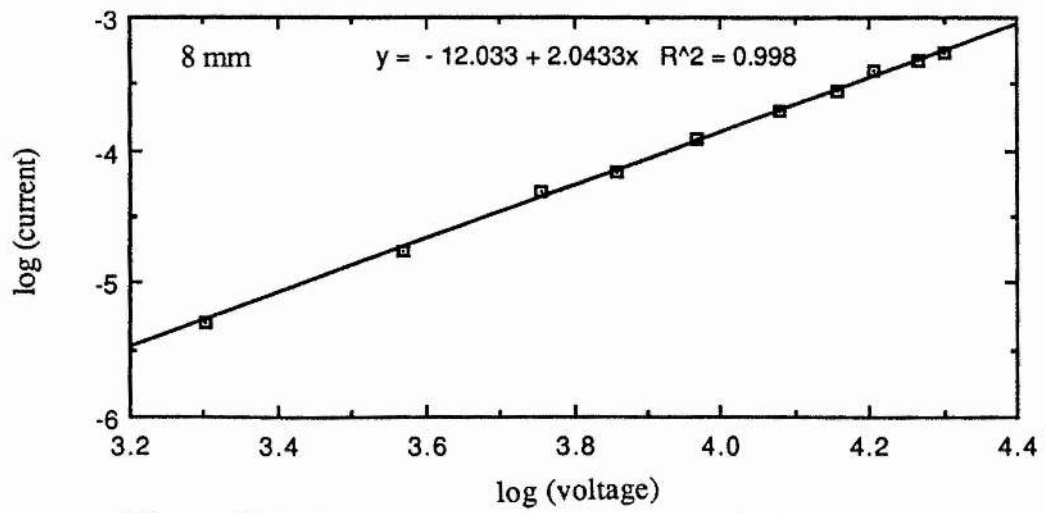

Figure II.2.6.2: The Characteristics of the Electron Gun as a Function of Electrode Spacing

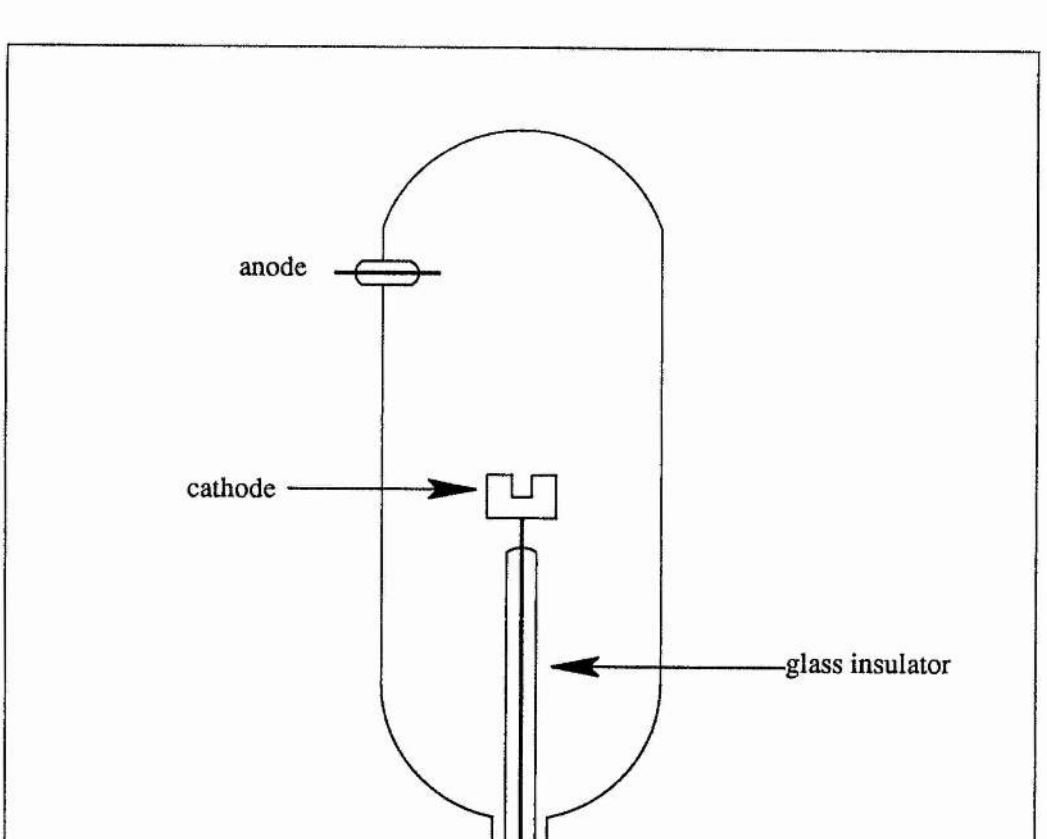

Figure II.2.7.1: Simple High Voltage Electron Gun

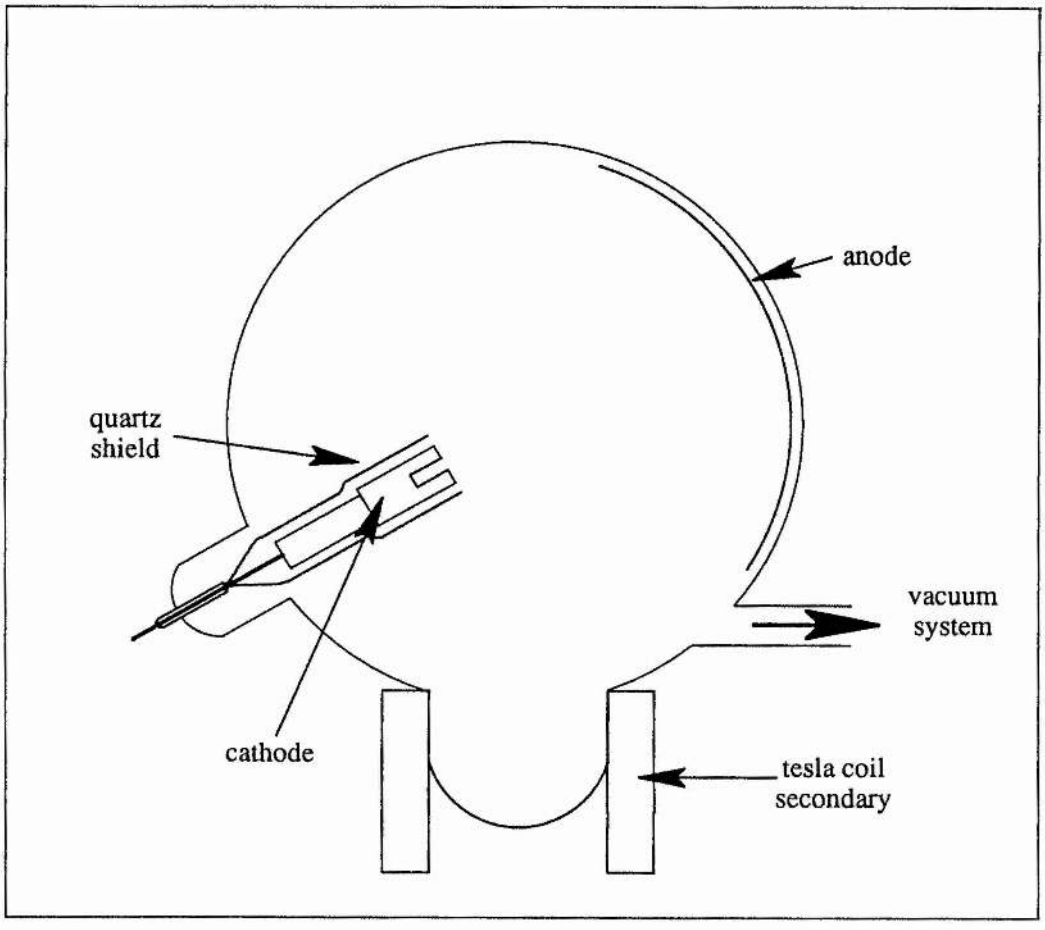

Figure II.2.7.2: The High Voltage Electron Gun Mk II

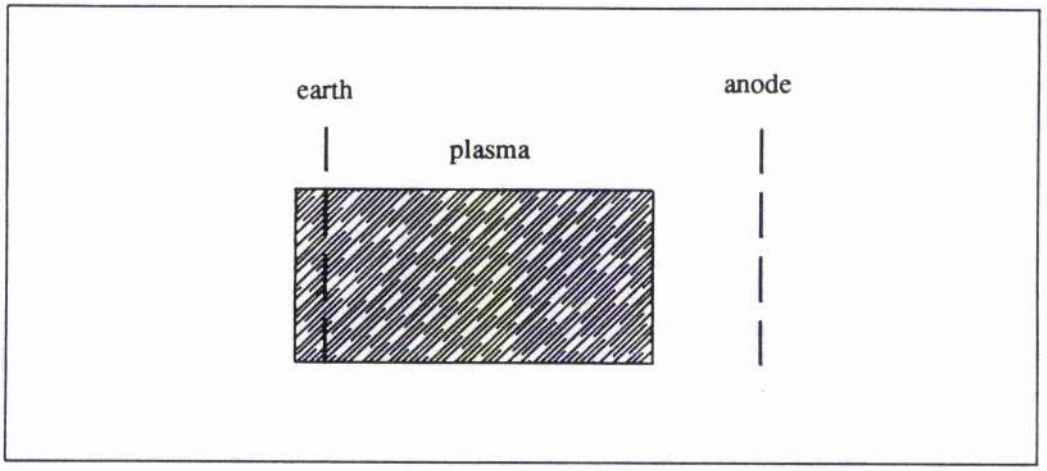

Figure II.3.1.1: Simple Plasma Cathode

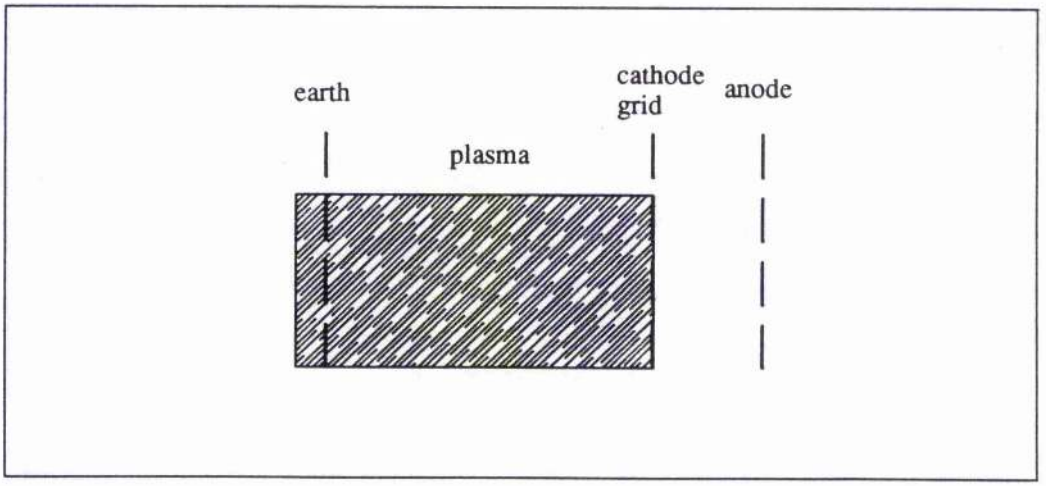

Figure II.3.1.2: Schematic Diagram of Plasma Cathodes

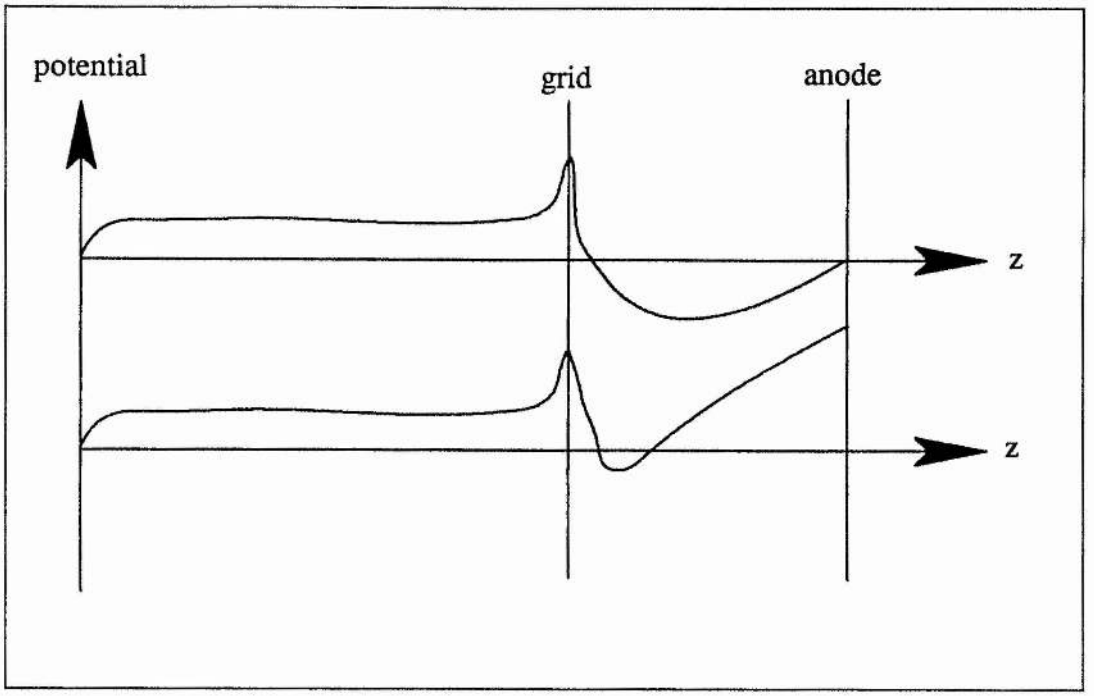

Figure II.3.1.3: The Field Distribution in a Grid-Controlled Plasma Cathode

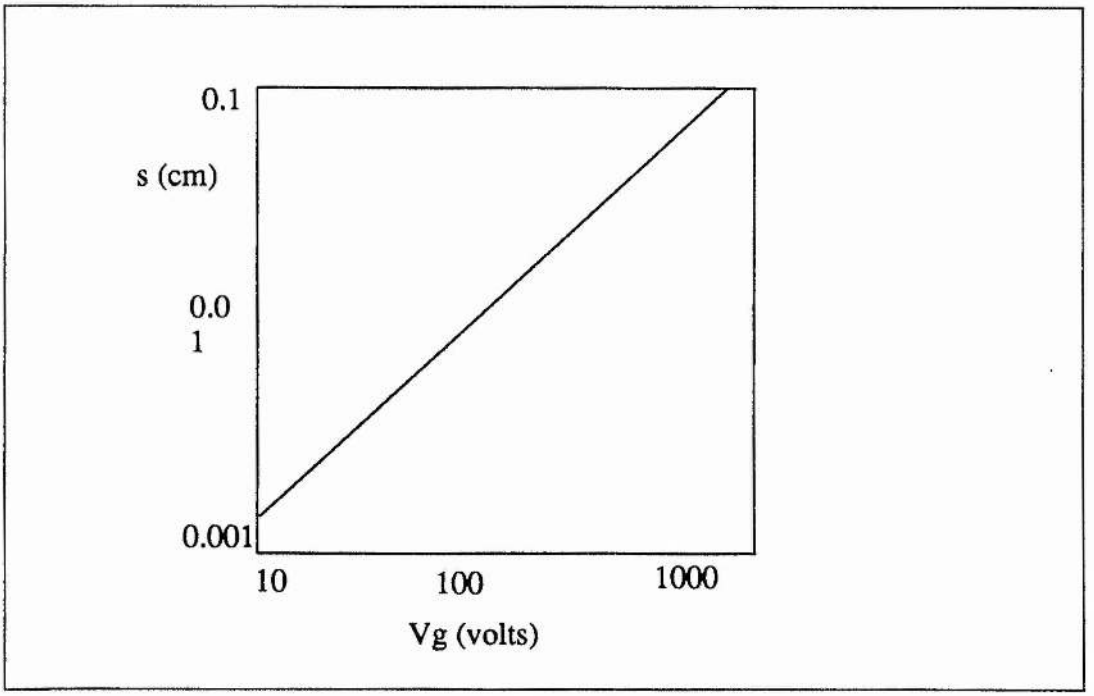

Figure II.3.2.1: The Sheath Thickness as a Function of the Grid Bias Voltage

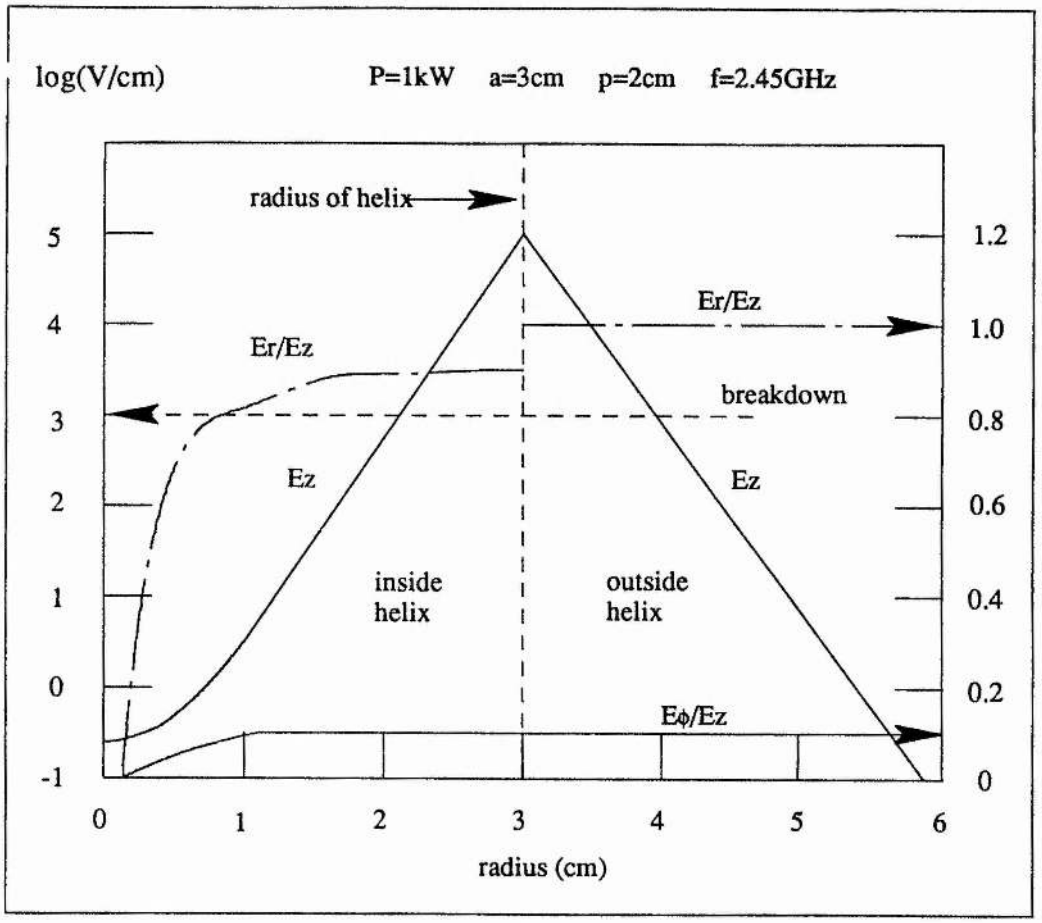

Figure II.3.7.1: The RF Fields Produced by a Microwave Helix

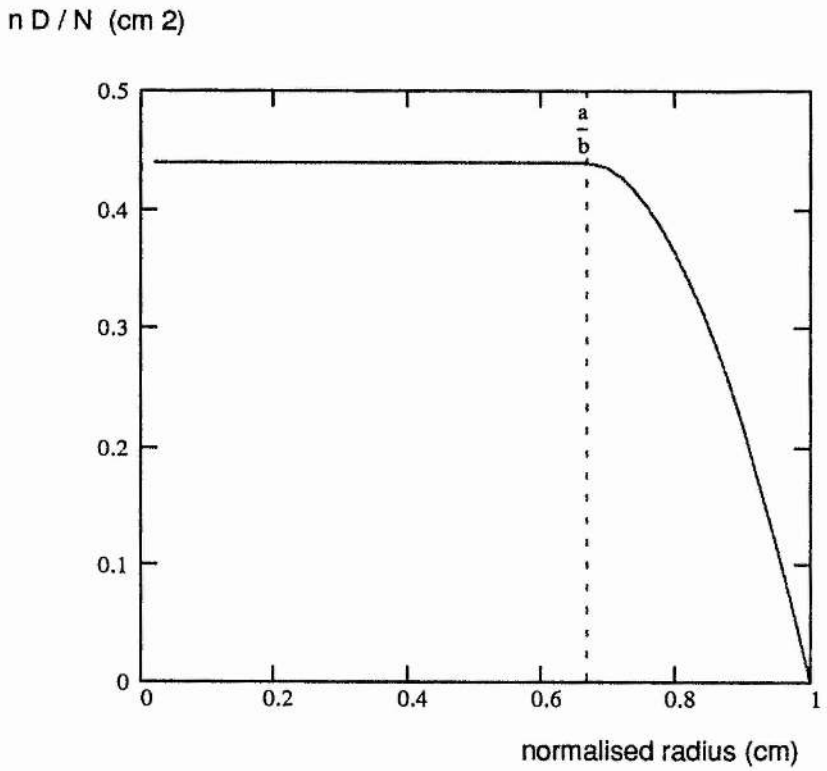

Figure II.3.7.2: The Plasma Density Produced by a Microwave Helix with a Uniform Ionisation Rate

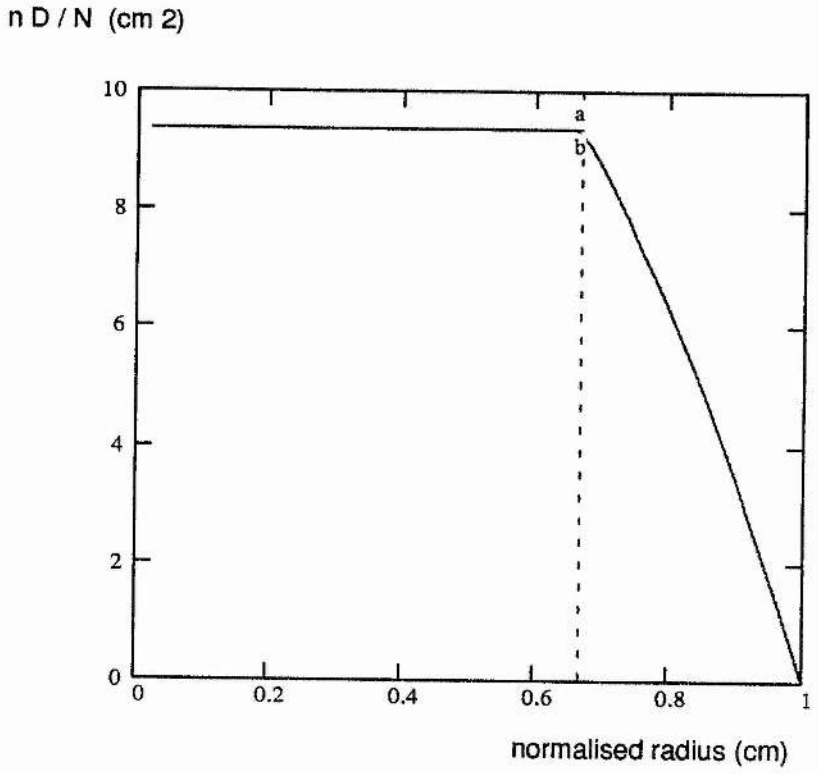

Figure II.3.7.3: The Plasma Density Produced by a Microwave Helix with a Linear Ionisation Rate

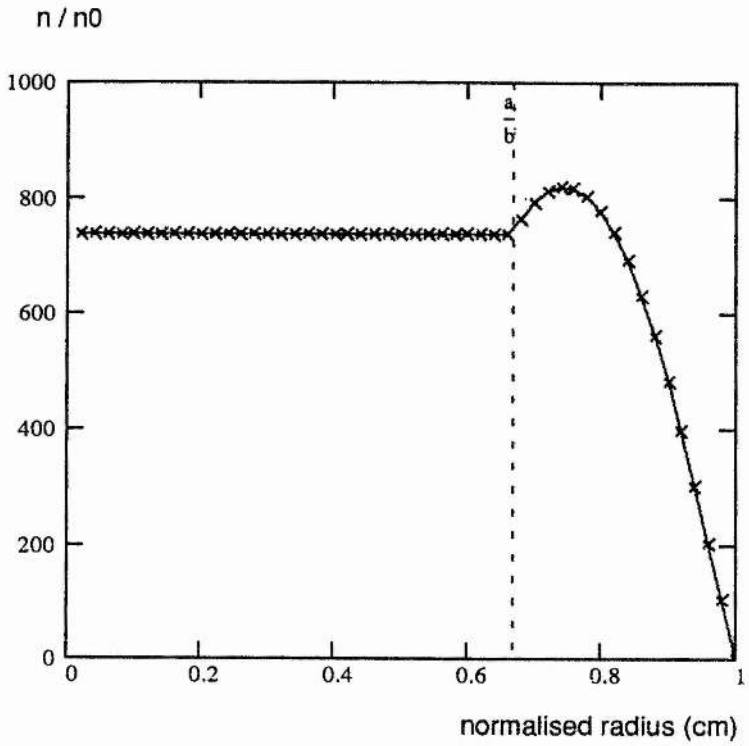

Figure II.3.7.4: The Plasma Density Produced by a Microwave Helix with a Linear Ionisation Rate which is a Function of the Local Plasma Density

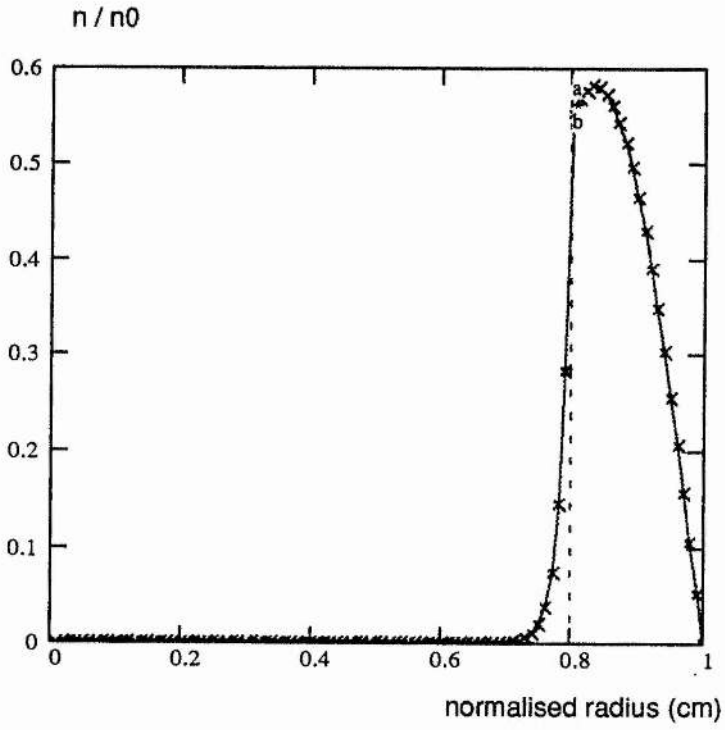

Figure II.3.7.5: The Plasma Density Produced by a Microwave Helix with Recombination

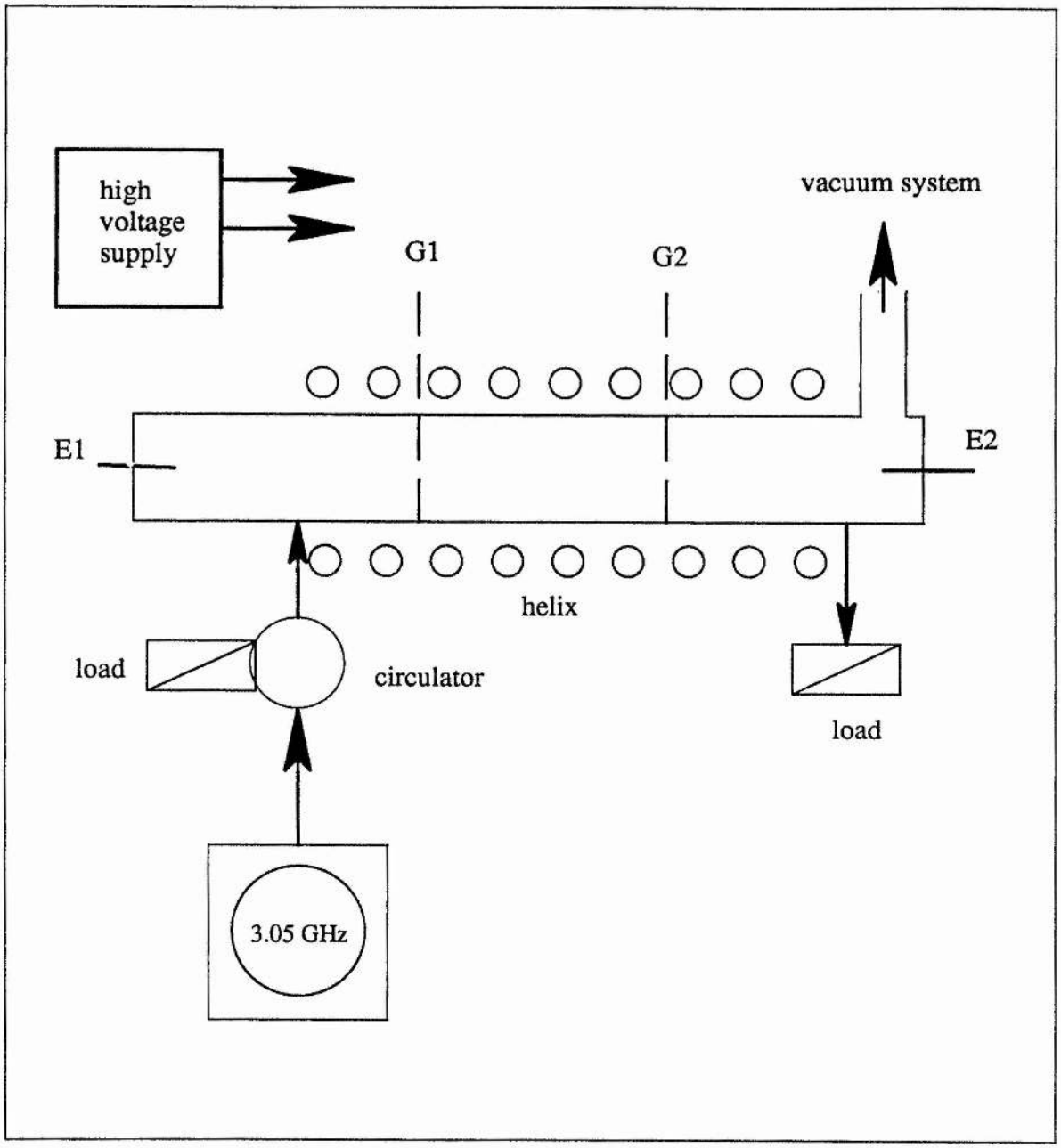

Figure II.3.8.1: Experimental Configuration for Testing the RF Plasma Cathode

Figure II.3.8.2: Discharge characteristics at 2.5 mbar (Hydrogen)

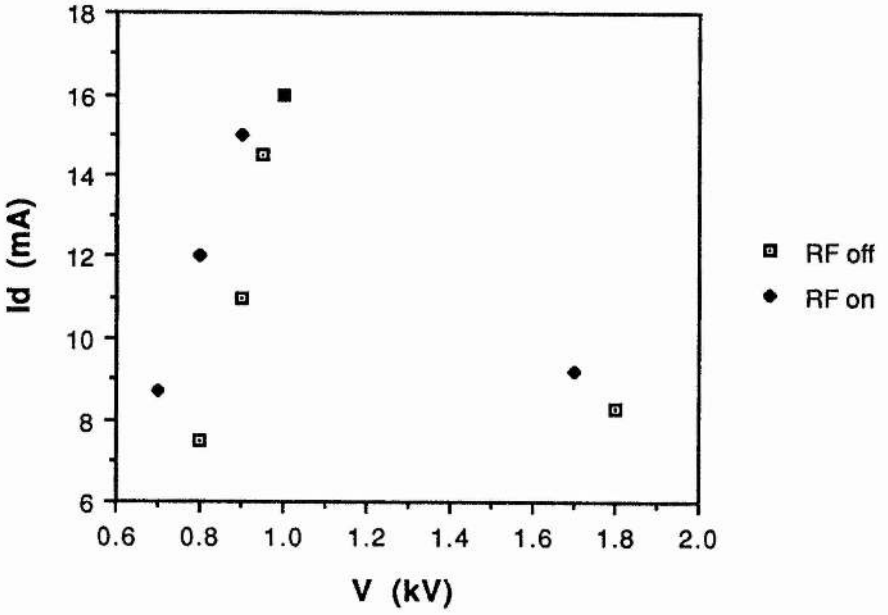

Figure II.3.8.3: Discharge characteristics at 0.45 mbar (Hydrogen)

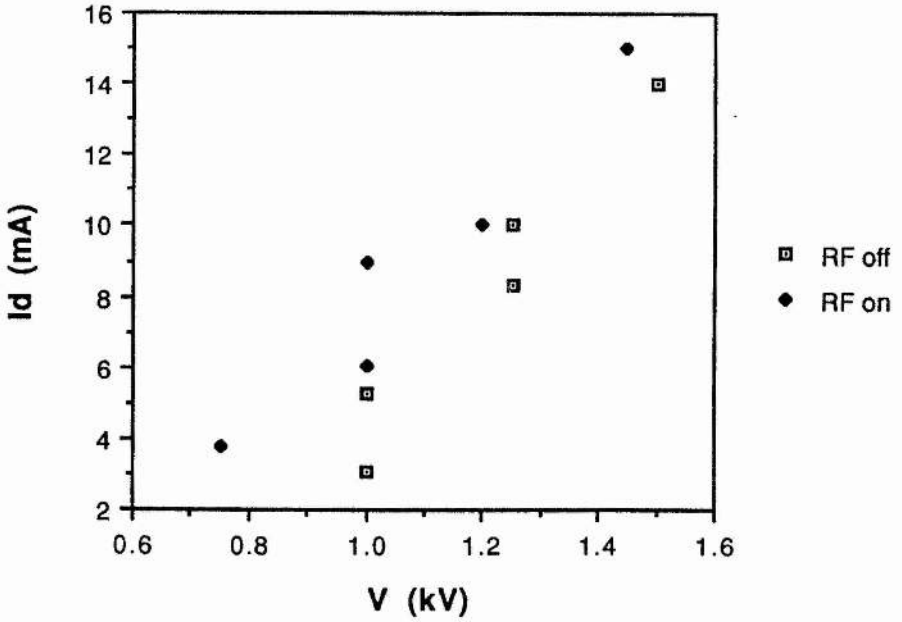

Figure II.3.8.4: Discharge characteristics at 0.23 mbar (Hydrogen)

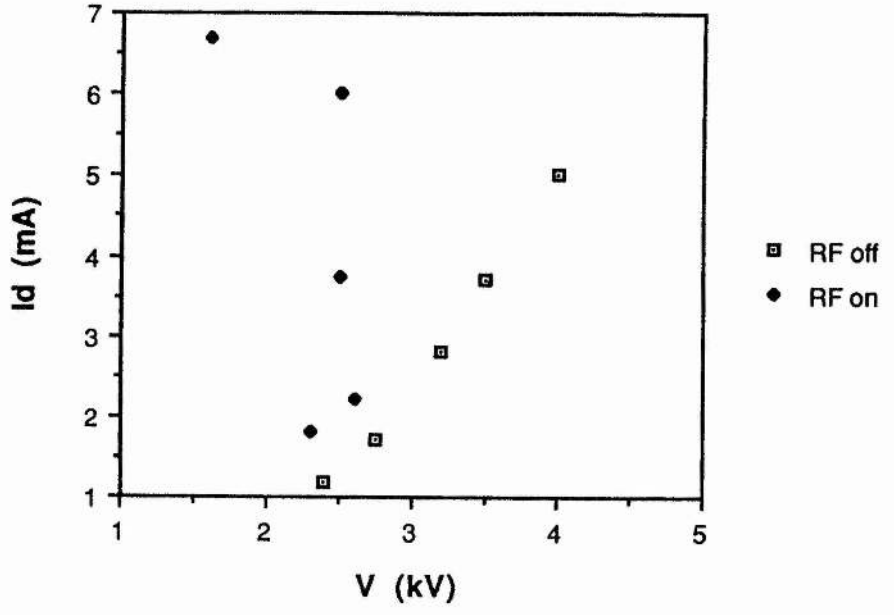

Figure II.3.8.5: Discharge characteristics at 0.115 mbar (Hydrogen)

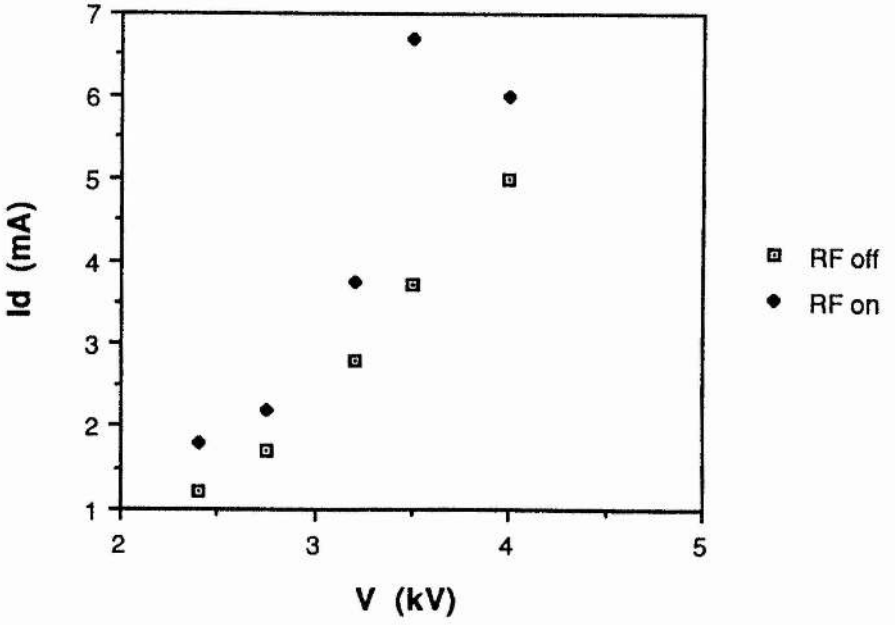

Figure II.3.8.6: Effect of RF discharge at 2.5 mbar (Hydrogen)

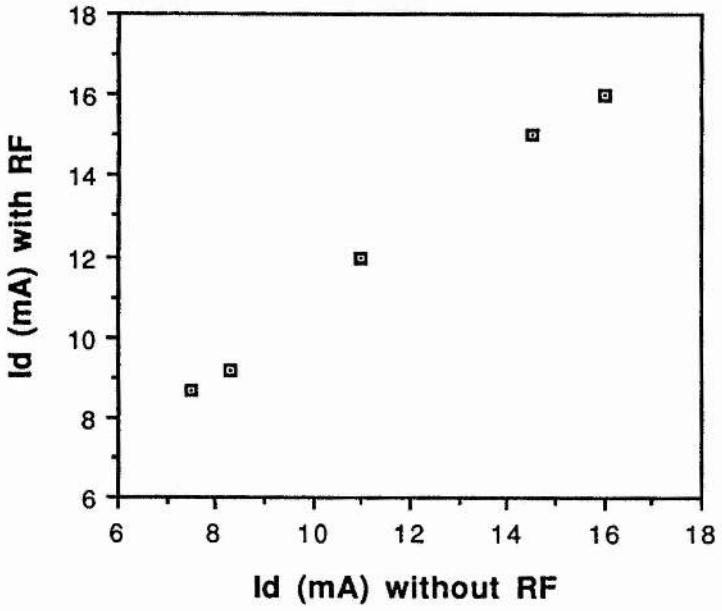

Figure II.3.8.7: Effect of RF discharge at 0.45 mbar (Hydrogen)

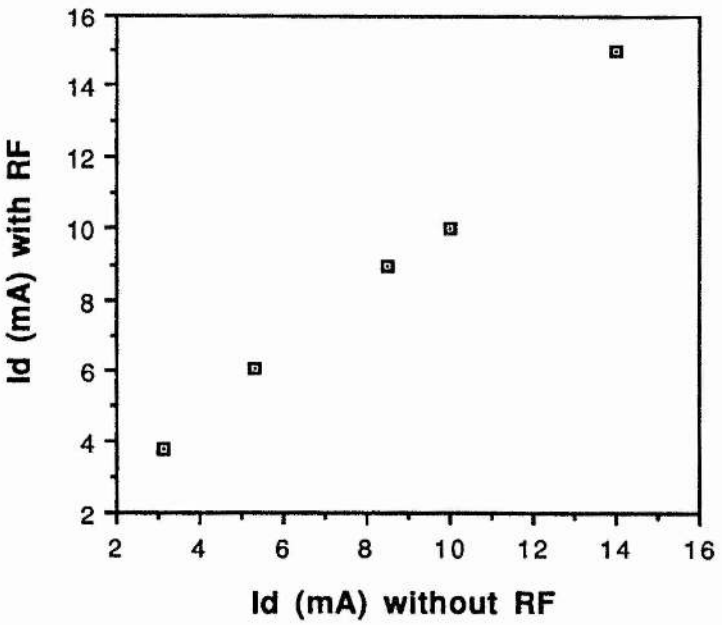

Figure II.3.8.8: Effect of RF discharge at 0.23 mbar (Hydrogen)

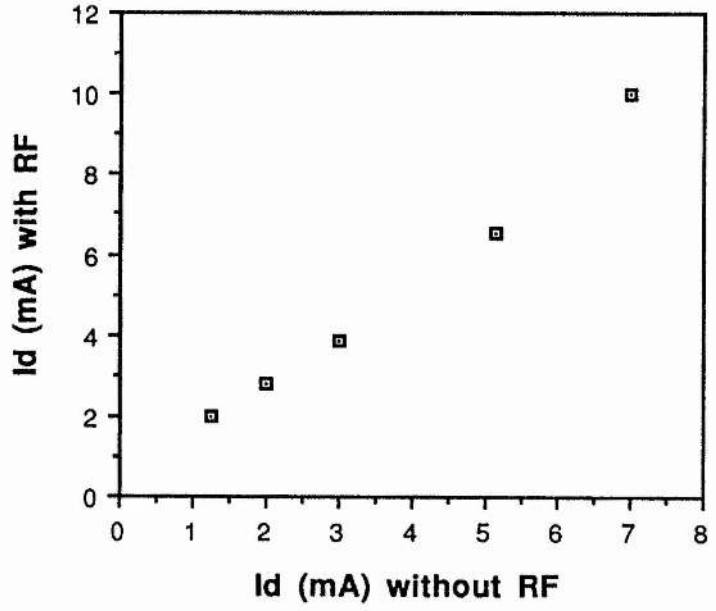

Figure II.3.8.9: Effect of RF discharge at 0.115 mbar (Hydrogen)

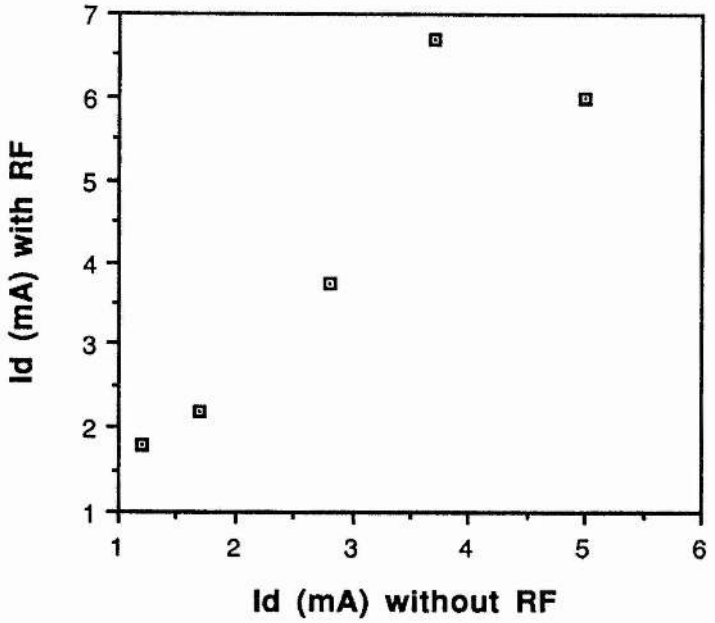

Figure II.3.8.10: Effect of RF discharge in Hydrogen

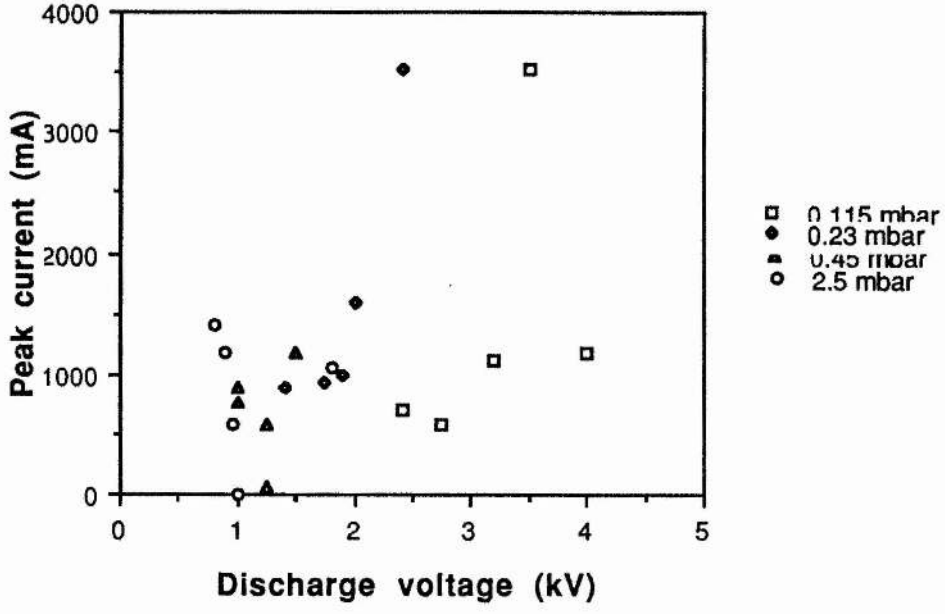

Figure II.3.8.11: Effect of RF discharge in Hydrogen

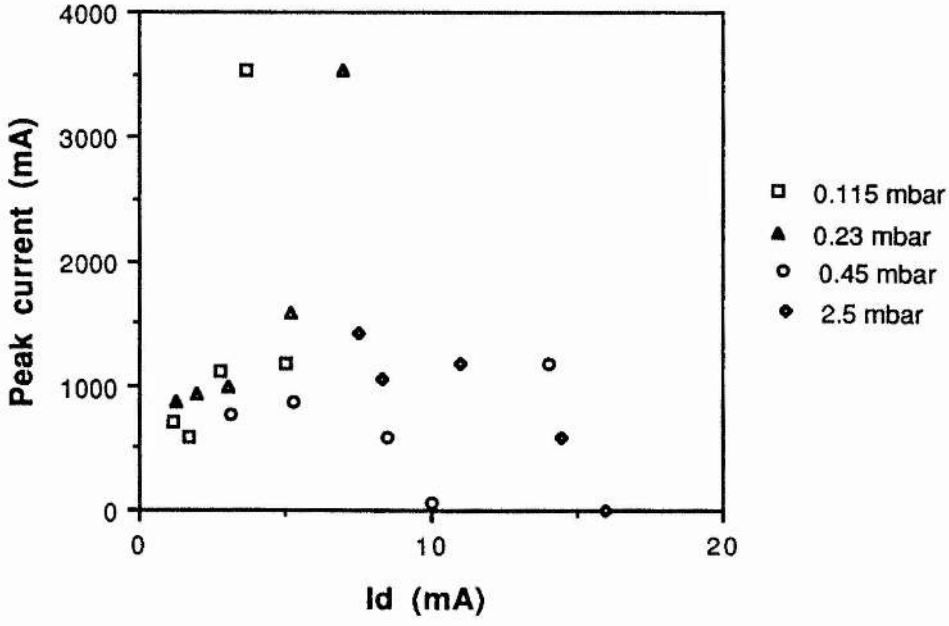

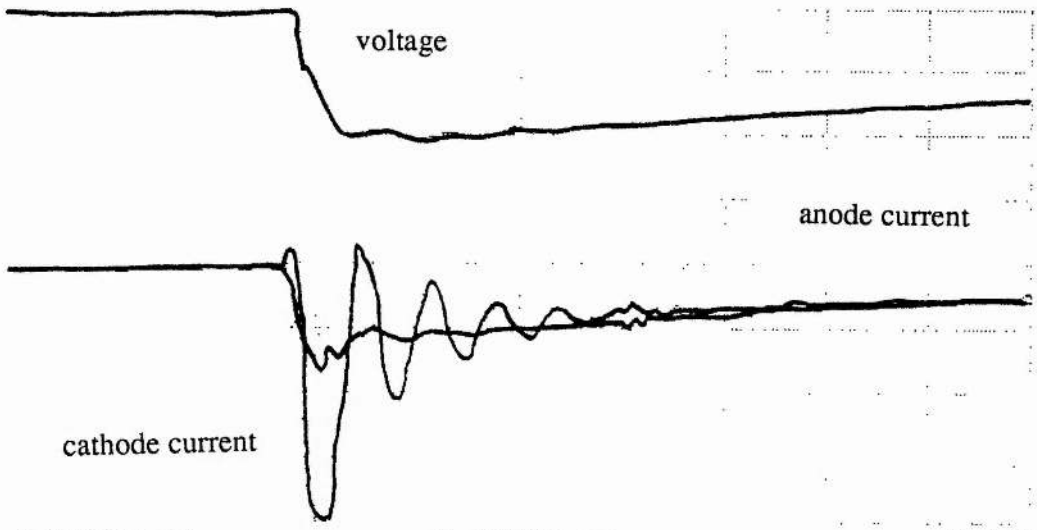

-2.83198 us 2.16802 us 7.16802 us

Channel 1 =	10.00 mVolts/div	Offset =	0.000 Volts
Channel 3 =	10.00 mVolts/div	Offset =	0.000 Volts
Channel 4 =	1.000 Volts/div	Offset =	-2.000 Volts
Timebase =	1.00 us/div	Delay =	2.16802 us

Voltage (top trace) 1 kV/div

Anode Current 100 mA/div

Cathode Current 100 mA/div

Figure II.3.8.12

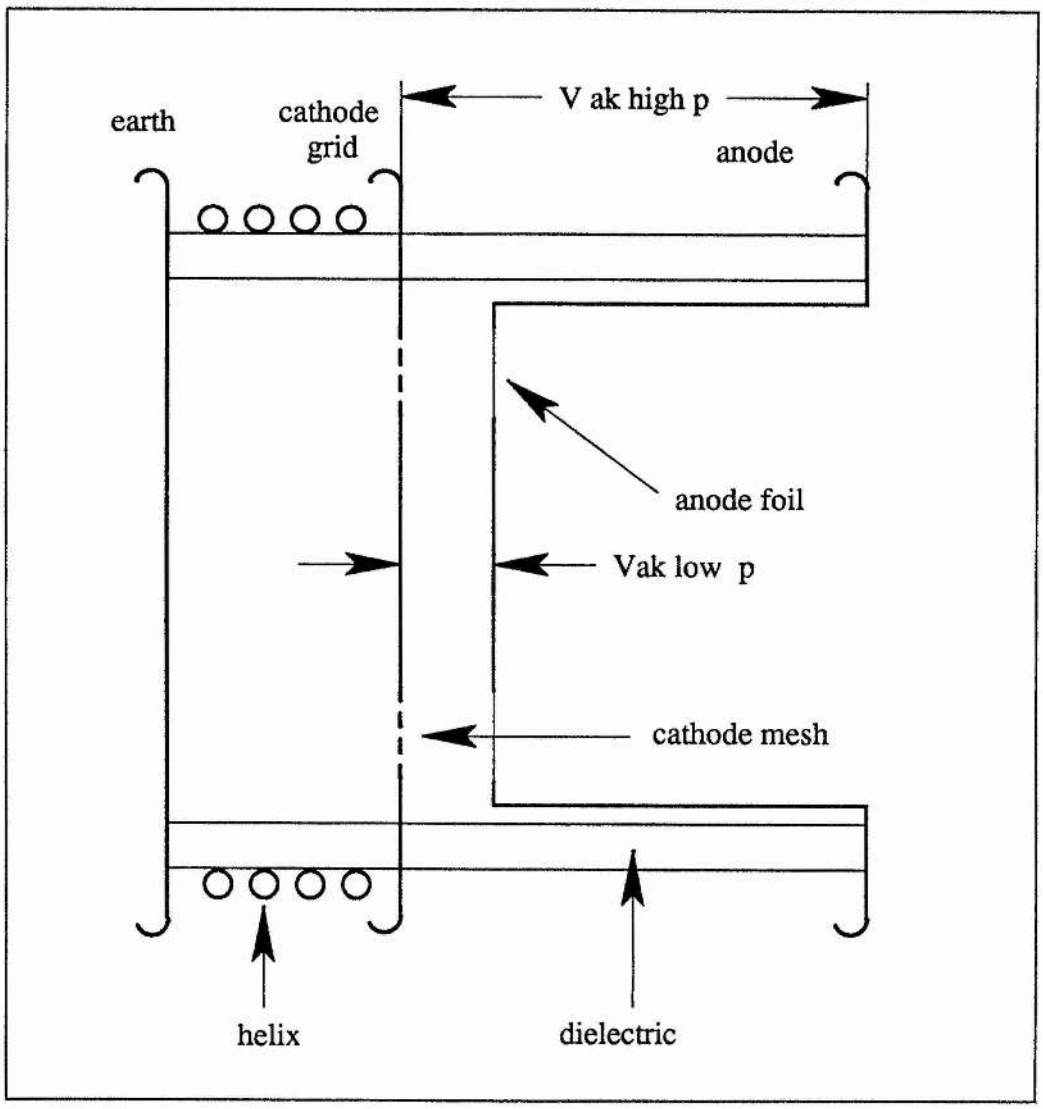

Figure II.3.11.1: Electron Gun with Plasma Cathode

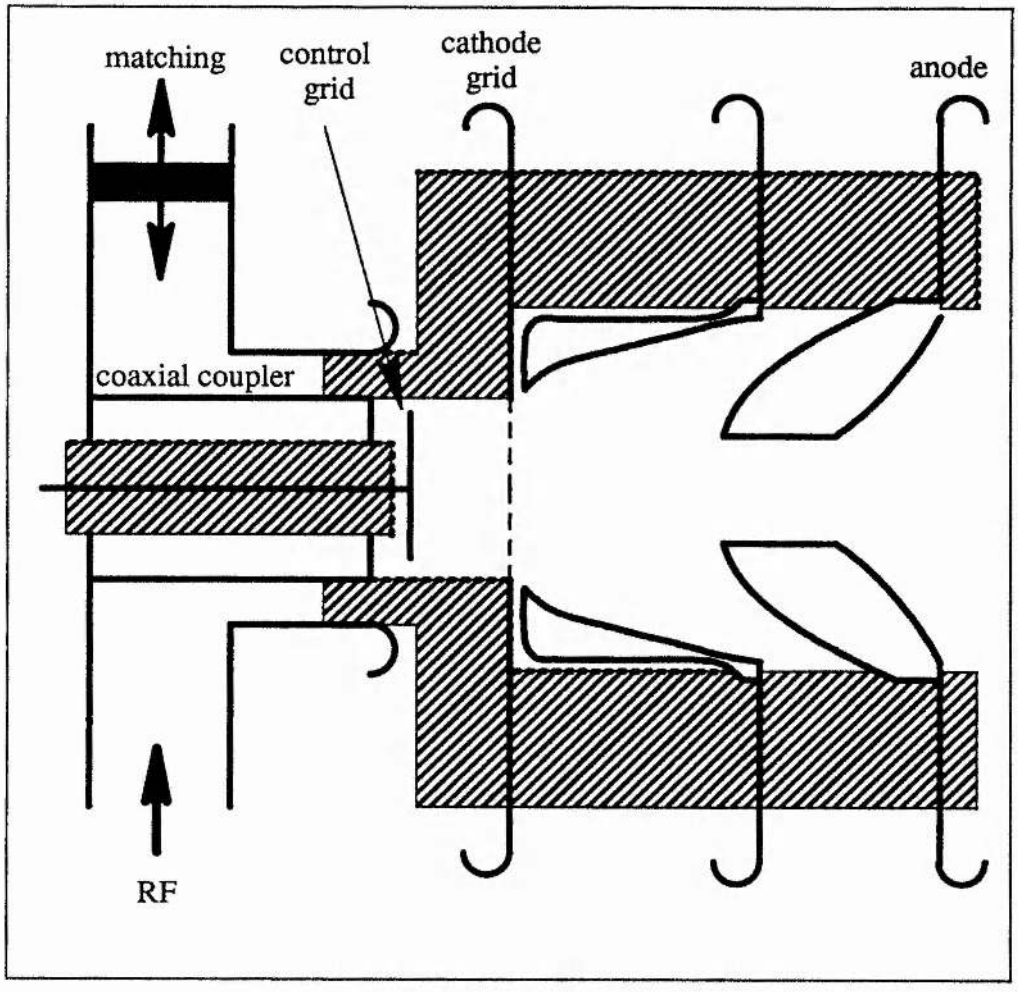

Figure II.3.12.1: Electron Gun with a Pierce Cathode

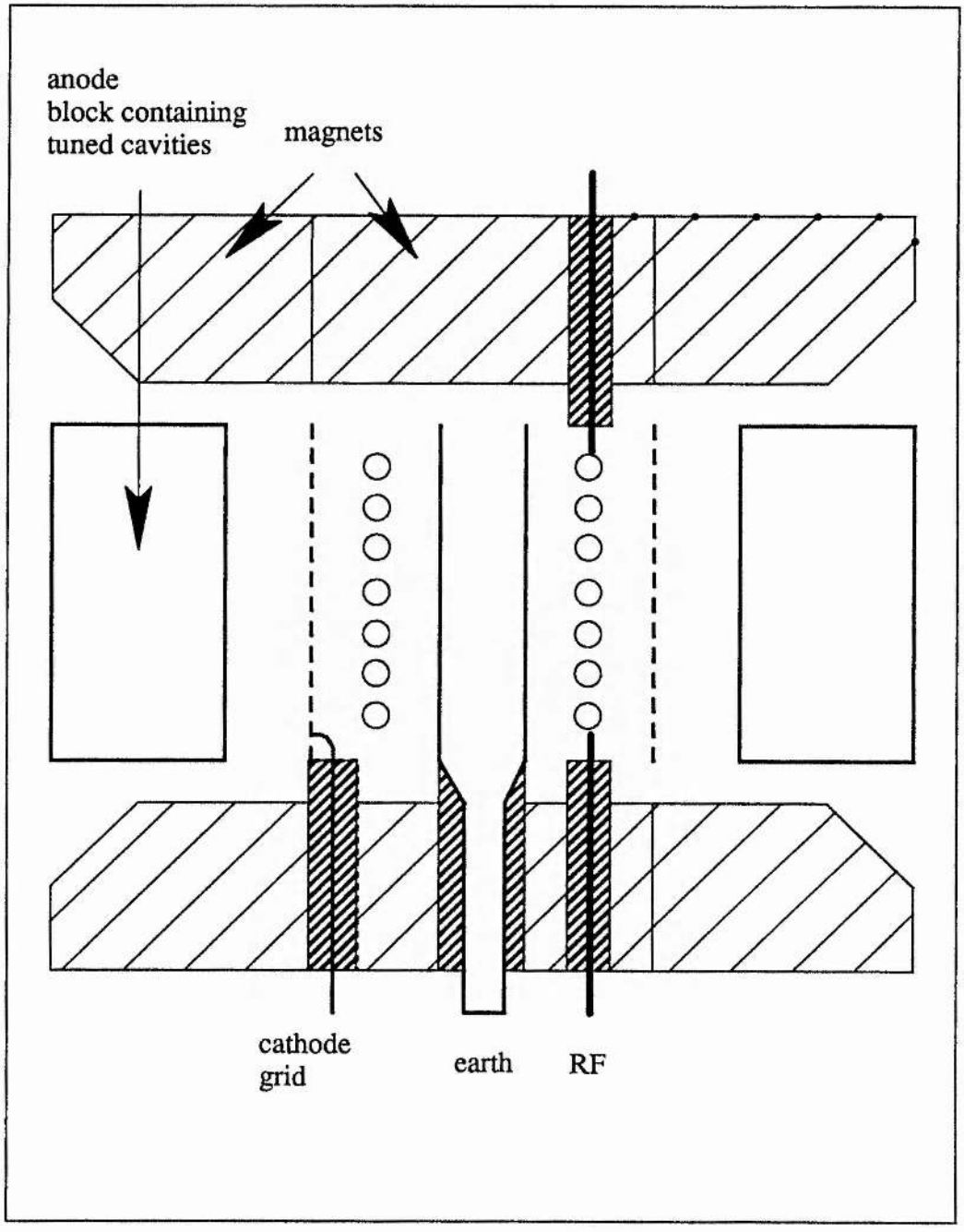

Figure II.3.13.1: Magnetron Incorporating an RF Plasma Cathode

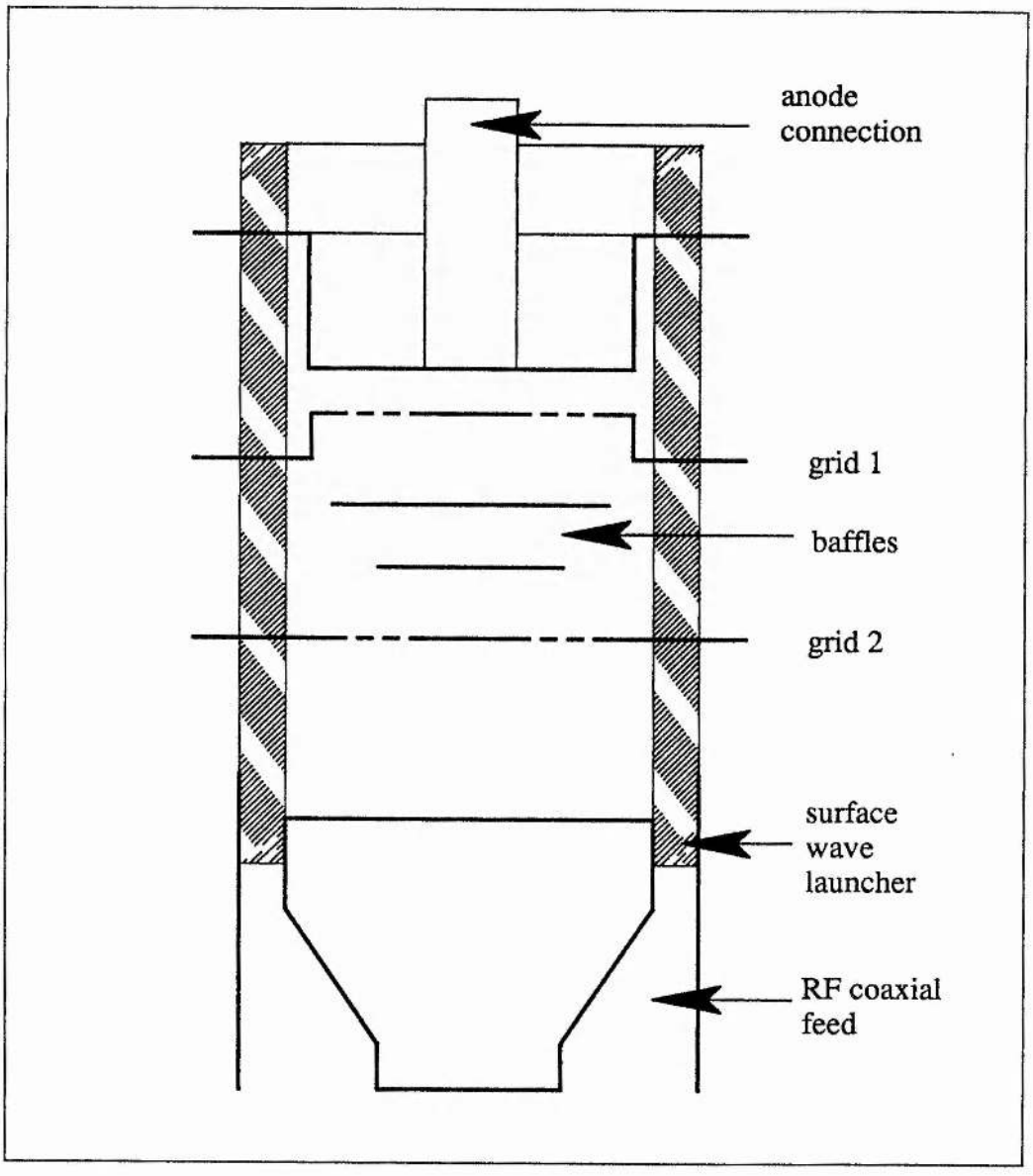

Figure II.3.14.1: Thyratron with Surface Wave RF Plasma Cathode

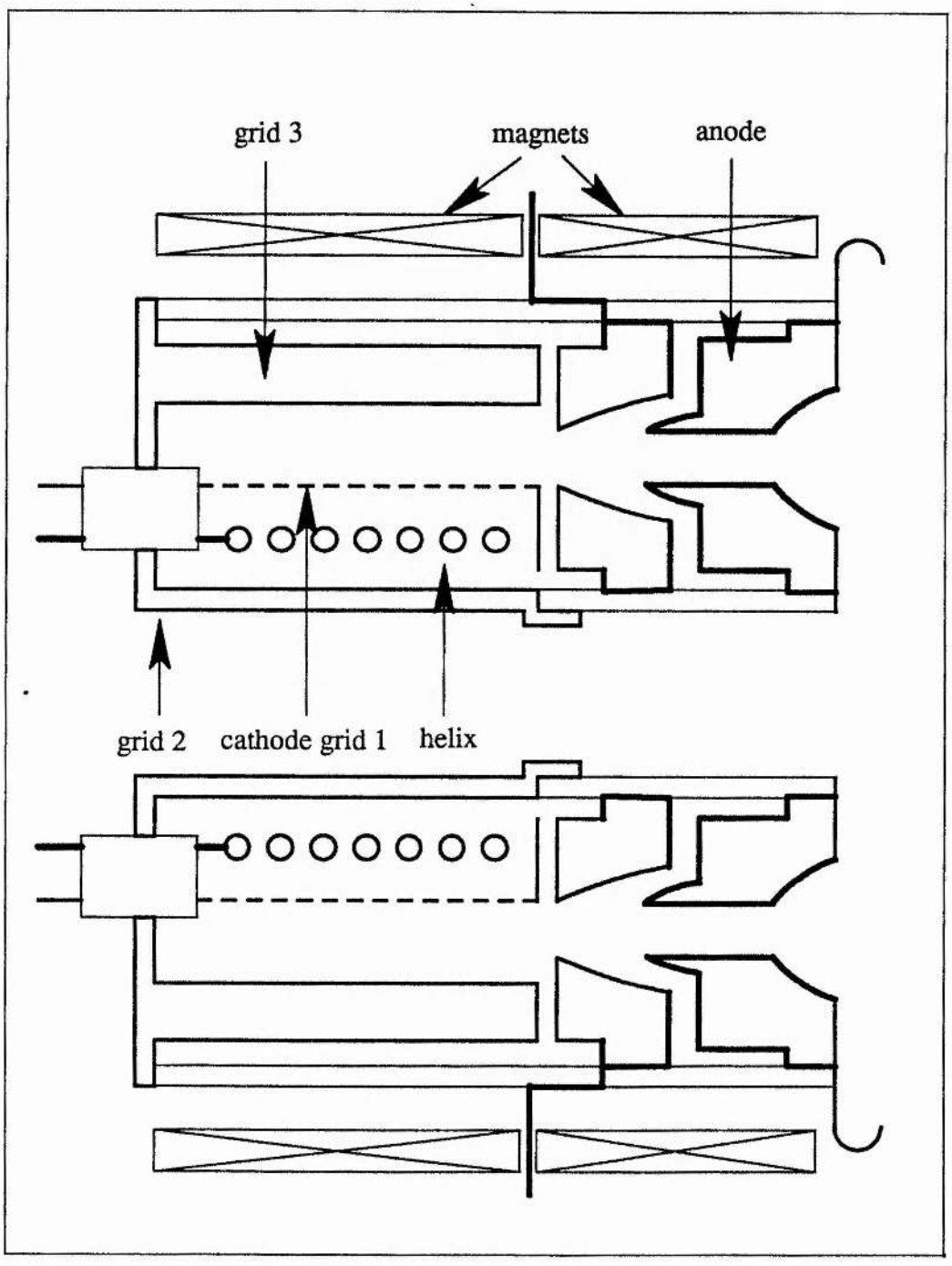

Figure II.3.15.1: High Power Electron Gun with RF Plasma Cathode

CHAPTER III

PLASMA WAVEGUIDES

III.1 Introduction

The investigation of the propagation of electromagnetic waves in ionised media has received attention since Heaveside postulated the existence of an ionised layer in the atmosphere in 1902. Much of the early work on plasma waves and oscillations in the ionosphere was undertaken[1] by Langmuir, Tonks, Appleton and Hartree around 1930. Over the next two decades the theoretical and experimental investigations were progressed by Vlasov[2], Landau[3] and Alfven[4], among others. When controlled fusion research began in earnest in 1952, the rate of publication in the field of plasma physics increased rapidly and the number of plasma "waves" rose with every new theory. In 1963, Allis, Buchsbaum and Bers published a unifying monograph[5] which brought together all of the previous work and rationalised the various theories using rigourous derivations. Simultaneously, Trivelpiece and Gould were developing the theory of slow wave propagation in plasma waveguides[6] using approximate solutions of Maxwell's equations.

Plasma research has continued, primarily in the cosmological, controlled fusion and themonuclear fields (high pressure, high density plasmas) and for switching applications (thyratrons, etc). The work of Trivelpiece *et al* has led to the investigation of plasma-based high power microwave generators[7]. This is the inspiration for, and the basis of, the research presented in this chapter.

The solution of Maxwell's wave equations in a conducting medium has become a standard textbook problem. A familiar result is the existence of a cut-off frequency below which propagation cannot occur. This cut-off frequency corresponds to a natural resonance of the charged particles in the medium and is called the plasma frequency. When, however, the conducting medium is anisotropic or bounded, the propagation properties change and propagation below the plasma frequency is possible.

Complete solutions of Maxwell's equations are extremely difficult in all but the simplest cases. Throughout our treatment, we consider only linear responses of the plasma and sinusoidal oscillations of the fields. In section III.2 we follow the method of Allis *et al* in the development of a general formulation of Maxwell's equations in a plasma with uniformity in one dimension (the **z** direction). The electric and magnetic field equations are, in general, coupled, and must be solved simultaneously. We shall consider the conditions in which the field equations decouple into independent equations which are solvable in term of known functions.

The conditions for propagation below the cut-off frequencies of a plasma-loaded waveguide are of particular interest. Such waves generally have phase velocities less than the velocity of light, that is, they are slow waves. In section III.3 we develop an approximate solution for the plasma-waveguide system by assuming *a priori* the slow wave nature of the solutions. This enables us to write down analytic forms for the dispersion relation, field equations and power flow and obtain a physical insight into the behaviour of the plasma loaded waveguide.

A study of wave propagation in plasma loaded waveguides is of interest in two application areas of this thesis. Firstly, as a method of plasma generation in relation, for example, to the RF plasma cathode of section II.3. The main requirement for this application is to maximise the efficiency by maximising the ratio of field strength to power flow. We shall see that this condition is optimised when the wave frequency correpsonds to a plasma resonance. Secondly, in the next chapter we introduce novel

plasma waveguide microwave switches. These devices exploit the propagation characteristics of plasma loaded waveguides and ideally require minimum field strengths for maximum power flow.

III.2 Maxwell's Equations in a Plasma with Uniformity in One Dimension

III.2.1 General Formulation

We begin with Maxwell's equations for the complex vector electric and magnetic fields:

$$\nabla \mathbf{x} \mathbf{E} = -j\omega\mu_0 \mathbf{H} \tag{III.2.1.1}$$

$$\nabla \mathbf{x} \mathbf{H} = j\omega\varepsilon_0 \underline{\mathbf{k}}.\mathbf{E} \tag{III.2.1.2}$$

$$\nabla.(\varepsilon_0 \underline{\mathbf{k}}.\mathbf{E}) = 0 \tag{III.2.1.3}$$

$$\nabla.(\mu_0 \mathbf{H}) = 0 \tag{III.2.1.4}$$

where the coefficients of the tensor dielectric coefficient $\underline{\mathbf{k}}$ are given by:

$$\underline{\mathbf{k}} = \begin{bmatrix} k_{11} & -k_{12} & 0 \\ k_{21} & k_{22} & 0 \\ 0 & 0 & k_{33} \end{bmatrix} \tag{III.2.1.5}$$

$$k_{33} = 1 - \alpha^2 \tag{III.2.1.6}$$

$$k_{11} = k_{22} = 1 - \frac{\alpha^2(1-\beta_+\beta_-)}{(1-\beta_-^2)(1-\beta_+^2)} \tag{III.2.1.7}$$

$$k_{21} = k_{12} = j\frac{\alpha^2(\beta_- - \beta_+)}{(1-\beta_-^2)(1-\beta_+^2)} \tag{III.2.1.8}$$

$$\alpha^2 = \frac{Ne^2}{\varepsilon_0\omega^2}\frac{m_+ + m_-}{m_+ m_-} = \frac{\omega_p^2}{\omega^2} \qquad \text{(III.2.1.9)}$$

$$\beta_{+/-} = \frac{eB_0}{m_{+/-}\omega} = \frac{\omega_{c+/-}}{\omega} \qquad \text{(III.2.1.10)}$$

In these equations, N is the number density of ionised atoms, m_+ and m_- are the ion and electron masses, ω_p is the plasma frequency and ω_c is the cyclotron frequency. The relations for the dielectric coefficients given above are valid for a collisionless plasma in the "temperate" regime. (A plasma is defined to be "temperate" if the thermal velocities are intermediate between the induced particle velocities and the phase velocities of the electromagnetic waves.) These are reasonable assumptions for discharge plasmas.

The wave equation for **E** is derived in the usual way, by taking the curl of III.2.1.1 and applying a standard vector identity we get

$$\nabla^2\mathbf{E} + k_0^2\mathbf{k}.\mathbf{E} - \nabla(\nabla.\mathbf{E}) = 0 \qquad \text{(III.2.1.11)}$$

where we have $k_0=\omega/c$ and $c=(\mu_0\varepsilon_0)^{-1/2}$.

For a system with uniformity in the z direction, and an otherwise arbitrary tensor medium, the solution for the electromagnetic fields satisfying Maxwell's equations have a z-dependence of the form $\exp(-\gamma z)$, where γ is an arbitrary complex function of the frequency. Hence the vector fields in equations III.2.1.1-4 are separable into transverse (denoted subscript T) and longitudinal (denoted subscript z) vector components. The separation is achieved by scalar and vector multiplication, respectively, of the longitudinal unit vector $\mathbf{i}_z$ with equations III.2.1.1 and 2. By this method we can manipulate equations III.2.1.1-4 to obtain a solution for the transverse fields in terms of the longitudinal fields:

$$\begin{bmatrix} P & R & Q & S \\ T & P & U & Q \\ -Q & -S & P & R \\ -U & -Q & T & P \end{bmatrix} \begin{bmatrix} \nabla_T E_z \\ \nabla_T H_z \\ \mathbf{i}_z \times \nabla_T E_z \\ \mathbf{i}_z \times \nabla_T H_z \end{bmatrix} = \begin{bmatrix} \mathbf{E}_T \\ \mathbf{H}_T \\ \mathbf{i}_z \times \mathbf{E}_T \\ \mathbf{i}_z \times \mathbf{H}_T \end{bmatrix} \qquad \text{(III.2.1.12)}$$

where we have

$$\mathbf{E} = \mathbf{E}_T + \mathbf{i}_z E_z \qquad \text{(III.2.1.13)}$$

$$\mathbf{H} = \mathbf{H}_T + \mathbf{i}_z H_z \qquad \text{(III.2.1.14)}$$

$$\nabla = \nabla_T + \mathbf{i}_z \frac{\partial}{\partial z} = \nabla_T + \mathbf{i}_z(-\gamma) \qquad \text{(III.2.1.15)}$$

$$\underline{\mathbf{k}}.\mathbf{E} = \underline{\mathbf{k}}_T.\mathbf{E}_T + \mathbf{i}_z k_{33} E_z \qquad \text{(III.2.1.16)}$$

$$\underline{\mathbf{k}}_T.\mathbf{E}_T = k_{11}\mathbf{E}_T + k_{12}\mathbf{i}_z \times \mathbf{E}_T \qquad \text{(III.2.1.17)}$$

$$k_0^2 = \omega^2 \mu_0 \varepsilon_0 = \frac{\omega^2}{c^2} \qquad \text{(III.2.1.18)}$$

$$k_r = k_{11} + 2jk_{12} \qquad \text{(III.2.1.19)}$$

$$k_l = k_{11} - jk_{12} \qquad \text{(III.2.1.20)}$$

and we have defined the following quantities:

$$R \equiv \frac{j\omega\mu_0 k_0^2 k_{12}}{D} \qquad \text{(III.2.1.21)}$$

$$P \equiv \frac{-\gamma(\gamma^2 + k_0^2 k_{11})}{D} \qquad \text{(III.2.1.22)}$$

$$Q \equiv \frac{\gamma k_0^2 k_{12}}{D} \qquad \text{(III.2.1.23)}$$

$$S \equiv \frac{j\omega\mu_0(\gamma^2+k_0^2k_{11})}{D} \qquad \text{(III.2.1.24)}$$

$$T \equiv \frac{\gamma^2 j\omega\varepsilon_0 k_{12}}{D} \qquad \text{(III.2.1.25)}$$

$$U \equiv \frac{-j\omega\varepsilon_0(\gamma^2k_{11}+k_0^2k_rk_l)}{D} \qquad \text{(III.2.1.26)}$$

$$D \equiv (\gamma^2+k_0^2k_{22})^2 + (k_0^2k_{12})^2 \qquad \text{(III.2.1.27)}$$

We can now write the wave equations for E_z and H_z in terms of the transverse separation of variables given by equations III.2 1.12 to 27.

$$\nabla_T^2E_z+aE_z = bH_z+\mathbf{b}_1.\nabla_TE_z+\mathbf{b}_2.\nabla_TH_z+\mathbf{b}_3.\mathbf{i}_z\times\nabla_TE_z+\mathbf{b}_4.\mathbf{i}_z\times\nabla_TH_z \qquad \text{(III.2.1.28)}$$

$$\nabla_T^2H_z+cH_z = dE_z+\mathbf{d}_1.\nabla_TE_z+\mathbf{d}_2.\nabla_TH_z+\mathbf{d}_3.\mathbf{i}_z\times\nabla_TE_z+\mathbf{d}_4.\mathbf{i}_z\times\nabla_TH_z \qquad \text{(III.2.1.29)}$$

where a,b,c and d are defined by

$$a \equiv \left(\gamma^2+k_0^2k_{11}\right)\frac{k_{33}}{k_{11}} \qquad \text{(III.2.1.30)}$$

$$b \equiv j\omega\mu_0\gamma\frac{k_{12}}{k_{11}} \qquad \text{(III.2.1.31)}$$

$$c \equiv \gamma^2 + k_0^2\frac{k_rk_l}{k_{11}} \qquad \text{(III.2.1.32)}$$

$$d \equiv -j\omega\varepsilon_0\gamma\frac{k_{12}k_{33}}{k_{11}} \qquad \text{(III.2.1.33)}$$

and we have

$$\begin{bmatrix} b_1 \\ b_2 \\ b_3 \\ b_4 \end{bmatrix} = \gamma \begin{bmatrix} P & -Q \\ R & -S \\ Q & P \\ S & R \end{bmatrix} \begin{bmatrix} \frac{\nabla_T k_{11}}{k_{11}} \\ \frac{k_{12}}{k_{11}} \frac{\nabla_T k_{12}}{k_{12}} \end{bmatrix} \qquad \text{(III.2.1.34)}$$

and

$$\begin{bmatrix} d_1 \\ d_2 \\ d_3 \\ d_4 \end{bmatrix} = j\omega\varepsilon_0 \left[\frac{\nabla_T k_{11}}{k_{11}} \begin{bmatrix} -Q & P \\ -S & R \\ P & Q \\ R & S \end{bmatrix} \begin{bmatrix} k_{11} \\ k_{12} \end{bmatrix} + \frac{\nabla_T k_{12}}{k_{12}} \begin{bmatrix} -Q & -P \\ -S & -R \\ P & -Q \\ R & -S \end{bmatrix} \begin{bmatrix} \frac{k_{12}^2}{k_{11}} \\ k_{12} \end{bmatrix} \right] \qquad \text{(III.2.1.35)}$$

Equations III.2.1.12,28 and 29 are explicit forms of Maxwell's equations for the inhomogeneous and anisotropic plasma described by the dielectric tensor $\underline{\mathbf{k}}$. In any particular problem, equations III.2.1.28 and 29 are solved and the results are substituted into equation III.2.1.12 to find the transverse fields. Application of the boundary conditions of the system then gives the determinantal equation for γ as a function of frequency and characteristic transverse dimensions of the system.

The equations for E and H are, in general, coupled. There are, however, some important cases in which the equations for E and H decouple and these are now considered.

III.2.2 Free-space Waveguide

In the absence of the plasma the dielectric tensor coefficients are $k_{21}=0$, $k_{11}=k_{22}=k_{33}=1$ and the equations for E_z and H_z decouple to give the familiar waveguide equations. The TM waves are given by:

$$H_z = 0 \tag{III.2.2.1}$$

$$\nabla_T^2 E_z + p_e^2 E_z = 0 \tag{III.2.2.2}$$

$$p_e^2 = \gamma^2 + k_0^2 \tag{III.2.2.3}$$

$$\mathbf{E}_T = \frac{-\gamma}{p_e^2} \nabla_T E_z \tag{III.2.2.4}$$

$$\mathbf{H}_T = \frac{-j\omega\varepsilon_0}{p_e^2} \mathbf{i}_z \times \nabla_T E_z \tag{III.2.2.5}$$

and the TE waves are given by

$$E_z = 0 \tag{III.2.2.6}$$

$$\nabla_T^2 H_z + p_h^2 H_z = 0 \tag{III.2.2.7}$$

$$p_h^2 = \gamma^2 + k_0^2 \tag{III.2.2.8}$$

$$\mathbf{H}_T = \frac{-\gamma}{p_h^2} \nabla_T H_z \tag{III.2.2.9}$$

$$\mathbf{E}_T = \frac{j\omega\mu_0}{p_h^2} \mathbf{i}_z \times \nabla_T H_z \tag{III.2.2.10}$$

For perfectly conducting waveguide walls, p^2 is an eigenvalue of equations III.2.2.2 and 7, determined by geometry and independent of frequency. By applying Green's theorem[5, p139] it can be shown that p^2 are positive real numbers. Hence the propagation constant is either real ($\gamma=\alpha$) or imaginary ($\gamma=j\beta$), representing a cut-off and a propagating wave, respectively. The cut-off frequencies, for which $\gamma=0$ are a function of geometry alone:

$$\omega_{co} = pc \qquad \text{(III.2.2.11)}$$

where c is the speed of light. The dispersion characteristics of the waves are then given by:

$$\alpha^2 = p^2 - k_0^2 \qquad \omega<\omega_{co} \qquad \text{(III.2.2.12)}$$

and

$$\beta^2 = k_0^2 - p^2 \qquad \omega>\omega_{co} \qquad \text{(III.2.2.13)}$$

III.2.3 Homogeneous, Isotropic Plasma Waveguides

For a waveguide which is filled with a homogeneous plasma with zero applied magnetic field we have $k_{21}=0$ and $k_{11}=k_{33}$. The TE and TM modes are independent and the dispersion relation is given by:

$$p^2 = \gamma^2 + k_0^2 k_{33} \qquad \text{(III.2.3.1)}$$

If the plasma is lossless, then k_{33} is real for all frequencies and the cut-offs occur at frequencies above the plasma frequency:

$$\omega_{co}^2 = \omega_p^2 + (pc)^2 \qquad \text{(III.2.3.2)}$$

The presence of a lossless, unmagnetised plasma which completely fills the waveguide simply shifts all of the free-space waveguide dispersion curves to higher frequencies and propagation constants. If the collision frequency is significant, then k_{33} is complex and frequency-dependent, so propagation is possible for all frequencies.

III.2.4 Inhomogeneous, Isotropic Plasma Waveguides

In the presence of an inhomogeneous, isotropic, unmagnetised plasma, we have $k_{12}=0$. Also, the dielectric coefficients k_{11} and k_{33} are equal and are finite functions of the transverse coordinates. Thus from equations III.2.1.21,23,25,31,33,34 and 35 the values of b,d,R,Q,T,$\mathbf{b}_2$,$\mathbf{b}_3$,$\mathbf{d}_1$ and $\mathbf{d}_4$ are zero and equations III.2.1.29 and 30 reduce to

$$\nabla_T^2 E_z + aE_z = \mathbf{b}_1.\nabla_T E_z + \mathbf{b}_4.\mathbf{i}_z \times \nabla_T H_z \qquad \text{(III.2.4.1)}$$

$$\nabla_T^2 H_z + cH_z = \mathbf{d}_2.\nabla_T H_z + \mathbf{d}_3.\mathbf{i}_z \times \nabla_T E_z \qquad \text{(III.2.4.2)}$$

and equation III.2.1.12 for the transverse fields in terms of the longitudinal fields reduces to

$$\mathbf{E}_T = \frac{-\gamma}{p^2}\nabla_T E_z + \frac{j\omega\mu_0}{p^2}\mathbf{i}_z \times \nabla_T H_z \qquad \text{(III.2.4.3)}$$

$$\mathbf{H}_T = \frac{-\gamma}{p^2}\nabla_T H_z + \frac{-j\omega\varepsilon_0 k_{33}}{p^2}\mathbf{i}_z \times \nabla_T E_z \qquad \text{(III.2.4.4)}$$

Equations III.2.4.1 and 2 are, in general, coupled, so E and H waves cannot exist separately. Furthermore, p^2 is no longer an eigenvalue, since k_{33} is a function both of transverse coordinates and of frequency, and, from equation III.2.1.30 it follows that p^2 is also a function of transverse dimensions and frequency. Problems of this nature are very difficult to solve.

The equations for E and H , however, decouple in the following two cases:

(i) if the plasma is inhomogeneous in only one of the transverse dimensions;

(ii) if the field solutions are independent of the other transverse dimension.

Let u_1 and u_2 be the transverse coordinates, k_{33} be a function of u_1 and consider solutions independent of u_2. With these assumptions the coupling terms in equations III.2.4.1 and 2 vanish and we get

$$\mathbf{b}_4.\mathbf{i}_z\times\nabla_T H_z = 0 \qquad \text{(III.2.4.5)}$$

$$\mathbf{d}_3.\mathbf{i}_z\times\nabla_T E_z = 0 \qquad \text{(III.2.4.6)}$$

and the solutions can be separated into E-waves:

$$H_z = 0 \qquad \text{(III.2.4.7)}$$

$$\nabla_T^2 E_z - \mathbf{b}_1.\nabla_T E_z + p^2 E_z = 0 \qquad \text{(III.2.4.8)}$$

$$\mathbf{E}_T = \frac{-\gamma}{p^2}\nabla_T E_z \equiv \mathbf{i}_1 E_1 \qquad \text{(III.2.4.9)}$$

$$\mathbf{H}_T = -\frac{j\omega\varepsilon_0 k_{33}}{p^2}\mathbf{i}_z\times\nabla_T E_z \equiv \mathbf{i}_2 H_2 \qquad \text{(III.2.4.10)}$$

$$\nabla_T^2 H_2 + cH_2 = \mathbf{d}_2.\nabla_T H_2 \qquad \text{(III.2.4.11)}$$

and H-waves:

$$E_z = 0 \qquad \text{(III.2.4.12)}$$

$$\nabla_T^2 H_z - \mathbf{d}_2.\nabla_T H_z + p^2 H_z = 0 \qquad \text{(III.2.4.13)}$$

$$\mathbf{H}_T = -\frac{\gamma}{p^2}\nabla_T H_z \equiv \mathbf{i}_1 H_1 \qquad \text{(III.2.4.14)}$$

$$\mathbf{E}_T = \frac{j\omega\mu_0}{p^2}\mathbf{i}_z\times\nabla_T H_z \equiv \mathbf{i}_2 E_2 \qquad \text{(III.2.4.15)}$$

$$\nabla_T^2 E_2 + p^2 E_2 = 0 \qquad \text{(III.2.4.16)}$$

Equation III.2.4.16 can be solved for certain simple functions $k_{33}(u_1)$.

III.2.5 Waveguide Partially Filled with Homogeneous Plasma

In the case where the plasma does not completely fill the waveguide the boundary conditions require consideration. At the waveguide wall the usual boundary conditions apply. At the plasma boundary, however, the charges are free to move and in the presence of electromagnetic fields the boundary will be perturbed. This perturbation can be analysed by replacing the first order perturbation in the boundary by an equivalent first order surface charge density on the unperturbed boundary. The charge that has moved across a unit area of the unperturbed boundary is

$$\rho_s = \sum_l \rho_{0l} \mathbf{n}.\mathbf{r}_{bl} \qquad \text{(III.2.5.1)}$$

where ρ_{0l} is the unperturbed charge density of species l, $\mathbf{r}_{bl}$ is the first order perturbation in position and $\mathbf{n}$ is the unit vector normal to the unperturbed boundary. Now we have

$$\mathbf{v}_{bl} = \frac{d\mathbf{r}_{bl}}{dt} = j\omega \mathbf{r}_{bl} \qquad \text{(III.2.5.2)}$$

and

$$j\omega m_l \mathbf{v}_{bl} = e\mathbf{E}_b \qquad \text{(III.2.5.3)}$$

where $\mathbf{v}_{bl}$ is the first order velocity modulation of the particle, m_l is the mass of species l and $\mathbf{E}_b$ is the total electric field at the boundary. For any real plasma boundary with free space it is not likely that there will be a discontinuity in density or complete neutrality, so there will be little variation of $\mathbf{E}_b$ with species. We neglect any variation in $\mathbf{E}_b$ and from equations III.2.5.1-3 obtain

$$\rho_s = \sum_l \frac{-\omega_{pl}^2}{\omega^2} \varepsilon_0 \mathbf{E}^p.\mathbf{n} \qquad \text{(III.2.5.4)}$$

where $\mathbf{E}^p$ is the first order electric field in the plasma at the unperturbed boundary. With the surface charge density of equation III.2.5.4 replacing the perturbation at the

boundary, the electric field at the unperturbed boundary is discontinuous by ρ_s/ε_0. Thus, we have the boundary condition for the edge of the plasma:

$$\mathbf{n}.(\varepsilon_0\mathbf{E}^a - \varepsilon_0 k_{33}\mathbf{E}^p) = 0 \qquad \text{(III.2.5.5)}$$

where $\mathbf{E}^a$ is the free-space electric field at the boundary. The tangential electric and magnetic fields are, as usual, continuous across the boundary. The field equations are given by

$$\nabla_T^2 E_z^i + p^2 E_z^i = 0 \qquad \text{(III.2.5.6)}$$

$$\nabla_T^2 H_z^i + p^2 H_z^i = 0 \qquad \text{(III.2.5.7)}$$

$$p2 = \gamma^2 + k_0^2 k_{33} \qquad \text{(III.2.5.8)}$$

$$\mathbf{E}_T^i = \frac{-\gamma}{p^2}\nabla_T E_z^i + \frac{j\omega\mu_0}{p^2}\mathbf{i}_z \times \nabla_T H_z^i \qquad \text{(III.2.5.9)}$$

$$\mathbf{H}_T^i = \frac{-j\omega k_{33}\varepsilon_0}{p^2}\mathbf{i}_z \times \nabla_T E_z^i - \frac{\gamma}{p^2}\nabla_T H_z^i \qquad \text{(III.2.5.10)}$$

and

$$\nabla_T^2 E_z^o + q^2 E_z^o = 0 \qquad \text{(III.2.5.11)}$$

$$\nabla_T^2 H_z^o + q^2 H_z^o = 0 \qquad \text{(III.2.5.12)}$$

$$q2 = \gamma^2 + k^2 \qquad \text{(III.2.5.13)}$$

$$k^2 = \omega^2\mu\varepsilon \qquad \text{(III.2.5.14)}$$

$$\mathbf{E}_T^o = \frac{-\gamma}{q^2}\nabla_T E_z^o + \frac{j\omega\mu}{q^2}\mathbf{i}_z \times \nabla_T H_z^o \qquad \text{(III.2.5.15)}$$

$$\mathbf{H}_T^0 = \frac{-j\omega\varepsilon}{q^2}\mathbf{i}_z \times \nabla_T E_z^o - \frac{\gamma}{q^2}\nabla_T H_z^o \qquad \text{(III.2.5.16)}$$

where the superscripts i and o signify regions inside and outside the plasma, respectively. Now let the radius of the waveguide be very large, and consider guided waves ($\gamma=j\beta$) which will have decaying fields outside the plasma, so that we have

$$q^2 < 0 \qquad \text{(III.2.5.17)}$$

and hence from equation III.2.5.13 we get

$$\beta^2 > k^2 \qquad \text{(III.2.5.18)}$$

Thus, these waves are slow waves with velocities less than the velocity of light. Also, from equations III.2.5.8 and 18, when we have $\mu\varepsilon > \mu_0\varepsilon_0$, we obtain

$$p^2 < 0 \qquad \text{(III.2.5.19)}$$

Then from equations III.2.5.6 and 11, subject to equation III.2.5.5, we see that E_z is largest at the plasma boundary. That is, these waves may be described as surface waves. This mode of propagation does not exist in the homogeneously filled plasma waveguide.

III.2.6 Longitudinally Magnetised, Homogeneous Plasma Waveguides

The application of an external longitudinal magnetic field B_0 makes the plasma medium anisotropic, with $k_{21}\neq 0$ and $k_{11}\neq k_{33}$. For the homogeneous case, k_{11}, k_{21} and k_{33} are independent of transverse coordinates and the tensors **b** and **d** vanish. Equations III.2.1.28 and 29 reduce to

$$\nabla_T^2 E_z + aE_z = bH_z \qquad \text{(III.2.6.1)}$$

$$\nabla_T^2 H_z + cH_z = dE_z \qquad \text{(III.2.6.2)}$$

Equations III.2.6.1 and 2 can be rearranged to give a set of un-coupled fourth order equations:

$$[\nabla_T^4+(a+c)\nabla_T^2+(ac-bd)]E_z = 0 \qquad \text{(III.2.6.3)}$$

$$[\nabla_T^4+(a+c)\nabla_T^2+(ac-bd)]H_z = 0 \qquad \text{(III.2.6.4)}$$

Equations II.2.6.3 and 4 have standard solutions of the form $\exp(-j\mathbf{p}.\mathbf{r}_T)$ where

$$p^4-(a+c)p^2+(ac-bd) = 0 \qquad \text{(III.2.6.5)}$$

is the dispersion relation, relating the propagation constant to transverse wavenumbers p, frequency ω, and the plasma parameters ω_p and ω_b. In general, an infinite set of exponential functions is required for a complete solution. Equations III.2.6.1 and 2 can, however, also be reduced to an uncoupled set by seeking solutions for which

$$H_z = \frac{a-p^2E_z}{b} \qquad \text{(III.2.6.6)}$$

in equation III.2.6.1 and

$$H_z = \frac{dE_z}{c-p^2} \qquad \text{(III.2.6.7)}$$

in equation III.2.6.2. Now from equation III.2.6.5 we have

$$\frac{a-p^2}{b} = \frac{d}{c-p^2} \equiv h \qquad \text{(III.2.6.8)}$$

and equations III.2.6.1 and 2 reduce to

$$\nabla_T^2+p^2E_z = 0 \qquad \text{(III.2.6.9)}$$

and $$\nabla_T^2+p^2H_z = 0 \qquad \text{(III.2.6.10)}$$

We then seek solutions for values of p^2, as given by equation III.2.6.5. Since equation III.2.6.5 is of fourth order in p, then two independent solutions of each of equations III.2.6.9 and 10 are required. Thus, we may write

$$E_z = E_{z1}+E_{z2} \qquad \text{(III.2.6.11)}$$

and

$$H_z = hE_{z1}+hE_{z2} \qquad \text{(III.2.6.12)}$$

The functions E_{z1} and E_{z2} are independent solutions of equation III.2.6.9 corresponding to distinct values of p^2. From equations III.2.6.8, 11 and 12 and III.2.1.12, the transverse fields are then given by:

$$\begin{bmatrix} \mathbf{E}_T \\ \mathbf{H}_T \\ \mathbf{i}_z\times\mathbf{E}_T \\ \mathbf{i}_z\times\mathbf{H}_T \end{bmatrix} = \begin{bmatrix} \frac{-1}{\gamma} & \frac{R}{b} & \frac{-1}{\gamma}\frac{k11}{k12} & \frac{S}{b} \\ \frac{\gamma}{b} & \frac{P}{b} & 0 & \frac{Q}{b} \\ \frac{1}{\gamma}\frac{k11}{k12} & \frac{-S}{b} & \frac{-1}{\gamma} & \frac{R}{b} \\ 0 & \frac{-Q}{b} & \frac{\gamma}{b} & \frac{P}{b} \end{bmatrix} \left[\begin{pmatrix} \nabla_T \\ p_2^2\nabla_T \\ \mathbf{i}_z\times\nabla_T \\ p_2^2\mathbf{i}_z\times\nabla_T \end{pmatrix} E_{z1} + \begin{pmatrix} \nabla_T \\ p_1^2\nabla_T \\ \mathbf{i}_z\times\nabla_T \\ p_1^2\mathbf{i}_z\times\nabla_T \end{pmatrix} E_{z2} \right] \qquad \text{(III.2.6.13)}$$

III.3 Slow-wave Solutions

III.3.1 Introduction

It has been shown in section III.2 that the equations for **E** and **H** in a plasma loaded waveguide form a coupled set of second order differential equations. Apart from a few special cases the solution of the field equations is non-trivial. It was also shown that when the plasma does not completely fill the waveguide, or in the presence of a longitudinal magnetic field, propagation at frequencies below the plasma frequency is possible. These modes may have $\beta>k_0$, that is the phase velocity of the wave in the

plasma loaded guide may be less than c. In this regime we may invoke the quasi-static approximation ("QSA"), first proposed by Trivelpiece and Gould[6].

The quasi-static approximation assumes that the phase velocity of the wave is extremely slow compared to the velocity of light, such that the velocity of light can be regarded as infinite. In this case, the electric and magnetic fields are essentially static and satisfy

$$\mathbf{H} \equiv 0 \tag{III.3.1.1}$$

$$\nabla \times \mathbf{E} \equiv 0 \tag{III.3.1.2}$$

$$\nabla . \mathbf{D} = \nabla . (\varepsilon_0 \underline{\mathbf{k}} . \mathbf{E}) \equiv 0 \tag{III.3.1.3}$$

Now equation III.3.1.2 means that we can define **E** to be the gradient of a scalar potential function Φ with the usual $\exp(-\gamma z)$ dependence:

$$\mathbf{E} \equiv -\nabla \Phi \tag{III.3.1.4}$$

so from equations III.3.1.3,4 and III.2.1.5,13-17 and using the standard vector identities:

$$\nabla . \mathbf{A} = \frac{1}{r}\frac{\partial}{\partial r}(rA_r) + \frac{1}{r}\frac{\partial A_\theta}{\partial \theta} + \frac{\partial A_z}{\partial z} \tag{III.3.1.5}$$

and

$$\nabla f = \begin{bmatrix} \dfrac{\partial f}{\partial r} \\ \dfrac{1}{r}\dfrac{\partial f}{\partial \theta} \\ \dfrac{\partial f}{\partial z} \end{bmatrix} \tag{III.3.1.5}$$

we obtain

$$\nabla_T^2 \Phi + p^2 \Phi = 0 \tag{III.3.1.6}$$

$$p^2 = \gamma^2 \frac{k_{33}}{k_{11}} \qquad \text{(III.3.1.7)}$$

$$E_z = \gamma\Phi \qquad \text{(III.3.1.8)}$$

$$E_T = -\nabla_T\Phi \qquad \text{(III.3.1.9)}$$

For regions outside the plasma these relations become

$$\nabla_T^2\Phi^o + \gamma^2\Phi^o = 0 \qquad \text{(III.3.1.10)}$$

$$E_z^o = \gamma\,\Phi^o \qquad \text{(III.3.1.11)}$$

$$E_T^o = -\nabla_T\Phi^o \qquad \text{(III.3.1.12)}$$

At the (perfectly conducting) waveguide wall, we have

$$\mathbf{n}\times\mathbf{E} = 0 \qquad \text{(III.3.1.13)}$$

and at the boundary between the plasma and free space, we have

$$\mathbf{n}.(\varepsilon_0\underline{\mathbf{k}}.\mathbf{E} - \varepsilon_0\mathbf{E}^o) = 0 \qquad \text{(III.3.1.14)}$$

III.3.2 Finite Longitudinal Magnetic Field

Equations III.3.1.6 and 10 can be solved in terms of known functions to give the potential function. Application of the boundary conditions III.3.1.13 an 14 then give the full dispersion relation and the fields can be obtained from III.3.1.8,9,11 and 12. As the case of particular interest we consider a circular waveguide, radius b, partially filled with a longitudinally magnetised plasma column of radius a and seek propagating solutions for which $\gamma=j\beta$ and ω is real. The solution of equations III.3.1.6 and III.3.1.10 are

$$\Phi = [AJ_m(pr) + BY_m(pr)]\, e^{j(m\theta+\omega t)}\, \gamma z \qquad 0 < r < a \qquad \text{(III.3.2.1)}$$

and

$$\Phi^o = [CI_m(\beta r) + DK_m(\beta r)]\, e^{j(m\theta+\omega t)}\, \gamma z \qquad a < r < b \qquad \text{(III.3.2.2)}$$

where J_m, Y_m, I_m and K_m are Bessel functions of the first and second kind and modified Bessel functions of the first and second kind, respectively, all of order m, and A, B, C and D are arbitrary constants to be determined from the boundary conditions.

The first condition, that the fields must be finite on the axis, requires that B=0. The boundary condition at the waveguide wall, equation III.3.1.13, is

$$\nabla\times\mathbf{E}(b) = 0$$

$$\Rightarrow\nabla\times[\mathbf{E}_T(b)+\mathbf{i}_z(b)] =0$$

$$\Rightarrow\nabla\times[-\nabla_T\Phi^o(b)+\mathbf{i}_z\gamma\Phi^o(b)] = 0$$

$$\Rightarrow\Phi^o(b) = 0 \qquad \text{(III.3.2.3)}$$

since all of the terms are proportional to Φ^o. Equation III.3.2.3 can be achieved by setting

$$C = C' K_m(\beta b) \qquad \text{(III.3.2.5)}$$

$$D = -C' I_m(\beta b) \qquad \text{(III.3.2.6)}$$

where C' is an arbitrary constant. The second boundary condition, that the potential must be continuous at r=a so (that the electric field is finite), can be satisfied by choosing

$$A = \frac{1}{J_m(pa)} \qquad \text{(III.3.2.4)}$$

$$C' = \frac{1}{I_m(\beta a)K_m(\beta b) - I_m(\beta b)K_m(\beta a)} \qquad \text{(III.3.2.5)}$$

Finally, the condition III.3.1.14 that the normal component of the displacement be continuous is applied. We have

$$\Phi = \frac{J_m(pr)}{J_m(pa)} e^{j(m\theta+\omega t)-\gamma z} \qquad 0 < r < a \qquad \text{(III.3.2.6)}$$

$$\mathbf{E}_T = -\nabla_T \Phi$$

$$= \begin{bmatrix} -p \dfrac{J'_m(pr)}{J_m(pa)} e^{j(m\theta+\omega t)-\gamma z} \\ -\dfrac{1}{r} \dfrac{J_m(pr)}{J_m(pa)} jm\, e^{j(m\theta+\omega t)-\gamma z} \end{bmatrix} \qquad \text{(III.3.2.7)}$$

inside the plasma and

$$\Phi^o = \frac{I_m(\beta r)\, K_m(\beta b) - K_m(\beta r)\, I_m(\beta b)}{I_m(\beta a)\, K_m(\beta b) - K_m(\beta a)\, I_m(\beta b)} e^{j(m\theta+\omega t)-\gamma z} \qquad a < r < b \qquad \text{(III.3.2.8)}$$

$$\mathbf{E}_T^o = \begin{bmatrix} -\dfrac{\beta I'_m(\gamma r)\, K_m(\beta b) - \beta K'_m(\beta r)\, I_m(\beta b)}{I_m(\beta a)\, K_m(\beta b) - K_m(\beta b)\, I_m(\beta a)} e^{j(m\theta+\omega t)-\gamma z} \\ -\dfrac{I_m(\beta r)\, K_m(\beta b) - K_m(\beta r)\, I_m(\beta b)}{I_m(\beta a)\, K_m(\beta b) - K_m(\beta a)\, I_m(\beta b)} jm\, e^{j(m\theta+\omega t)-\gamma z} \end{bmatrix} \qquad \text{(III.3.2.9)}$$

outside the plasma. Now using equation III.2.1.16

$$\underline{\mathbf{k}}.\mathbf{E} = \underline{\mathbf{k}}_T.\mathbf{E}_T + \mathbf{i}_z k_{33} E_z$$

we obtain

$$\mathbf{n}.\underline{\mathbf{k}}.\mathbf{E} = \mathbf{n}.(\underline{\mathbf{k}}_T.\mathbf{E}_T) \qquad \text{(III.3.2.10)}$$

and from equation III.3.2.7

$$\mathbf{n}.\underline{\mathbf{k}}.\mathbf{E}_T = \left[-k_{11}\, p \frac{J_m'(pr)}{J_m(pa)} e^{j(m\theta - \gamma z + \omega t)} - \frac{k_{12}}{r} \frac{J_m(pr)}{J_m(pa)} \right] e^{j(m\theta + \omega t) - \gamma z}$$

(III.3.2.11)

Substituting from equations III.3.2.9 and 11 into equation III.3.1.14 with r=a, we obtain

$$k_{11}\, pa \frac{J_m'(pa)}{J_m(pa)} + jmk_{12} - \beta a \frac{I_m'(\beta a)\, K_m(\beta b) - K_m'(\beta a)\, I_m(\beta b)}{I_m(\beta a)\, K_m(\beta b) - K_m(\beta a)\, I_m(\beta b)} = 0 \qquad \text{(III.3.2.12)}$$

Equation III.3.2.12 is the dispersion relation for the longitudinally magnetised plasma column in a waveguide. Its solution requires numerical techniques. In order to confirm the results of the numerical simulation we solve the dispersion relation for the simpler case of the plasma–filled waveguide. In this case the solution for the potential is given by

$$\Phi = AJ_m(pr) \qquad 0 < r < b \qquad \text{(III.3.2.13)}$$

and the boundary condition III.3.2.3 that the potential must vanish at the waveguide surface r=b gives

$$J_m(pb) = 0 \Rightarrow pb = \eta_{m\nu} \qquad \text{(III.3.2.14)}$$

where $\eta_{m\nu}$ is the ν^{th} root of the Bessel function of order m. Thus, p is simply a numerical constant whose value depends on the waveguide radius and the mode of interest. Using equation III.3.1.7 we may write

$$\frac{\gamma b}{\eta_{m\nu}} = \sqrt{\frac{k_{11}}{k_{33}}} \qquad \text{(III.3.2.15)}$$

Substituting for k_{11} and k_{33} and neglecting the ion frequencies compared to the electron frequencies we obtain an analytic form for the dispersion relation:

$$\frac{\gamma b}{\eta_{m\nu}} = \sqrt{\frac{1 + \dfrac{\omega_p^2}{\omega_c^2 - \omega^2}}{1 - \dfrac{\omega_p^2}{\omega^2}}} \qquad \text{(III.3.2.16)}$$

A graph of equation III.3.2.16 is shown in Figure III.3.2.1. For a propagating mode we have required that γ be imaginary and non-zero ($\gamma = j\beta$) and only the solutions which meet this criterion are shown. From the figure we see that there are two for the longitudinally magnetised plasma filled waveguide. The first pass-band extends from $\omega=0$ up to ω_p or ω_c, whichever is the smaller, and consists of forward wave modes. The second pass-band extends from $\omega=\omega_p$ up to $(\omega_p^2+\omega_c^2)^{1/2}$ and consists of backward wave modes. The phase velocity is given by ω/β and the group velocity by $d\omega/d\beta$.

In order to generate the slow wave solutions we have assumed that the ac magnetic field is zero. In order to calculate the power flow, however, we need to find an approximate value for the magnetic field since the time averaged power flow is given by

$$P = \int_A \mathrm{Re}\,\frac{1}{2}\,\mathbf{E}_T \times \mathbf{H}_T^{*} \cdot i_z \, da \qquad \text{(III.3.2.17).}$$

Let the magnetic field be coupled to the currents that arise from the interaction of the quasi-static electric fields with the charges. From Maxwell's equations (III.2.1.2,4), equations III.1.8,9 and III.2.13 we are able to calculate all of the required fields. We get

$$E_r = A\,\frac{j}{\beta}\,p\,J_m'(pr) \qquad \text{(III.3.2.18)}$$

$$E_\theta = A\,\frac{m}{\beta r}\,J_m(pr) \qquad \text{(III.3.2.19)}$$

$$E_z = A\,J_m(pr) \qquad \text{(III.3.2.20)}$$

$$H_\theta = -j\,\frac{\omega}{\beta^2}\,\varepsilon_0\,A\left[-k_{11}pJ_m'(pr) - k_{12}\,\frac{m}{r}\,J_m(pr)\right] \qquad \text{(III.3.2.21)}$$

$$H_r = \frac{-\omega}{\beta^2}\,\varepsilon_0\,A\left[k_{12}pJ_m'(pr) + k_{22}\,\frac{m}{r}\,J_m(pr)\right] \qquad \text{(III.3.2.22)}$$

In equations III.3.2.18 to 22 the exponential propagation factor is omitted for clarity. The longitudinal component of the Poynting vector is then given by

$$\mathbf{E}_T \times \mathbf{H}_T^{*} \cdot i_z = \frac{A^2 \omega \varepsilon_0}{\beta^3}\left[-p^2\left[J_m'(pr)\right]^2 k_{11} - \frac{pm}{r}\,2J_m(pr)J_m'(pr)k_{12} + \frac{m^2}{r^2}\left[J_m(pr)\right]^2 k_{22}\right] \qquad \text{(III.3.2.23)}$$

The evaluation of the integral in equation III.3.2.17 is generally non-trivial. For the axially symmetric modes (m=0), however, all but the first term of equation III.3.2.23 are equal to zero and equations III.3.2.17 and 23 reduce to

$$P = \frac{1}{2}\frac{A^2\omega\varepsilon_0}{\beta^3} p^2 k_{11} \int_0^b J_1^2(pr)\,(2\pi r\,dr) \qquad \text{(III.3.2.24)}$$

Integrating by parts and noting equation III.3.2.14 for the boundary condition we obtain

$$P = A^2 \frac{\pi}{2}\frac{\omega}{\beta^3}\varepsilon_0 k_{11}\eta_{0v}^2 J_1^2\left[\eta_{0v}^2\right] \qquad \text{(III.3.2.25)}$$

We are now able to evaluate the constant A and, hence, the magnitudes of the fields as a function of the average power which propagates in the waveguide. Figure III.3.2.2 shows A as a function of the normalised plasma frequency for typical values of the cyclotron frequency. The fields in the stop-bands correspond to real values of γ where the power flow is purely reactive (imaginary). Clearly, the fields become very large in the vicinity of plasma resonances; this defines the conditions for optimal plasma generation in the waveguide (see section II.3.6). In order to minimise the fields for a given power flow, the guide radius should be large, the plasma frequency high and the ratio of the signal frequency to the plasma frequency should be small.

Returning now to the problem of a plasma column in a waveguide, we consider the solution of equation III.3.2.12. The results of a numerical solution of the dispersion relation are shown in Figure III.3.2.3. One major difference between this case and the plasma filled guide is that there is no longer a cut-off at the cyclotron frequency because of the surface wave effects described in section III.2.5. Propagation is possible down to zero longitudinal magnetic field.

Approximate values for the magnetic fields can be calculated in a similar manner to the derivation of equations III.3.2.21 and 22. The transverse electric fields are given by equations III.3.2.7 and 9 from which we deduce that the magnetic field inside the plasma is

$$H_\theta = \frac{j\omega\varepsilon_0}{-\gamma}\left[\frac{-k_{11}pJ'_m(pr)}{J_m(pa)} + \frac{k_{12}m}{r}\frac{J_m(pr)}{J_m(pa)}\right] \qquad \text{(III.3.2.26)}$$

and, for the magnetic field outside the plasma, we get

$$H_\theta^o = \frac{j\omega\varepsilon_0}{-\gamma}\left[-k_{11}\beta\frac{I'_m(\beta r)K_m(\beta b) - K'_m(\beta r)I_m(\beta b)}{I_m(\beta a)K_m(\beta b) - K_m(\beta a)I_m(\beta b)}\right.$$

$$\left. + k_{12}m\frac{I_m(\beta r)K_m(\beta b) - K_m(\beta r)I_m(\beta b)}{I_m(\beta a)K_m(\beta b) - K_m(\beta a)I_m(\beta b)}\right] \qquad \text{(III.3.2.27)}$$

where the exponential factor has been omitted. The total power flow P for the axially symmetric modes is then the sum of the power flows inside and outside the plasma, given by

$$P = \frac{\pi\beta\omega\varepsilon_0}{J_0^2(pa)}\frac{k_{33}}{k_{11}}\int_0^a J_1^2(pr)r\,dr + \pi\omega\varepsilon_0 k_{11}\int_a^b\left[\frac{I_1(\beta r)K_0(\beta b) - K_1(\beta r)I_0(\beta b)}{I_0(\beta a)K_0(\beta b) - K_0(\beta a)I_0(\beta b)}\right]^2 r\,dr$$

(III.3.2.28)

An analytic evaluation of the power flow, however, is difficult to obtain, even for the zeroth order mode, since there is no longer a convenient boundary condition to simplify the integrals in equation III.3.2.28.

The second major difference between a plasma filled waveguide and a plasma column in a waveguide is that the plasma column can exhibit Faraday rotation of the plane of polarisation of a wave but the plasma filled waveguide cannot. A polarised wave is

formed by the superposition of two angular modes having the same order and opposite sign, that is modes described by the indices +m and –m. If the phase velocities (ω/β) of the two modes are different, then the plane of polarisation of the composite wave will rotate as the wave propagates in the z-direction. For +m and –m modes to have different phase velocities, the solution of the dispersion relation (III.3.2.12 and 16) for constant ω must have different values for the +m and –m branches. This condition is true for equation III.3.2.12 with a<b but not for equation III.3.2.16. Thus, Faraday rotation can only occur if the plasma does not completely fill the waveguide.

Clearly, from the occurrence of the terms k_{11} and k_{12} in equation III.3.2.12, the difference in phase velocity between the +m and –m modes, and hence the Faraday rotation, is a function of the plasma and cyclotron frequencies. Approximate numerical solutions of the dispersion relation for a plasma column in a waveguide with m=1 and m=–1 are shown in Figure III.3.2.4. For constant ω/ω_p, the phase difference per unit length of the guide is

$$\frac{\partial\phi}{z} = \partial\beta = \left|\beta_+ - \beta_-\right| \qquad \text{(III.3.2.29)}$$

and the composite wavenumber is

$$\beta' = \frac{\beta_+ - \beta_-}{2} \qquad \text{(III.3.2.30)}$$

Thus, the distance in guide wavelengths for one complete rotation of the plane of polarisation is

$$\frac{z}{\lambda'} = \frac{\beta_+ - \beta_-}{2\left|\beta_+ - \beta_-\right|} \qquad \text{(III.3.2.31)}$$

This parameter is plotted as a function of frequency in Figure III.3.2.5. The sensitivity of the Faraday effect to the plasma and cyclotron frequencies is evident from the figure.

III.3.3 Conclusions

The quasistatic approximation has been used to model the propagation of electromagnetic waves in a circular waveguide which contains a longitudinally magnetised plasma. The QSA assumes that the RF magnetic fields in Maxwell's equations are negligible and the electric fields are calculated from the resulting wave equation. The disperion relations have been derived and solved for the cases of a plasma-filled waveguide and a plasma column in a waveguide. Propagation at velocities smaller than the velocity of light is possible for frequencies smaller than a cut-off frequency which is a function of the plasma and cyclotron frequencies.

For propagating modes, the RF magnetic fields have been estimated by assuming that they arise solely from the interactions of the RF electric fields with the plasma. The resulting field equations have been manipulated to give the magnitudes of the fields in terms of the power flow. Near the plasma and cyclotron frequencies (resonances) the field magnitudes become very large for moderate values of the power flow. Therefore, in order to utilise a propagating mode for plasma generation, the signal frequency should be close to one of the resonances. The cyclotron resonance is the natural choice since its value does not depend on the plasma density. Conversely, if the plasma-loaded waveguide is to be used for the transmission of high RF powers, then the resonant frequencies should be significantly higher than the signal frequency. That is, the plasma frequency and the cyclotron frequency should be as high as possible.

Waveguides which contain a magnetised plasma column which does not completely fill the waveguide exhibit Faraday rotation of the plane of polarisation. This effect is a function of the plasma parameters and varies approximately quadratically with the plasma frequency.

III.4 Summary

An empty waveguide has a cut-off frequency below which propagation does not occur. When, however, a plasma is introduced into the waveguide a new set of modes appears with frequencies below the waveguide cut-off frequency. The characteristics of the plasma waves depend on the geometry and the plasma parameters; they are summarised in Table III.4.1.

	plasma filled guide	partially filled guide
$\omega_c=0$	$\omega_{cop}=\omega_{co}+\omega_p$ P=0 for $\omega<\omega_{cop}$	Forward surface wave $0<\omega<\omega_p$
$0<\omega_c<\omega_p$	Forward wave: $0<\omega<\omega_c$ Backward wave: $\omega_p<\omega<(\omega_p^2+\omega_c^2)^{1/2}$	Surface / electromagnetic wave axially symmetric modes $\omega_{co}=\omega_p$ higher order modes $\omega_{co}>\omega_p$
$\omega_c=\omega_p$	Forward wave: $0<\omega<\omega_p$ Backward wave: $\omega_p<\omega<2^{1/2}\,\omega_p$	
$\omega_c>\omega_p$	Forward wave: $0<\omega<\omega_p$ Backward wave: $\omega_p<\omega<(\omega_p^2+\omega_c^2)^{1/2}$	Faraday rotation
ω_c=infinity	TM forward wave: $0<\omega<\omega_p$	TM forward wave cut off frequencies as above Faraday rotation

Table III.4.1: Summary of propagation in plasma-loaded waveguides.

For applications which require a microwave sustained discharge, the pump wave should have a frequency close to one of the plasma resonances, in which case, the field strengths become very large for relatively small RF powers. Conversely, for plasma waveguide applications in microwave power components the signal frequency should be very different from the plasma resonances so that the signal fields do not perturb the equilibrium of plasma generation.

III.5 References

[1] Propagation of electromagnetic waves in a refracting medium in a magnetic field, D. R. Hartree,Proc. Cambridge Phil. Soc., **27**, p143, 1931.

[2] Vibrational properties of an electron gas, A. A. Vlasov, Sov. Phys. JETP, **8**, p291 1938.

[3] Electron plasma oscillations, L. D. Landau, J. Phys. (USSR), **10**(25) p25, 1946.

[4] Cosmical Electrodynamics, H. Alfven, Clarendon Press, Oxford, 1950.

[5] Waves in Anisotropic Plasmas, W. P. Allis, S. J. Buchsbaum, A. Bers, MIT Press, 1963.

[6] Slow-Wave Propagation in Plasma Waveguides, A. W. Trivelpiece, San Fransisco Press, 1967.

[7] Relativistic plasma microwave oscillator, M. V. Kuzelev, F. Kh. Mukhametzyanov, M. S. Rabinovich, A. A. Rukhadze, P. S. Strelkov and A. G. Shkvarunets, Sov. Phys. JETP, **56**(4), p780, 1982

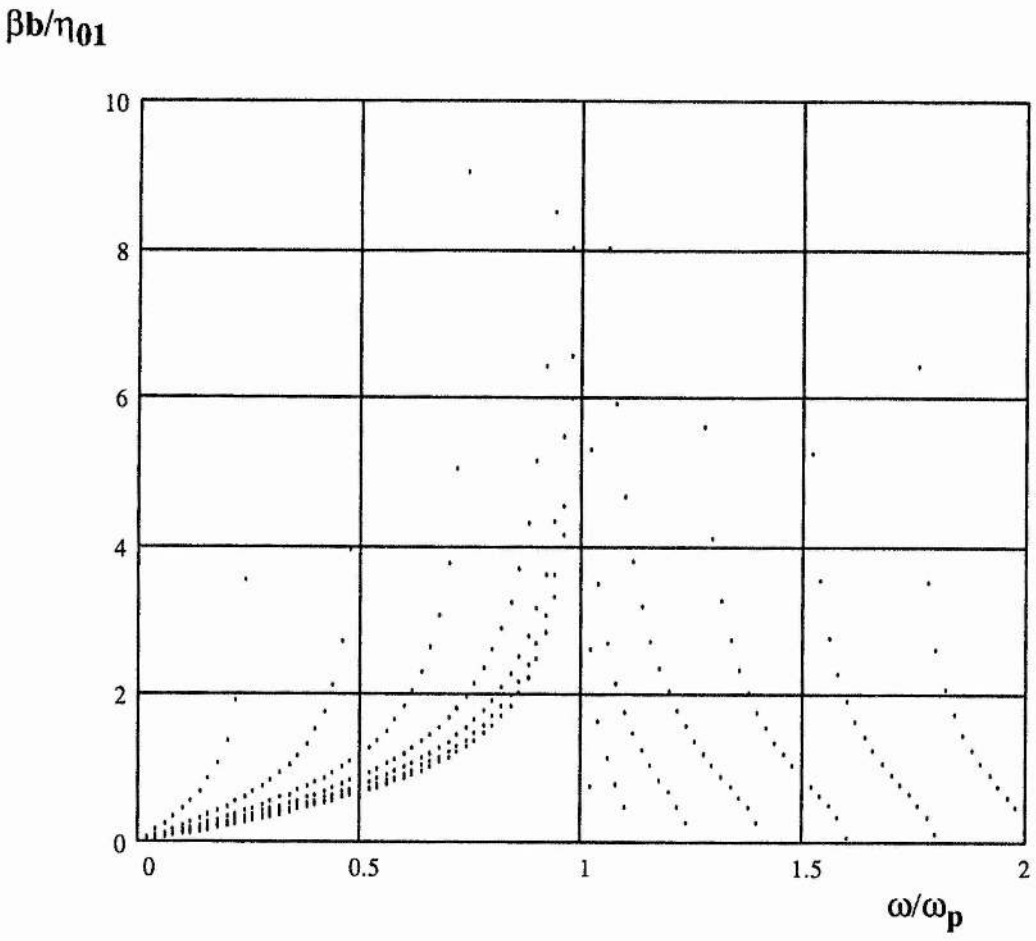

Figure III.3.2.1: The Dispersion Relation for a Plasma-Filled Waveguide for Different Values of the Cyclotron Frequency

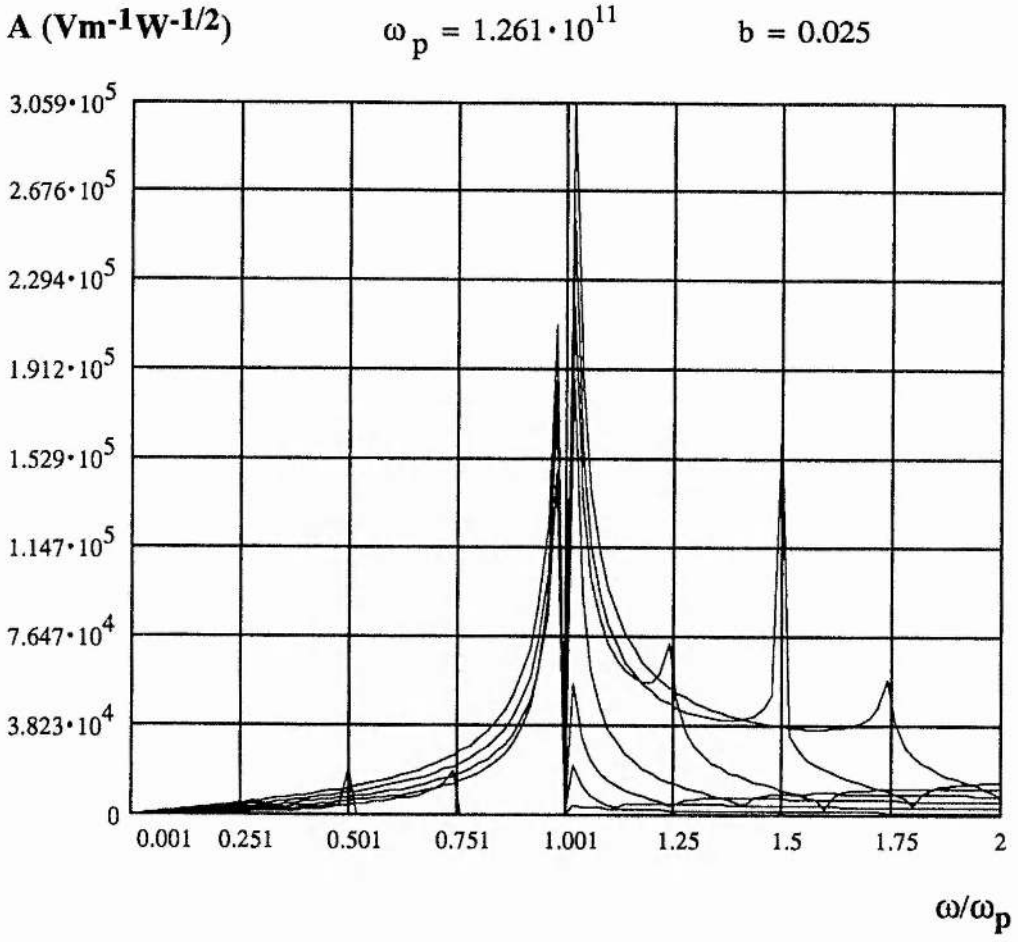

Figure III.3.2.2: The Magnitude of the Electric Field in a Plasma-Filled Waveguide for Different Values of the Cyclotron Frequency

$a = 0.03 \quad b = 0.05 \quad B = 0.005$

$\omega_{\chi} = 8.791 \cdot 10^{8} \qquad \omega_{\pi} = 3.987 \cdot 10^{10}$

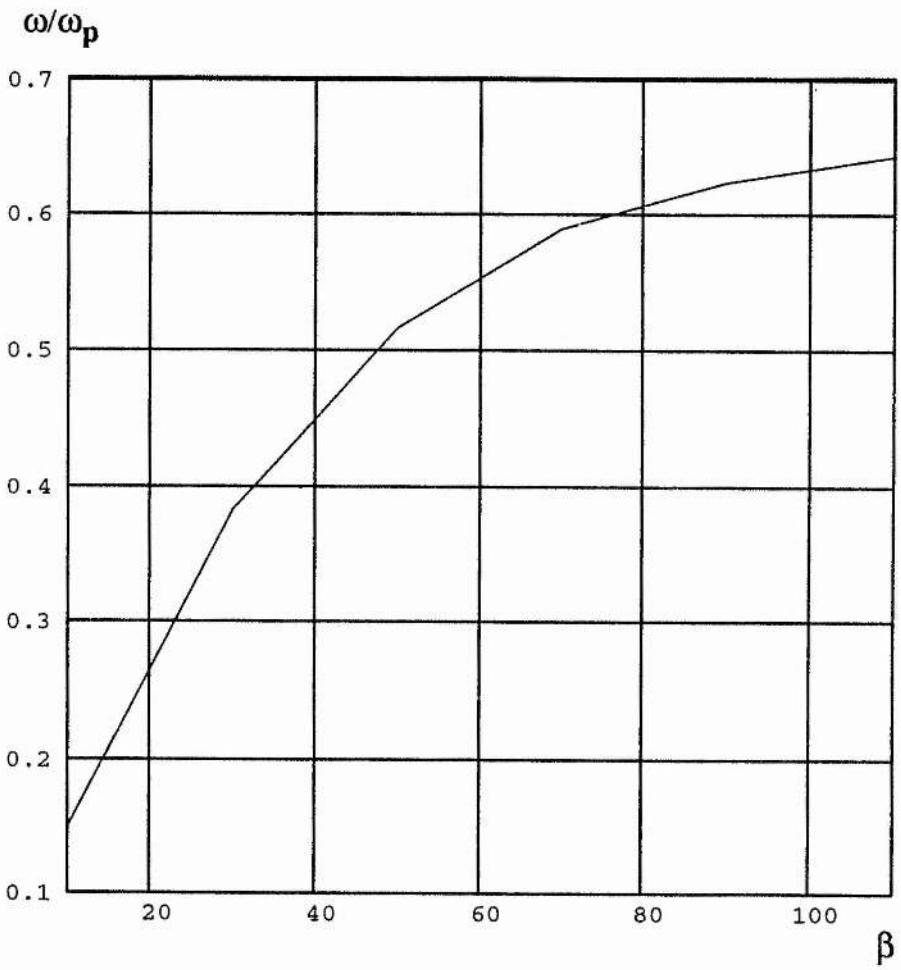

Figure III.3.2.3: The Dispersion Relation for a Plasma Column in a Waveguide

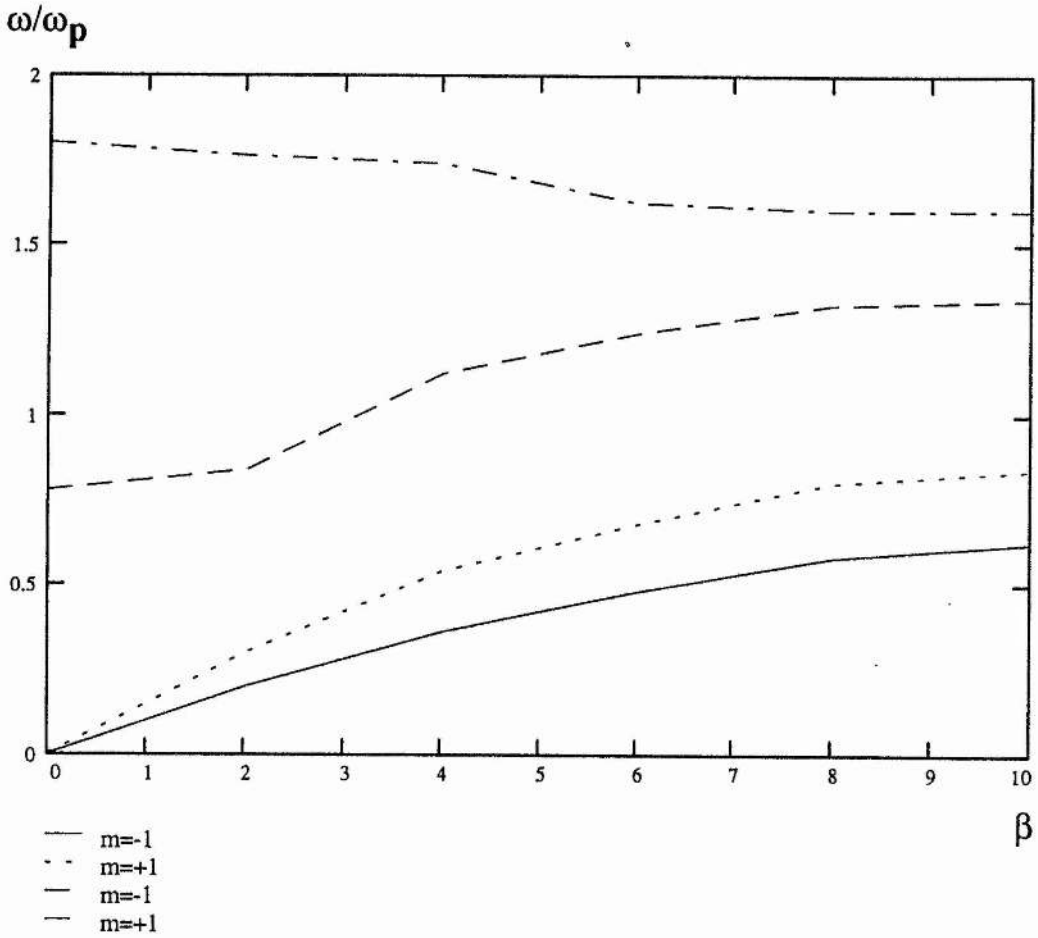

Figure III.3.2.4: The Dispersion Relation for the Components of a Linearly Polarised Wave for a Plasma Column in a Waveguide

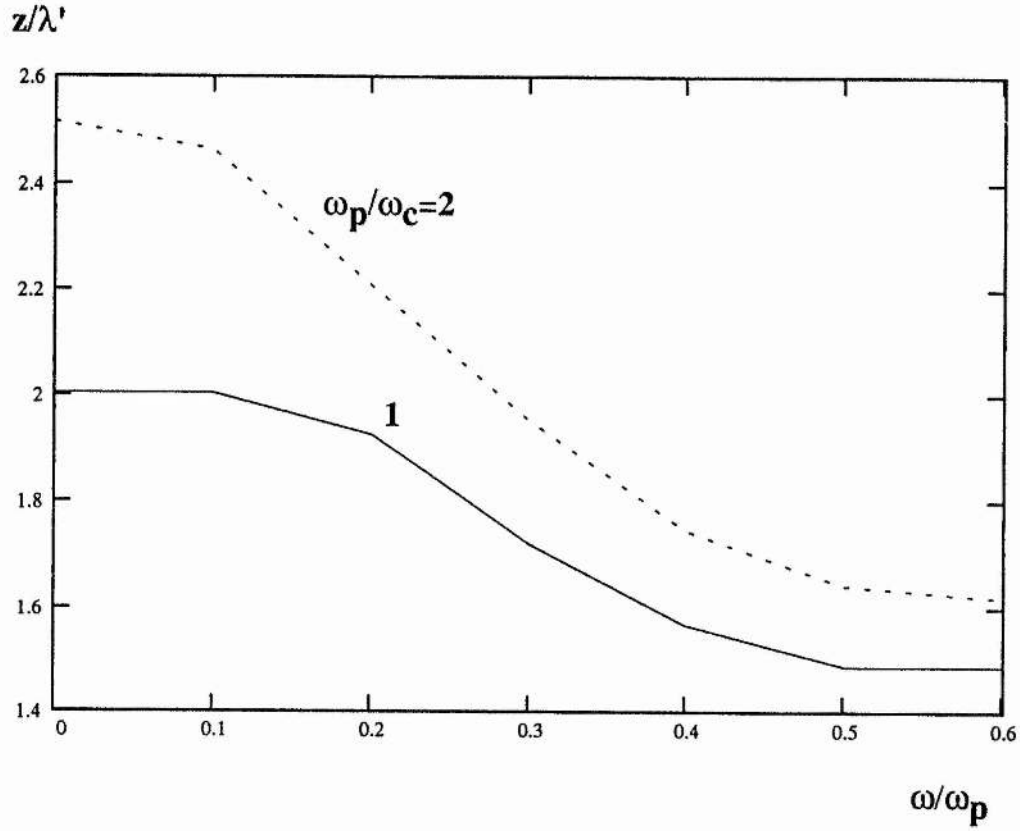

Figure III.3.2.5: Faraday Rotation in a Plasma Waveguide

CHAPTER IV

PLASMA SWITCHING AND PULSE COMPRESSION IN PLASMA WAVEGUIDES

IV.1 Introduction

IV.1.1 Background

Over the last few years there has been an increasing requirement for short pulse, extremely high power (multi-gigawatt) microwave generators. The application areas include controlled fusion, particle accelerators, electromagnetic pulse generators and ultrawideband radar. Many new types of microwave sources such as relativistic magnetrons, superpower travelling wave tubes and free electron lasers have been developed in an attempt to meet with these requirements. All such devices achieve increased peak output powers by increasing the peak electrical power drawn from the supply. There are, however, a number of disadvantages associated with this approach which can limit its usefulness with regard to the afore-mentioned applications.

If the peak electrical power is increased by increasing the peak current, then strong (more than one tesla) magnetic fields are required. Furthermore, high power modulators are bulky and expensive. Alternatively, if the peak power is increased by increasing the operating voltage, then electrical breakdown and diode gap-closure may occur. Additionally, high voltage power supplies, such as Marx generators, operate at low repetition rates.

Alternative methods of increasing the peak power output of a microwave source have been investigated by several researchers. These employ techniques for pulse sharpening to amplify the output of a microwave pulse generator at the expense of the pulse duration. The pulse sharpening schemes fall broadly into two categories: resonant cavity switching and dispersive pulse compression.

IV.1.2 Cavity Dumping

Cavity dumping was proposed as a means of microwave pulse amplification as early as 1964[1]. The basic principle is that energy is stored in a microwave cavity from a source of power P_i for a period τ_i and then released by some mechanism into the load in time τ_o. The output power is then given simply by

$$P_o = P_i \frac{\tau_i}{\tau_o} \qquad \text{(IV.1.2.1)}$$

Clearly this explanation is highly simplified and the effects of loss and mismatch feature in the more sophisticated analysis which follows.

The first experiments in microwave cavity dumpling employed mechanical waveguide switches and met with limited success. Birx *et al* proposed a plasma waveguide switched cavity dumping scheme with a superconducting resonator which gave a power gain of one order of magnitude (1978)[2]. Their system is explained with reference to Figure IV.1.2.1. A superconducting resonator, excited by a low power microwave source, is coupled to arm 1 of a waveguide H-plane T section. Arm 2 couples to a matched load of impedance Z_L and arm 3 contains a gas discharge tube (a TR cell) placed in front of a moveable short. With the discharge off, the tube is effectively transparent to microwaves and reflection occurs at the short. The position of the short is chosen so that arm 2 is located at a minimum of the standing wave field and therefore has a low coupling coefficient with the resonator. When the discharge tube is activated

and a plasma with a sufficiently high number density is formed (such that $\omega_p > \omega$) the microwave fields are reflected at the discharge tube. If the tube is appropriately located, then the standing wave pattern shifts and arm 2 is now located at a field maximum and couples strongly with the resonator. Thus, the stored energy is delivered, through arm 2, to the load in a time characteristic of the transit time of the resonator.

An improved system[3] replaces the discharge tube with a high energy electron beam which is fired through a foil section in the waveguide wall to produce the reflecting plasma layer in a low pressure gas. Using this technique Birx achieved a power gain of the order of 10^4 with an output pulse duration of 15 ns. The electron gun, however, required a 450 kV, 10 kA Marx bank charged blumlein - specifications which are typical for superpower TWT and beam-plasma sources.

A useful analysis of microwave resonant cavity dumping has been given by Alvarez[4]. The stored energy W(t) in a cavity is given by

$$W(t) = \gamma W^* \left[1 - e^{-\alpha t}\right]^2 \qquad \text{(IV.1.2.2)}$$

where we have

$$W^* = P_i \tau_i \qquad \text{(IV.1.2.3)}$$

$$\gamma = 4\beta(1+\beta)^{-2}$$

$$\alpha = \frac{1+\beta}{2\tau_i} = \frac{\kappa}{\tau_i}$$

$$\tau_i = \frac{Q_0}{\omega}$$

$$\beta = \frac{Q_0}{Q_e}$$

and charging begins at t=0. The power of the pump signal is P_i, its frequency is ω and the parameter β is the input coupling factor from the source. The external quality factor, Q_e, refers to the reradiation of power back out through the coupling port. The intrinsic Q of the cavity, Q_0, relates to the losses due to resistive dissipation in the cavity and the overall, or loaded, cavity Q is given by

$$\frac{1}{Q_L} = \frac{1}{Q_0} + \frac{1}{Q_e} \qquad \text{(IV.1.2.4)}$$

We are also able to write down a number of equations governing the build up of energy in the cavity. The instantaneous power dissipation due to cavity losses is

$$\Pi = \frac{W\omega}{Q_0} = \frac{W}{\tau_i} \qquad \text{(IV.1.2.5)}$$

The rate of energy storage is obtained by differentiating equation IV.1.2.2 :

$$\frac{dW}{dt} = \frac{W^*}{\tau_i}(1+\beta)\frac{e^{-\alpha t}}{1-e^{-\alpha t}} \qquad \text{(IV.1.2.6)}$$

The net power flow into the cavity, Φ_i, must account for the rate of energy storage (equation IV.1.2.6) plus the power dissipated in the walls (equation IV.1.2.5) and is given by

$$\Phi_i = P_i\gamma\left[1-e^{-\alpha t}\right]\left[1+\beta\, e^{-\alpha t}\right] \qquad \text{(IV.1.2.7)}$$

For sub-critical coupling (β less than or equal to unity), the maximum power is coupled into the cavity in the asymptotic limit (t tends to infinity). In the case of super-critical coupling, the power coupled into the cavity reaches a maximum value at time

$$t_{max} = \frac{2}{1+\beta}\ln\left[\frac{2\beta}{\beta-1}\right]\tau_i \qquad \text{(IV.1.2.8)}$$

Now, let us assume that energy is stored in the cavity until some time t_c when the coupling parameter β suddenly increases to a value of β' to generate the output pulse. The energy stored in the cavity is given by

$$E_s(t_c) = \int_0^{t_c} \Phi_i(t)\, dt \qquad \text{(IV.1.2.9).}$$

In the energy extraction mode (β') the external Q of the cavity Q_e' is much smaller than the initial value Q_e and the extracted power is given by

$$P_0 = \frac{\omega}{Q_e'} \int_0^{t_c} \Phi_i(t)\, dt \qquad \text{(IV.1.2.10)}$$

As an example, consider the case where there is critical coupling (β=1) during the energy storage stage and the fill-time is long enough so that we have $E_s(t_c)=P_iQ_0/\omega$. The peak power output P_0 immediately after switching is then given by

$$P_o = \frac{E_s(t_c)\,\omega}{Q_e'} = \frac{P_iQ_0}{Q_e'} \qquad \text{(IV.1.2.11)}$$

and the power gain is

$$G = \frac{P_o}{P_i} = \frac{Q_0}{Q_e'} \qquad \text{(IV.1.2.12)}$$

The output power may be taken out of the input port and fed to the load via a circulator or out of a separate port. In the latter case, some power will be re-emitted from the input port, but the magnitude is determined by the original Q_e and is generally small compared to the main output power.

IV.1.3 Dispersive Compression

Early radar systems employed a transmitter pulse compression system which made use of the dispersive properties of waveguide modes. Modern radar systems generally handle the pulse compression in the receiver circuitry. Recent applications for ultrashort microwave pulses, such as wideband radar, have rekindled the interest in waveguide pulse compression systems. Manheimer and Ripin[5] (1986) have proposed a dispersive pulse compression system based on a plasma-loaded waveguide. They propose to obtain plasma densities up to 10^{14} cm^{-3} at up to 100% ionisation using a plasma gun with a magnetic selector and mirror system. Compression of either chirped or fixed frequency pulses is achieved, the latter by altering the plasma parameters in time by methods such as an inverse theta pinch.

The compression of a chirped pulse is explained with reference to Figure IV.1.3.1. The compression medium is assumed to exhibit normal dispersion in the frequency range (f, f+δf) with a corresponding variation in group velocity (v, v–δv). The input pulse has a duration of τ and is chirped from f+δf to f over the duration of the pulse. The consequence of these conditions is that as the pulse propagates down the dispersion line, the trailing edge of the pulse, having a higher group velocity, catches up with the leading edge of the pulse. If the length of the dispersion line is L and the leading edge of the pulse enters the line at t=0, then the leading edge exits the line at

$$t_l = \frac{L}{v-\delta v} \qquad \text{(IV.1.3.1)}$$

and the trailing edge exits the line at

$$t_t = \tau + \frac{L}{v} \qquad \text{(IV.1.3.2)}$$

The compressed pulse length is then

$$\tau' = \tau + \frac{L}{v} - \frac{L}{v-\delta v} \qquad \text{(IV.1.3.3)}$$

and neglecting terms of the order of $\delta v/v$ we obtain

$$\tau' = \tau - \frac{L\delta v}{v^2} \qquad \text{(IV.1.3.4)}$$

The power gain, assuming no loss, is then given by

$$G = \frac{P_o}{P_i} = \frac{\tau v^2}{v^2\tau - L\delta v} \qquad \text{(IV.1.3.5)}$$

Equation IV.1.3.5 predicts infinite gain when $v^2\tau = L\delta v$. In reality the compression ratio is limited by departures from the ideal pulse and dispersion characteristics and, at higher powers, by losses and non-linear effects.

Dispersive compression can be achieved for monochromatic sources by altering the characteristics of the dispersion line as a function of time. Manheimer and Ripin suggest that this temporal variation can be achieved in a highly ionised (≅100%) plasma waveguide using magnetic field effects. The pulse power equipment required for this purpose adds an extra degree of complexity and needs accurate timing.

A much simpler, passive mechanism for dispersive compression in a plasma loaded waveguide is proposed, based on the results of Chapter III. For simplicity, the analysis is given for a plasma-filled waveguide in an infinite longitudinal magnetic field. In principle, pulse compression should occur in an analogous manner for other propagating plasma-loaded waveguide configurations.

The solution of the dispersion relation of a plasma filled guide is given by equation III.3.2.16. The group velocity for an infinite magnetic field is obtained by differentiation, from which we get

$$v = \frac{d\omega}{d\beta} = b\,\omega_p \frac{\eta_{mv}^2}{\left(\beta^2 b^2 + \eta_{mv}^2\right)^{\frac{3}{2}}} \qquad \text{(IV.1.3.6)}$$

Furthermore, from the solution of equation III.3.2.25 shown in Figure III.3.2.2, the magnitudes of the fields are a function of the guide and plasma parameters, the power flow and the frequency. By choosing the values of these parameters the field strengths can be varied over a wide range.

Consider a microwave pulse propagating along the magnetised plasma waveguide. If the magnitudes of the fields in the pulse are such that a small proportion of the pulse energy is lost in producing further ionisation, then the tail of the pulse will see a higher plasma density than the leading edge. The plasma frequency is proportional to the number density to the power one half, so from equation IV.1.3.6, it follows that the tail of the pulse will catch up with the leading edge to produce pulse compression.

In practice the fields in a plasma-filled guide may be so large that a significant proportion of the pulse energy is lost in ionisation processes. The magnitudes of the fields can, however, be reduced with a corresponding increase in power flow if the plasma does not completely fill the waveguide. In this case the plasma loaded waveguide retains its dispersive nature with respect to the plasma frequency.

To see that only a small fraction of the pulse energy is required to produce a significant change in plasma density we can use the experimental results given in sections II.3.8 and 9 in which plasma densities of the order of 10^{12} cm^{-3} are maintained by an ionisation rate of the order of 10^{18} $cm^{-3}s^{-1}$. Assuming an ionisation energy of the order of 15 eV, this corresponds to an absorbed power flux of the order of 2 W cm^{-2}. The only problem, then, is to control the amount of absorption of the RF field. Operation at a frequency which is far removed from the plasma resonances reduces the fields and the resonant absorption. The fields also decrease as the waveguide radius

increases and the proportion of the volume of the waveguide which is filled with plasma decreases.

IV.2 Novel Plasma Waveguide Closing Switch

IV.2.1 Introduction

The design of a novel waveguide closing switch for applications such as microwave cavity dumping is presented. The operation of the switch relies on the fact that plasma loaded waveguides, in general, have a pass-band below the cut-off frequency of the empty waveguide. Thus, a waveguide section can be switched from a non-propagating mode to a propagating mode by the generation of a suitable plasma within the waveguide.

Consider the waveguide transition shown in Figure IV.2.1.1. The waveguide section to the right of the transition has a radius such that its lowest cut-off frequency is lower than the frequency of operation and it therefore appears as an infinite impedance. The reflection coefficient is

$$\rho = \frac{Z_0 - Z_1}{Z_0 + Z_1} = -1 \qquad \text{(IV.2.1.1)}$$

and so the transition is perfectly reflecting. (We use the subscript '0' to denote quantities to the left of the transition and '1' for quantities to the right.) When a suitable plasma is generated in the cut-off section the impedance Z_1 drops and the switch closes. The reflection coefficient for the switch in the closed state is not just the value given by equation IV.2.1.1. The reflection coefficient must be calculated from the electromagnetic scattering matrix for the transition which takes into account the field

matching conditions. Without deriving the quantities for a particular system, an important identity for matching purposes is given by

$$\frac{\int_{\Sigma} \mathbf{F}_0 . \mathbf{F}_1^* \, d\sigma}{F_0 F_1} \equiv 1 \qquad \text{(IV.2.1.2)}$$

where $\mathbf{F}_i$ are the field vectors with magnitude F_i. Equation IV.2.1.2 describes the spatial correlation between the fields in the two sections of waveguide. For example, it was found in Chapter III that for an infinitely strong longitudinal magnetic field only TM modes can exist in the plasma-loaded waveguide. Thus we expect that only a TM mode of the appropriate order will match into this particular plasma waveguide.

Rather than directly match the two sections of the switch, a matching transformer can be used. This may take the form of a stub-tuning system, transformer sections or an adiabatic transition. However, for very fast pulses the use of direct matching or an adiabatic transition are preferred as these methods give the largest bandwidth.

IV.2.2 Waveguide Equivalent of an Optical Saturable Absorber

Optical cavity dumping is commonly implemented using a saturable absorber. The saturable absorber is typically a dye which is normally opaque but rapidly bleaches after absorbing some critical amount of optical radiation. It is, therefore, a self-switching device. After switching there is some finite recovery time before the dye returns to its opaque state.

The plasma waveguide closing switch shown in Figure IV.2.2.1 behaves in an exactly analogous manner to an optical saturable absorber in a laser cavity. As the fields in the resonator build up in accordance with equation IV.1.2.2 some ionisation occurs in the

cut-off waveguide section. The longitudinal magnetic field confines the plasma in the transverse directions but allows longitudinal diffusion to occur. The plasma density increases until the cavity fields can match into a propagating mode of the waveguide. Rapid ionisation of the guide occurs and the switch closes, dumping the stored energy into the load. After the end of the power pulse the waveguide switch has a recovery time characteristic of the plasma decay in the afterglow.

The design of a waveguide saturable absorber ("WSA") is considered with reference to the results of Chapter III, together with section IV.2. The starting point is that the operating frequency should be smaller than the lowest free-space waveguide cut-off frequency. For a circular free-space waveguide of radius b, the cut-off frequencies given by equation III.2.2.11 are, for TE modes:

$$f_{cmv}^{TE} = \frac{\eta'_{mv}}{2\pi b\sqrt{\mu_0\varepsilon_0}} \qquad \text{(IV.2.2.1)}$$

and for TM modes:

$$f_{cmv}^{TM} = \frac{\eta_{mv}}{2\pi b\sqrt{\mu_0\varepsilon_0}} \qquad \text{(IV.2.2.2)}$$

where

$$J_m(\eta_{mv}) = 0 \qquad \text{(IV.2.2.3)}$$

$$J'_m(\eta'_{mv}) = 0 \qquad \text{(IV.2.2.4)}$$

and J_m is a Bessel function of order m, and J'_m is its derivative. The first few modes, in order of increasing cut-off frequency, are TE_{11}, TM_{01}, TE_{21}, TE_{01}/TM_{11} and so on.

For a waveguide radius of 2.5 cm, for example, the cut-off frequency of the lowest TE_{11} mode is 3.5 GHz.

The fact that the plasma is generated by the main power flux in the switch section means that, even with a strong axial magnetic field, the plasma will fill the waveguide, albeit with some radial density distribution. Now it was concluded from the solution of equation III.3.2.25 for the power flow in a plasma-filled guide that the power is maximised when we have $f<<f_p$. The plasma frequency is expressed conveniently as

$$f_p = 8.98 \times 10^3 \, n_e^{\frac{1}{2}} \quad \text{Hz} \qquad \text{(IV.2.2.5)}$$

where the electron number density n_e refers to cm^{-3}. Typical microwave sustained plasmas have number densities of the order of 10^{13} cm^{-3} which correspond to plasma frequencies of the order of 30 GHz.

For a 3 GHz Waveguide Saturable Absorber (WSA), a switch radius of 2.5 cm satisfies the free-space waveguide cut-off criterion. Reference to Figure III.3.2.2 shows that with these parameters and a typical plasma frequency of 30 GHz, the maximum field strengths are less than the order of 100 V m^{-1} $W^{-1/2}$. With a propagating power of 1 MW the field strengths may be as high as 100 kV m^{-1}. There are two implications of such field strengths. First of all, the discrepancy between the switch propagation characteristics and the free-space waveguide characteristics reduces the matching to the switch. Secondly, breakdown effects and nonlinear plasma response are important. Depending on the particular conditions, these nonlinear responses may provide additional pulse compression in the manner described in section IV.1.3.

The WSA is, then, a potentially useful device for cavity dumping applications. There are, however, two areas in which its performance may be less than ideal. The first has already been discussed and relates to the high field strengths which may occur. The ultimate limiting factors on this restriction are the maximum attainable plasma density

and the waveguide cut-off condition. The second area of the WSAs performance which may in some instances be unsatisfactory is that of shot-to-shot variation. Because the switch breaks down spontaneously under the influence of the fields from the stored energy it is impossible to determine the exact moment that breakdown occurs. Thus, the breakdown conditions may vary between shots in an unpredictable manner. In some applications accurate timing and reproducibility may be important.

IV.2.3 Triggered Waveguide Switch

The problems of shot-to-shot reproducibility and high field strengths anticipated in the waveguide saturable absorber may both be solved in the proposed triggered waveguide switches ("TWS"). The main features of the TWS are shown in Figure IV.2.3.1. Reproducibility of a plasma waveguide switch can be improved if plasma generation is triggered at some fixed time in the charging cycle. A number of triggering mechanisms are feasible, using such techniques as electrical discharge, optical and electron beam preionisation. To begin with, however, we consider a waveguide switch which is triggered using the microwave helical discharge described in section II.3.7.

In section IV.2.2 it was shown that because the WSA is filled with plasma, the maximum waveguide radius (from the free-space cut-off condition) limits the maximum power controlled by the switch. The power flow in the switch can be increased (and the matching to the free-space waveguide improved) if the plasma does not completely fill the waveguide. Now it was shown in sections II.3.7 and 8 that a helical structure excited by a microwave signal generates electric fields which are very intense close to the helix. With no applied magnetic field, a plasma which is either annular or fills the volume may be generated, depending on the gas pressure. In the presence of an intense longitudinal magnetic field, however, the plasma can be confined to a thin annular region surrounding the helix. A waveguide containing such a plasma

can handle much higher peak powers than a plasma-filled waveduide and is more easily coupled into the main waveguide system.

In terms of the plasma produced by the microwave helix, the intense magnetic field acts to decrease the transverse diffusion coefficients in the plasma, which greatly reduces the wall losses. The number density of charged particles in the annular plasma will, therefore, be high so that the operating frequency can be further removed from the plasma resonance. This condition also increases the power flow for a given RF field strength.

Careful consideration must be given to the design of the helix for the following reason. A free-space waveguide containing a helical slow wave structure can support propagating modes with frequencies below the cut-off frequency of the waveguide. It is possible, then, that when the switch is in the off state there may be sufficient leakage to seriously reduce the Q of the resonator. It is even possible that the coupling from the resonator onto the helical structure might be sufficient to cause the switch to close before it is triggered. (This effect may, in fact, be put to good use in a WSA device.) In order to avoid leakage and self triggering the helically loaded waveguide must be designed so that it is poorly matched to the resonator until the trigger signal is applied. In the implementation shown, this is achieved by stopping the helix short of the end of the switch. When the switch is triggered the remaining gap fills with plasma which diffuses along the magnetic field lines.

In Chapter III it was found that the microwave fields in a waveguide partially filled with plasma are greatest near the plasma boundary. In the case of a waveguide loaded with an annular plasma, then, the fields also have an annular form. In attempting to satisfy the spatial matching condition IV.2.12, we require a waveguide mode for the resonator and output coupler which has this annular form. One option would be to choose one of the axially symmetric modes of a circular waveguide. However, the problem with this choice is that, since the cut-off frequency of a circular waveguide

increases with the order of the mode, the resonator and output coupler radii must be increased and this has a deleterious effect on the coupling.

A much better choice for the resonator and output coupler is the coaxial geometry shown in Figure IV.2.3.1. Coaxial waveguide allows a TEM mode (with no lower cut-off frequency) which can couple strongly to the plasma waveguide mode since the change in structure of the field in the transformation between the guided wave and the plasma wave is minimal. This is consistent with the results of Kuzelev *et al* who use a coaxial output coupler in their relativistic plasma Cerenkov maser[6] which operates at powers in excess of 100 MW.

The use of a coaxial coupling geometry also lends itself particularly well to glow discharge electron beam (GDEB) triggering of the microwave waveguide switch. An example of how this might be implemented is shown in Figure IV.2.3.2. In the open state the switch section is, as usual, below cut-off. When the GDEB is switched on, an annular plasma is rapidly formed and the microwave switch closes by the plasma waveguide mechanism discussed in Chapter III. In this configuration it is also possible that the electron beam may itself provide some coupling through the switch section. There is also the possibility that the electron beam may drive a Cerenkov instability in the plasma waveguide system. To obtain significant power levels from this instability would, however, require very high electron beam powers. For applications of the plasma waveguide switch where the specific intention is to generate high peak power microwaves without the need for high peak power driving circuitry, the Cerenkov instability is unlikely to be significant.

IV.3 Conclusions

The results of an analysis of microwave discharges and plasma loaded waveguides has resulted in the proposal of novel methods of high power microwave pulse compression.

Pulse compression allows very high peak powers to be obtained from microwave sources of moderate power, at the expense of the pulse duration. A high power microwave pulse propagating along a plasma loaded waveguide can interact with the plasma and background gas to produce spatio-temporal dispersive compression of the pulse. The effect can be controlled by means of the waveguide radius, the plasma frequency and geometry and externally applied magnetic fields to produce a working dispersive pulse compression system.

Resonant cavity dumping schemes for microwave pulse compression require efficient, high power waveguide switches. A new kind of high power microwave waveguide switch has been proposed. The switch relies on the property of plasma loaded waveguides that propagating modes exist below the normal cut-off frequency of the waveguide. A waveguide transition which normally has a reflection coefficient of unity because of a section below cut-off can be transformed into a highly transmitting transition by the generation of a (magnetised) plasma in the waveguide.

In a self-triggering implementation of the microwave plasma waveguide switch the plasma is generated initially by the action of the evanescent fields in the cut-off waveguide. When the stored energy is high enough, a plasma of sufficient density to switch the waveguide into a propagating mode is formed. Rapid ionisation occurs, thus driving the switch into a transmitting mode and dumping the stored energy into the load.

In an externally triggered implementation, the plasma is created by a helical microwave discharge. Under the influence of an external magnetic field the plasma is in the form of a thin annulus. This arrangement increases the power flow in the switch and allows the insertion loss to be minimised by using coaxial waveguide couplers. Furthermore, the external trigger allows accurate timing of the switch and reduces shot-to-shot variations.

In another implementation of external triggering for the plasma waveguide switch, the plasma is produced by a glow discharge electron beam. An advantage of this technique is that a high level of isolation can be achieved in the off-state and that self-triggering consequently represents less of a problem.

IV.4 References

[1] Rome Air Development Centre Technical Report, C. Buntschuh and M. Gilden, RADC-TDR-64-204 (1964) (unpublished).

[2] Microwave power gain utilizing superconducting resonant energy storage, D. Birx, Appl. Phys. Lett. **32**(1) p68, 1978.

[3] Microwave energy compression using a high-intensity electron beam switch, D. Birx and D. Scalapino, J. Appl. Phys. **51**(7) pp3629-3631, 1980.

[4] Some properties of microwave resonant cavities relevant to pulse-compression power amplification, R. A. Alvarez, Rev. Sci. Instrum. **57**(10) pp2481-2488, 1986.

[5] High power microwave pulse compression, W. Manheimer and B. Ripin, Phys. Fluids **29**(7) pp2283-2291, 1986.

[6] Relativistic plasma microwave oscillators, M. V. Kuzelev, F. Kh. Mukhametzyanov, M. S. Rabinovich, A. A. Rukhadze, P. S. Strelkov and A. G. Shkvarunets, Sov. Phys. JETP **56**(4) p780, 1982.

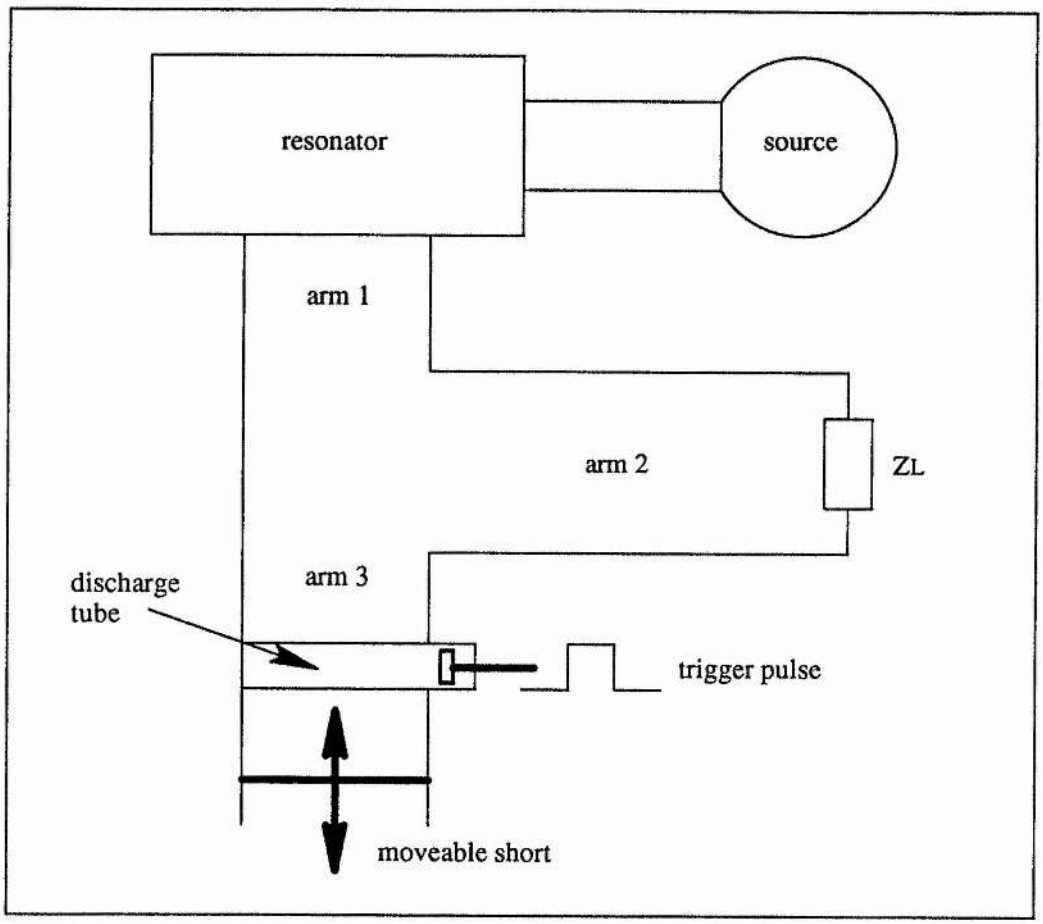

Figure IV.1.2.1: Cavity Dumping Using a TR Cell

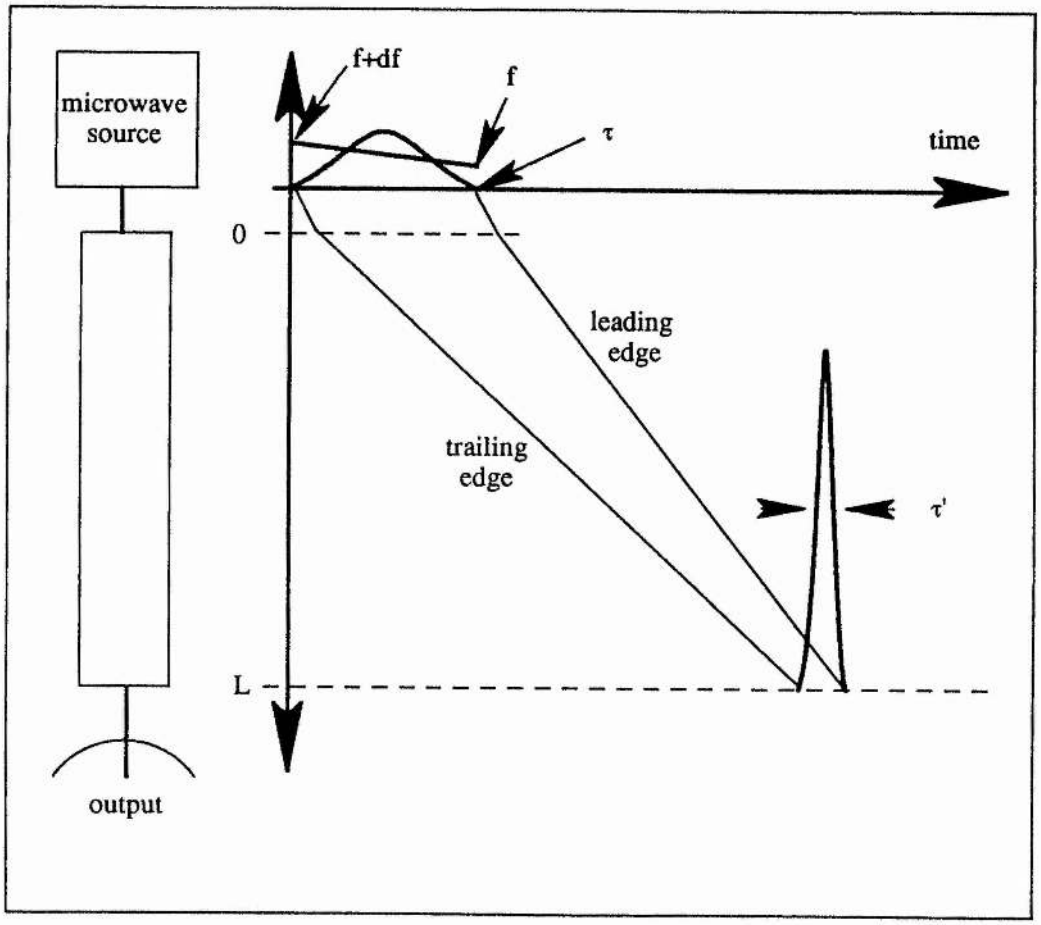

Figure IV.1.3.1: Dispersive Pulse Compression

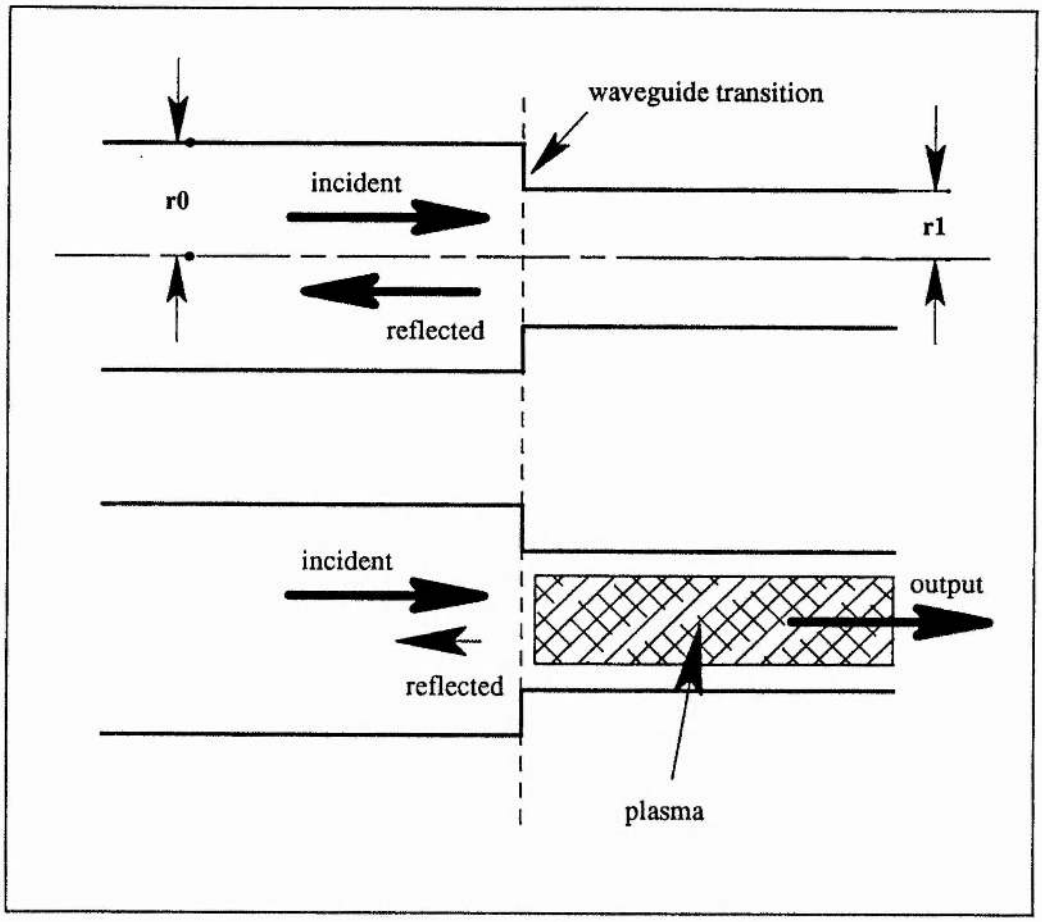

Figure IV.2.1.1: Schematic Diagram of the Plasma Waveguide Switch

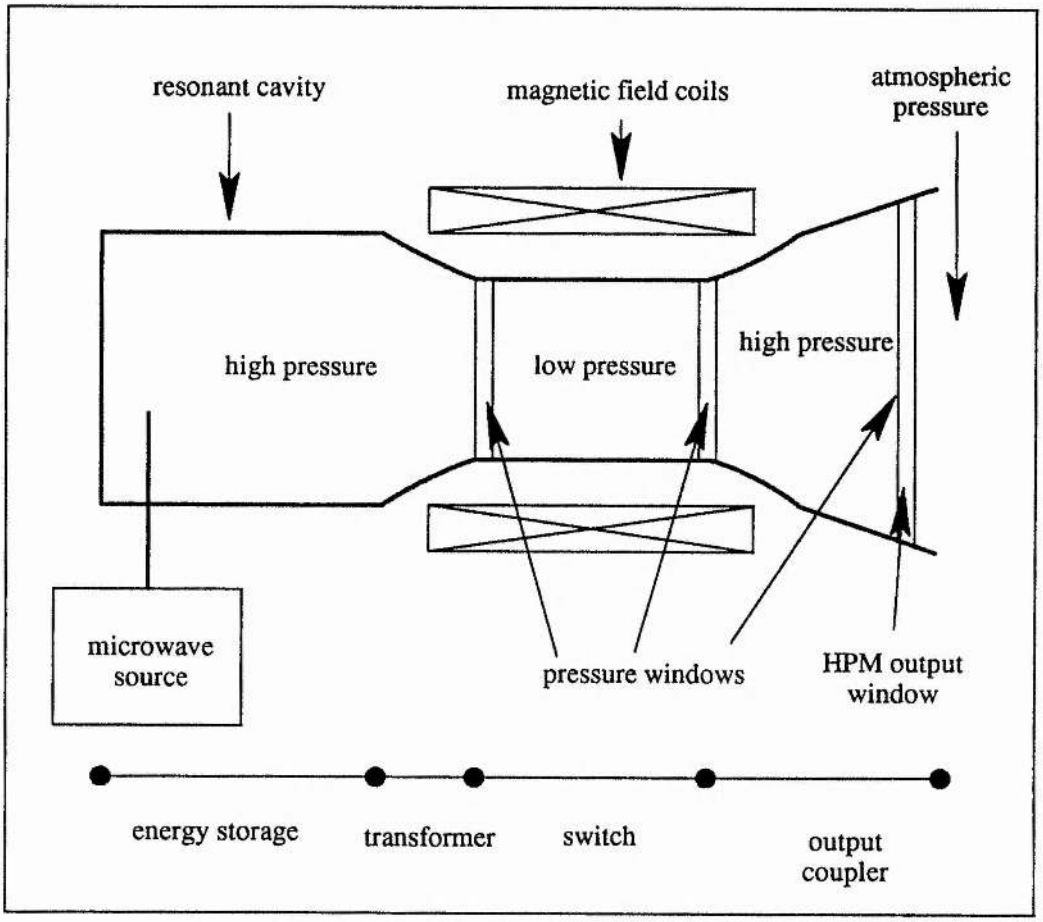

Figure IV.2.2.1: A Pulsed Microwave Source Employing the Waveguide Saturable Absorber

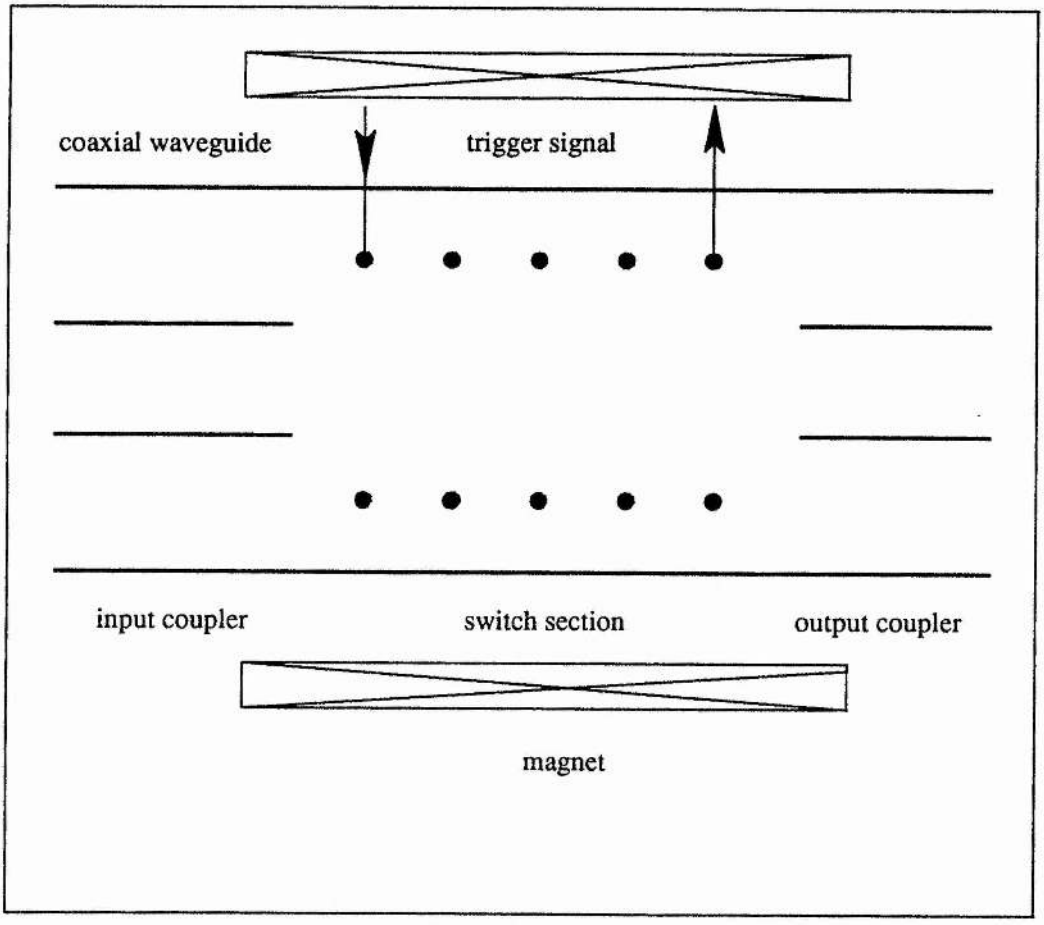

Figure IV.2.3.1: A Microwave Helix-Triggered Plasma Waveguide Switch

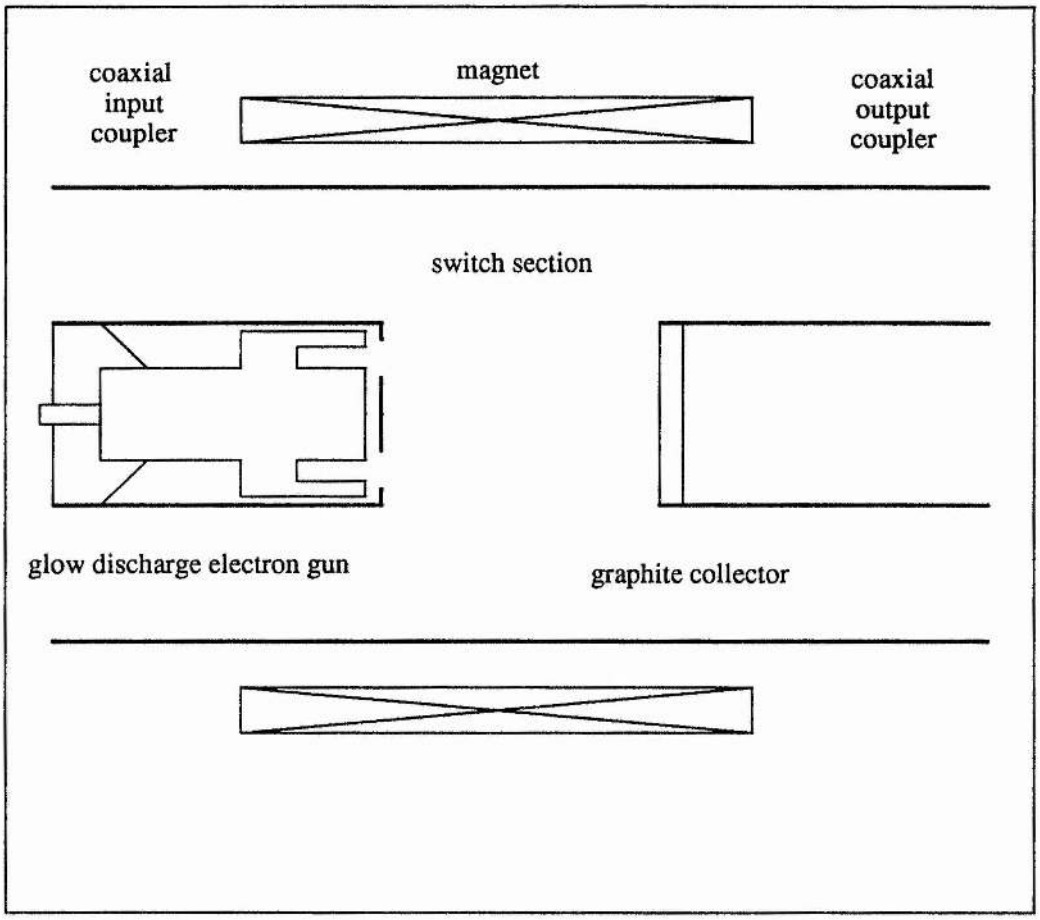

Figure IV.2.3.2: A Glow Discharge Electron Beam-Triggered Plasma Waveguide Switch

CHAPTER V

THE GLOW DISCHARGE INVERTED MAGNETRON

V.1 Introduction

Since its introduction in 1921 the magnetron has developed into one of the most efficient and rugged sources of microwave radiation at decimetre through sub-centimetre wavelengths[1-3]. In conventional magnetrons voltages up to a few tens of kilovolts are applied between the anode block and a thermionic cathode, giving microwave output powers up to hundreds of kilowatts with conversion efficiencies which can be in excess of 70%.

In the late 1970's the relativistic magnetron was developed to produce higher power microwaves[4-12]. These devices typically employ field emission cathodes at several hundred kilovolts relative to the anode structure to produce currents up to several hundred kiloamps, and are capable of delivering microwave pulses into the gigawatt range (although the conversion efficiency is typically less than 30%).[13]

There are several problem areas associated with the operation of a relativistic magnetron. The design of modulators capable of producing high peak voltages and powers at high repetition rates is both difficult and expensive. An associated problem is that of electrical breakdown: the physical dimensions of the magnetron and its supporting structure are restricted by the insulation characteristics required to support the high voltages used to drive the magnetron. All relativistic magnetrons have so far operated at much lower conversion efficiencies than conventional magnetrons (typically

lower than 30%) which can lead to thermal management problems when stable operation at high average powers is required. Furthermore, the bombardment of the anode block by high energy electrons damages the anode structure: the useful lifetime of an anode block may be only a few tens of shots.[14]

In order to support an azimuthally rotating Brillouin space-charge cloud, the applied magnetic field must exceed a critical value B_0 given by the Hull criterion:

$$B_0 = \frac{m_0 c}{e d_e}\left[\gamma_0^2 - 1\right]^2 \qquad \text{(V.1.1)}$$

where we have

$$\gamma_0 = \left[1 + \frac{eV}{m_0 c^2}\right] \qquad \text{(V.1.2)}$$

with

$$d_e = \frac{r_a^2 - r_c^2}{2\, r_a} \qquad \text{(V.1.3)}$$

and the other symbols have their usual meaning. For field emission the anode-cathode gap, and hence d_e, is small; for relativistic operation, the diode operating voltage V is large. Thus large magnetic fields (typically of the order of one tesla) are required to meet the Hull criterion. This either greatly increases the overall weight of the device (if the magnetic field is derived from a permanent magnet) or introduces an additional power supply and thermal management problem (if an electromagnet is used).

An undesirable phenomenon associated with field emission across a narrow gap is that of gap closure: the plasma sheath formed around the cathode drifts across the anode-cathode gap to produce a short-circuit. Although the high magnetic field does have an insulating effect, gap closure is probably a major cause of the RF pulse shortening seen in relativistic magnetrons.[14]

The design of a new type of magnetron, the "Glow Discharge Inverted Magnetron" (GDIM), is presented. The GDIM (Figure V.1.1) has three main features:-

(i) The electron beam is derived from a cold cathode glow discharge in a low pressure filler gas.

(ii) The electron beams are emitted from the cavities of the slow-wave structure.

(iii) The cathode surrounds the anode coaxially, i.e the magnetron is inverted.

(iiv) The slow wave circuit appears on the cathode, not the anode block.

In sections V.2,3 and 4 the general principles underlying the above features are discussed, drawing on the results of previous research to demonstrate the plausibility of the device. In section V.5 the design of a strapped, slot-type GDIM is presented. Although there are certain advantages to other magnetron geometries (eg rising sun, slot-and cavity), the slot structure is somewhat easier to analyze in terms of RF circuit characteristics and electron beam formation dynamics, and strapping is a convenient means of separating the desired operating mode. The analysis takes no account of space charge due to ionization of the filler gas, as the resulting Poisson equation is intractable. The use of strapping provides an extra degree of freedom with which to tune the magnetron to compensate for possible space-charge effects.

V.2 Formation of Electron Beam

Published results show that electron beams with current densities of the order of 20 A cm^{-2} can be generated in a pulsed, cold cathode glow discharge in helium at a

pressure of the order of 1 mbar.[15,16] In particular, beam formation and the current density are enhanced if the cathode is slotted[16] (Figure II.2.4.1). It has further been found that for a glow discharge in helium at this pressure the optimum dimensions for the cathode slot are a depth of 1.5 cm and a diameter of 4 mm. Any increase in the slot depth above 1.5 cm results in no change in the beam current (this is relevant to the rising sun GDIM).

For electron beam formation it is imperative that the discharge should not be allowed to develop into a hollow cathode discharge (HCD) which has a low impedance and effectively shorts the anode-cathode gap. We therefore arrange for the discharge to occur in the negative-gradient region (left-hand side) of the Paschen curve (Figure II.2.1.2). The minimum anode-cathode distance (i.e between the slots) is set such that the breakdown voltage across this short gap is higher than the operating voltage of the magnetron. An electron beam is then formed only where breakdown can occur – along the long path from inside a cathode slot to the anode.

General magnetron theory[2,3] shows that for good Brillouin cloud formation (required for efficient magnetron operation), the initial electron velocity should be radial. The (DC) field configuration around the cathode slots during beam formation (see Figure II.2.4.1) acts to focus the electron beam so that the electron trajectories are very nearly perpendicular to the surface of the cathode. The mechanism of beam formation in the GDIM tends to produce a beam with the desired radial velocity characteristic.

Furthermore, the current densities attainable with a non-relativistic, cold cathode glow discharge are more than an order of magnitude higher than those obtainable from a thermionic cathode. This suggests that the microwave power output from a GDIM might be an order of magnitude greater than that from a conventional magnetron, if a high conversion efficiency can be achieved.

V.3 Magnetron Geometry

In a conventional magnetron the anode, being the outermost electrode, is generally earthed and a negative voltage is applied to the cathode. Any electrons which acquire an axial velocity tend to sink to the earth structure. This forms a shunt current in parallel with the resonant system which reduces the conversion efficiency of the magnetron. This problem is usually overcome by the use of end-hats which are electrically connected to the cathode.

At higher voltages there is a tendency for electrical breakdown and arcing to occur between the end-hats and the anode. For this reason, end-hats are rarely employed in relativistic magnetrons. Even for operating voltages of the order of tens of kilovolts electrical breakdown can be a problem.

In the inverted magnetron the cathode forms the outer structure so in this case it is the cathode which is earthed, with a positive voltage being applied to the anode. Now any electrons, with axial velocities, that sink to earth are simply returning to the cathode potential and so do not form a shunt current in parallel with the anode-cathode circuit.

Conventionally, the slow-wave structure has been placed on the anode block. This leads to problems in coupling the microwave power out of an inverted magnetron. In most inverted magnetrons the power is extracted coaxially from the centre of the magnetron. This is not an ideal solution and better results have been obtained by coupling the microwave power through large apertures in the cathode (Figure V.3.1). This method, however, introduces loading asymmetries and also disrupts the electric field configuration.

In the GDIM the slow-wave structure appears on the cathode, so power can be extracted from one or more of the resonators in the usual manner (see Figure V.5.2). It is not immediately clear that there is a coupling mechanism between the RF circuit of the GDIM and the space-charge cloud. We postulate that strong coupling appropriate for

efficient microwave generation is possible and propose two possible mechanisms to justify this postulate.

V.4 RF Signal Coupling

In order to study the propagation of signals across the Brillouin cloud we analyze a planar geometry and neglect collision, thermal spread and relativistic effects. The analysis is treated as a perturbation problem, taking Brillouin flow as the unperturbed state and neglecting second order effects. With reference to Figure V.4.1, the velocities are given by

$$\frac{dx}{dt} = \omega_B y + u \tag{V.4.1}$$

$$\frac{dy}{dt} = v \tag{V.4.2}$$

$$\frac{dz}{dt} = w \tag{V.4.3}$$

where, as usual, we have

$$\omega_B = \frac{eB}{m} \tag{V.4.4}$$

so that the Brillouin drift is $\omega_B y$. The Lorentz equation for the electron dynamics gives

$$\frac{d}{dt}(\omega_B y + u) = \frac{e}{m}\frac{\partial V}{\partial x} + \omega_B v \tag{V.4.5}$$

or, since dy/dt=v, we have

$$\frac{du}{dt} = \frac{e}{m}\frac{\partial V}{\partial x} \tag{V.4.6}$$

We also have

$$\frac{dv}{dt} = \frac{e}{m}\frac{\partial}{\partial y}\left[\frac{m\omega_B^2 y^2}{2e} + V\right] - \omega_B(\omega_B y + u) = \frac{e}{m}\frac{\partial V}{\partial y} - \omega_B u \tag{V.4.7}$$

where the Brillouin potential is given by

$$V_B = \frac{m\omega_B^2 y^2}{2e} \qquad \text{(V.4.8)}$$

and

$$\frac{dw}{dt} = \frac{e}{m}\frac{\partial V}{\partial z} \qquad \text{(V.4.9)}$$

The unperturbed Brillouin flow terms have been cancelled so that equations V.4.5-9 are for RF quantities only. Poisson's equation is:

$$\nabla^2 V = \frac{\rho}{\varepsilon} \qquad \text{(V.4.10)}$$

and conservation of charge considerations give:

$$\frac{d}{dt}\left[\frac{\varepsilon m\omega_B^2}{e} + \rho\right] = -\left[\frac{\varepsilon m\omega_B^2}{e} + \rho\right]\left[\frac{\partial(\omega_B y + u)}{\partial x} + \frac{\partial v}{\partial y} + \frac{\partial w}{\partial z}\right] \qquad \text{(V.4.11)}$$

Equation V.4.11 linearizes to give

$$\frac{\partial \rho}{\partial t} = -\frac{\varepsilon m\omega_B^2}{e}\left[\frac{\partial u}{\partial x} + \frac{\partial v}{\partial y} + \frac{\partial w}{\partial z}\right] \qquad \text{(V.4.12)}$$

The Brillouin state is uniform in x,z and t but not in y. We assume, therefore, that RF quantities vary as $\exp(j\omega t - j\beta x - j\gamma z)$. We further assume that β and γ are real and allow ω to be complex (i.e we consider the case of an oscillator rather than an amplifier). We can now substitute for the partial derivatives with respect to t, x and z in equations V.4.5-10 and 12 . The full time derivative is given by

$$\frac{d}{dt} = \frac{\partial}{\partial t} + \omega_B y \frac{\partial}{\partial x} = j\omega - j\omega_B y = j\omega_e \qquad \text{(V.4.13)}$$

where we have

$$\omega_e = \omega - \omega_B \beta y \tag{V.4.14}$$

Equations V.4.5-10 and 12 can now be simplified to give

$$u = -\frac{e\beta V}{m\omega_e} \tag{V.4.15}$$

$$v = -\frac{j}{\omega_e}\left[\frac{e}{m}\frac{\partial V}{\partial y} + \omega_B \frac{e\beta V}{m\omega_e}\right] = -j\frac{\partial}{\partial y}\left[\frac{eV}{m\omega_e}\right] \tag{V.4.16}$$

$$w = -\frac{e\gamma V}{m\omega_e} \tag{V.4.17}$$

$$\rho = \varepsilon\left[\frac{\partial^2}{\partial y^2 - \beta^2 - \gamma^2}\right]V \tag{V.4.18}$$

$$\left[\frac{\partial^2}{\partial y^2 - \beta^2 - \gamma^2}\right]V = \frac{\omega_B}{\omega_e}\left[\frac{\partial^2}{\partial y^2 - \beta^2 - \gamma^2}\right]\frac{\omega_B}{\omega_e}V \tag{V.4.19}$$

Rewriting equation V.4.19 in terms of the variable $s = \omega_e/\omega_B$, we are able to obtain a physical interpretation of the propagation equation. The recast equation is

$$\left[\frac{\partial^2}{\partial s^2} - 1 - \left(\frac{\gamma}{\beta}\right)^2 + (1-s^2)^{-2}\right][1-s^{-2}]^{1/2} V = 0 \tag{V.4.20}$$

We now see that, rather than the voltage, V, the quantity $(1-s^{-2})^{1/2} V$ propagates across the cloud under the influence of a "refractive index" which is a function of s. The results of a numerical solution of equation V.4.20 are shown in Figure V.4.2, where the velocity perturbation u=g(s) has been evaluated from equation V.4.15. For negative s the velocity perturbation is everywhere greater than unity, except at the plasma resonance s=–1 where its value is one. These results imply that it is possible for RF fields to couple from the resonant cavity formed between the anode and the cathode to the resonant slow wave structure on the cathode, in spite of the presence of the Brillouin cloud.

There is, in fact, a precedent for the inclusion of an RF circuit on the cathode of a crossed field microwave device. In the early 1980's Ratheon introduced the high gain crossed-field amplifier (CFA) which is similar in structure to a conventional CFA or amplitron, except that there is a slow wave structure on the cathode (which in this case is inside the anode i.e. the geometry is conventional). The principle of operation of the high gain CFA is also similar to that of a conventional CFA, with the additional feature that the signal to be amplified is introduced onto the cathode circuit. This RF signal propagates across the Brillouin cloud producing strong modulation of the space charge, thereby increasing the overall gain of the device by some 20 dB.

The GDIM relies on the property of RF signal propagation across the Brillouin cloud in order to couple the resonant system. There is another possible coupling mechanism which may greatly enhance the RF coupling in the GDIM and can be understood in terms of electron trajectories. If the DC conditions in the magnetron satisfy the Hull criterion then the electron cloud, in the absence of RF oscillations, can be considered to be rotating with an entirely azimuthal velocity (it is in a state of Brillouin flow). The Brillouin cloud is fed, however, by electron emission from the slots in the cathode. The electrons emitted from a slot in fact form a good beam. The electron beams are acted on by the electric and magnetic fields to bend their trajectories into the Brillouin flow . Now it is understood that an RF field can propagate in both forward and backward directions on an electron beam (a principle exploited in TWT's, BWO's, etc). It seems reasonable to suppose, then, that RF fields should be able to propagate through the Brillouin cloud in a GDIM in an analogous manner. Furthermore, since the electron beams leave the cathode with trajectories very nearly orthogonal to the cathode surface, the modes on the electron beams are able to couple strongly with the longitudinal modes in the slots which comprise the slow-wave structure.

V.5 Design of a Strapped GDIM

In this section the design of a strapped, slot-type magnetron having the following specification is described:

frequency = 3 GHz

peak output power = 100 MW

pulse duration = 1 μs

prf = 100 Hz

efficiency = 50 % (assumed)

operating voltage = 50 kV.

These are theoretical and assumed values which are used for the purpose of the design study. The effects of space charge other than the Brillouin cloud are assumed to be second order and are neglected in the prototype design equations. The slotted geometry is chosen as the optimal slot dimensions for electron beam formation are known from previous work to be a depth of 1.5 cm and a width of 4 mm (for helium at 1 mbar). In the presence of an externally applied magnetic field the electron beams form a Brillouin cloud which rotates around the anode with a velocity which depends on the radius relative to the cathode surface and the electron cyclotron frequency. It is assumed that gain is achieved for any microwave field which travels around the resonant slow -wave structure in synchronism with the inner edge of the Brillouin cloud. For efficient operation of the magnetron, the voltage at the inner edge of the Brillouin cloud is chosen to be of the order of ten per cent of the anode voltage.

The length of the cathode is chosen to be shorter than a half wavelength at the operating frequency in order to suppress any undesired longitudinal modes. The number of slots is then selected to give the desired operating current and this, together with the distance

between successive slots, determines the cathode radius. The anode radius is chosen such that the anode-cathode gap is small enough that breakdown can only occur adjacent to the cathode slots.

It can be shown easily that electrons emitted from the cathode will obtain an angular velocity given by:

$$\frac{d\theta}{dt} = \frac{\omega_c}{2}\left[1 - \frac{r_c^2}{r^2}\right] \qquad (V.5.1)$$

where r_c is the radius of the cathode and ω_c is the cyclotron radian frequency associated with the DC magnetic field B. The kinetic energy of an electron is gained at the expense of potential energy, so for electrons moving in near circular orbits at a radius r, the electron potential is given by

$$V(r) = \frac{eB^2}{8m}\left[\frac{r^2 - r_c^2}{r}\right]^2 \qquad (V.5.2)$$

The voltage at the edge of the Brillouin cloud is then

$$V_B = V(r_0) \qquad (V.5.3)$$

where r_0 is the radius at the edge of the Brillouin cloud. For the anode potential V_A required to maintain the Brillouin cloud, we obtain

$$V_A = V_B + \int_{r_a}^{r_0} E_r \, dr \qquad (V.5.4)$$

where r_a is the anode radius. This yields

$$r_a = \frac{r_c}{\frac{V_A}{V_B}\left[\frac{r_c}{r_0} - 1\right] + 1} \qquad (V.5.5)$$

The lumped element equivalent circuit of a segment of the strapped magnetron is shown in Figure V.4.2. The cathode slots act as quarter-wave resonators, terminated at one end and open at the other, so the resonant capacitance of a slot can be approximated by:

$$C = \varepsilon_0 l_c \frac{h}{2w} \tag{V.5.6}$$

where l_c is the length of the cathode, h is the slot depth and w is the width of the slot. We estimate the anode-cathode coupling capacitance per slot C_c by determining the proportional coaxial capacitance from the anode-cathode proximal areas and get

$$C_c = \frac{1}{N} 2\pi\varepsilon_0 \frac{l_c}{\log_e\left[\frac{r_c}{r_a}\right]\frac{p-w}{p}} \tag{V.5.7}$$

where p is the distance between the slots.

The π-mode (in which consecutive resonators have an RF phase difference of π radians) is separated by means of the strapping mechanism, which takes the form of two sets of parallel metal ribbons, one pair at each end of the cathode (Figure V.5.2). The straps are connected to alternate cathode segments so that a considerable shunt capacitance C_s is presented only at the frequency ω_π corresponding to the π-mode. The frequency of the π-mode in the strapped magnetron is lower than the unstrapped frequency and has a value given by

$$\omega_\pi = \frac{\omega_0}{\sqrt{1+\frac{C_s}{C}+\frac{C_c}{4C}}} \tag{V.5.8}$$

where ω_0 is the resonant frequency of the cathode slots. The value of ω_0 is chosen to make the length of the resonator slots at least 1.5 cm so that the electron beam current density is maximised.

Consideration of the phase delay per resonator yields the circumferential velocity of the π-mode at a radius corresponding to the edge of the Brillouin cloud:

$$v_B = \frac{2\omega_\pi}{N} r_0 \qquad \text{(V.5.10)}$$

Assuming that the velocity of electrons at the edge of the Brillouin cloud is entirely azimuthal we can then equate the electron kinetic energy to the loss of potential energy to give

$$V_B = m \frac{v_B^2}{2e} \qquad \text{(V.5.11)}$$

Finally, the strap dimensions required to produce the calculated strap capacitance are determined. The straps are most effective if they are placed close to the edge of the cathode at a radius r_s. The ratio of the width of the straps to the strap separation is then given by

$$\rho_s = N \frac{C_s}{4\pi\varepsilon_0 r_s} \qquad \text{(V.5.12)}$$

On the basis of the above design considerations the following parameters for the GDIM were produced:

N = 24	p = 6.00 mm
w = 4.00 mm	rc = 2.29 cm
l_c = 4.50 cm	h = 1.50 cm
V_A = 50 kV	I = 4 kA
$\omega_0 = 2\pi.5.10^9$ s^{-1}	$\omega_\pi = 2\pi.3.10^9$ s^{-1}

Table V.5.1: Design parameters for the Glow Discharge Inverted Magnetron

The calculated values of r_0, r_a, C_s, V_B and ρ parametrised by B are shown in Figures V.5.3-7.

V.6 Conclusions

The Gas Discharge Inverted Magnetron offers number of potential advantages over other types of magnetron. The high current density that can be derived from a pulsed, glow discharge at non-relativistic electron energies enables high output powers to be achieved using standard, high repetition rate pulsers. This is to be compared to relativistic magnetrons, which are generally driven by a Marx generator which is fundamentally incapable of high repetition rates. The glow discharge electron beam has a further desirable characteristic of being a cold-cathode phenomenon, meaning that the GDIM can be a cold-start device that does not require complex heaters.

The anode block of a conventional, relativistic magnetron has a lifetime which is limited, often to a few tens of shots, by the impact of high energy electrons. The slow wave structure on the anode is very sensitive to damage and the performance of the magnetron quickly degrades. The reduced operating voltage required for a GDIM lessens the impact damage. More importantly, the removal of the slow wave structure from the anode to the cathode block displaces the sensitive structure from the hostile anode region. Although the cathode does suffer bombardment by electrons and positive ions during the secondary emission process, these incident particles have not been accelerated through the entire diode potential and are thus less damaging to the slow wave structure. The location of the slow wave structure on the cathode block of the GDIM also simplifies microwave output coupling compared to other types of inverted magnetron, whilst preserving the other advantages of inverted magnetron geometry.

The performance of the GDIM will be greatly affected by the properties of the filler gas. The species present, and their partial pressures, influence the breakdown voltage (through Paschen's Law), the electron current and the space-charge characteristics. In this treatment we have ignored the presence of additional space charge due to the filler gas, but it is clear that control of the properties of the gas offers an additional degree of freedom of control over the magnetron. It may be possible rapidly to modulate the

output power or frequency of the magnetron by adjusting the pressure of the filler gas, thereby achieving such effects as frequency agility and pulse code modulation.

The principle area which has not been addressed in this treatment is that of thermal management. To obtain good thermal stability it is clear that forced cooling is required. The simple construction of the GDIM eases the engineering of the cooling system, although care would have to be taken to prevent overheating of the cathode in the regions surrounding the slots. Also, since it is likely that the implementation of the GDIM would exploit the cold-start capability of the device, the temperature gradients will be necessarily small. For example, for the device considered in this treatment, fabricated in copper, a stability of 250 kHz requires a temperature differential of the order of one degree centigrade across a cathode slot. The thermal contact with the coolant must be maximised, and for a water coolant a flow rate of about 2.5 litres per second would be required.

In the interest of simplicity the design presented is for a slot type magnetron. The rising sun geometry is generally preferred for operation at higher frequencies for which the construction of precision straps is prohibitively difficult. Provided that all of the cathode slots are more than 1.5 cm deep (for helium at 1 mbar) then all of the cathode slots in a rising sun GDIM would produce the same electron current. Interesting effects may occur if the slot depths differ from one another since each will have different RF resonances and produce different electron currents..

A GDIM employing slot and cavity resonators has the possible advantage, provided the slots are deep enough, of isolating the region where the electron beam is formed (the slots) from the cavity (inductive) resonators. This may improve performance both in terms of thermal management and the effect of electron beam formation processes on the cavity resonances.

V.7 References

[1] The Microwave Magnetron and Its Derivatives. William C Brown, IEEE Trans. Elec. Dev. **31**(11) p1595, Nov 1984.

[2] Microwave Magnetrons. Edited by G B Collins, McGraw Hill, New York, 1948.

[3] Crossed Field Microwave Devices. Edited by E Okress, Academic, New York, 1961.

[4] Microwave emission from pulsed, relativistic e-beam diodes. T J Orzechowski and G. Bekefi, Phys Fluids **22**(5) pp978-985, May 1979. Also Microwave emission from pulsed, relativistic e-beam diodes. Part II. The multiresonator magnetron. a Palevsky and G Bekefi. *ibid* pp 986-996.

[5] G Bekefi and T J Orzechowski, Phys. Rev. Lett. **37**, p379, 1976.

[6] G Bekefi and T J Orzechowski, Bull Am Phys Soc **21**, p571, 1976.

[7] T J Orzechowski, G Bekefi, A Palevsky, W M Black, S P Schlesinger, V L Granatstein, R K Parker, Bull Am Phys Soc **21**, p1112, 1976.

[8] A Palevsky, R J Hansman, Jr., G Bekefi, Bull Am Phys Soc **21**, p648, 1977

[9] A Palevsky and G Bekefi, Bull Am Phys Soc **23**, p588, 1978.

[10] N F Kovalev, B D Kol'chugin, V E Nechaev, M M Ofitserov, E I Soluyanov and M I Fuks, Pis'ma Zh. Tekh. Fiz **3**,p1048, 1977 [Sov. Tech. Phys. Lett. **3**, p430, 1977]; also V E Nechaev, M I Petelin and M I Fuks, Pis'ma Zh. Tekh. Fiz. **3**, p763, 1977 [Sov. Tech. Phys. Lett. **3**,p310, 1977].

[11] T H Martin, IEEE Trans. Nucl. Sci. **Ns-20**, p289, 1973.

[12] K R Prestwick, IEEE Trans. Nucl. Sci. **NS-22**, p975, 1975.

[13] Radiation measurements from an inverted relativistic magnetron. R A Close, A Palevsky and G Bekefi, J. Appl. Phys. **54**(7) pp4147-4151, July 1983.

[14] Operating Modes Of Relativistic Rising Sun and A6 Magnetrons. Todd A Treado, Wesley Doggett, Gary E Thomas, Richard S Smith III, Jeanne Jackson-Ford and David J Jenkins, IEEE Trans. Plas. Sci. **16**(2) pp237-248, April 1988.

[15] Study of Intense Electron Beams Produced by High-Voltage Pulsed Glow Discharges, H. F. Ranae-Sandoval, N. Reesor, B. T. Szapiro, C. Murray, J. J. Rocca, IEEE Trans. Plas. Sci. Vol. **PS-15**(4) pp361-374, 1987.

[16] DC Glow Discharge Electron Guns for the Excitation of Rare Gases, R. J. Carman, 1986, PhD Thesis (St And).

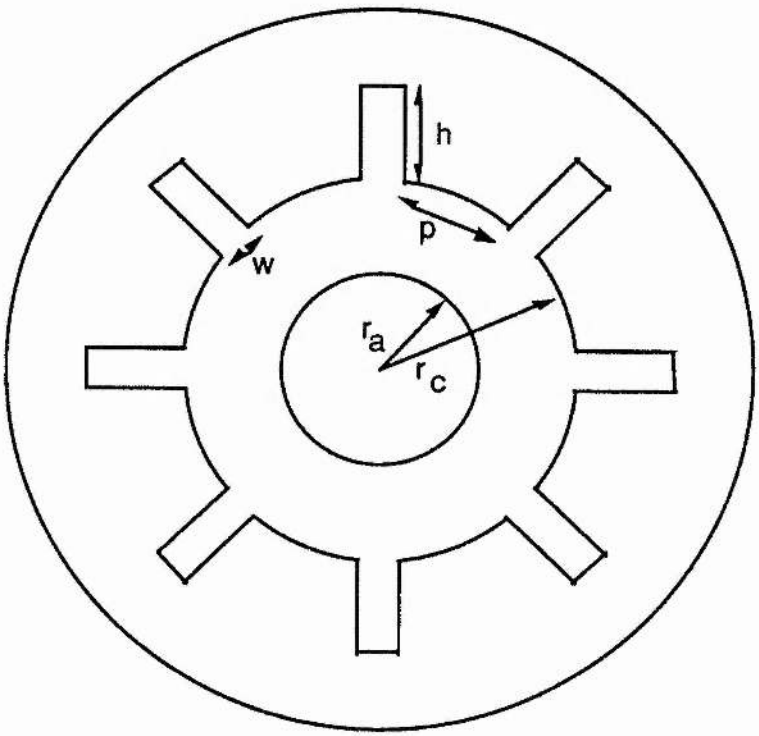

Figure V.1.1: Magnetron Dimensions

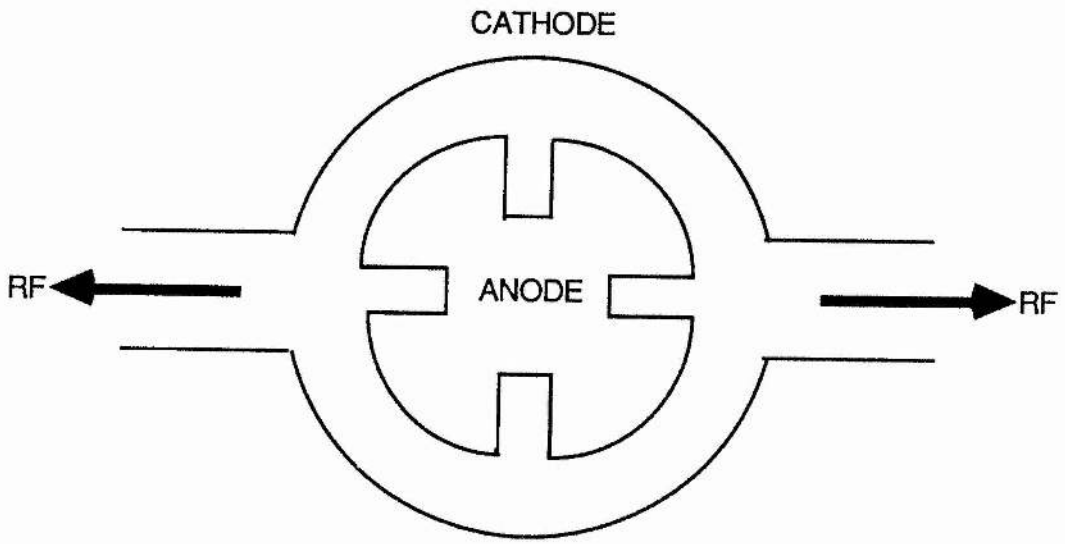

Figure V.3.1: Output Coupling in an Inverted Magnetron

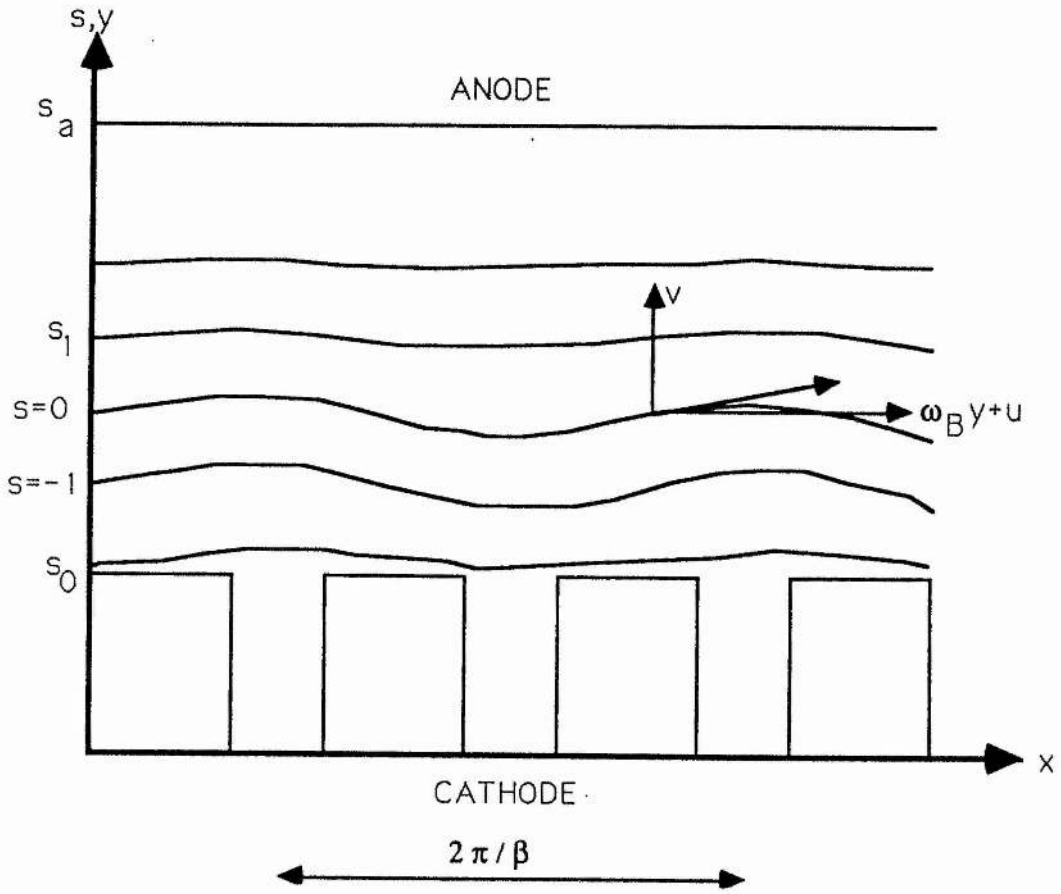

Figure V.4.1: Coordinate System for Calculation of Coupling through the Brillouin Cloud

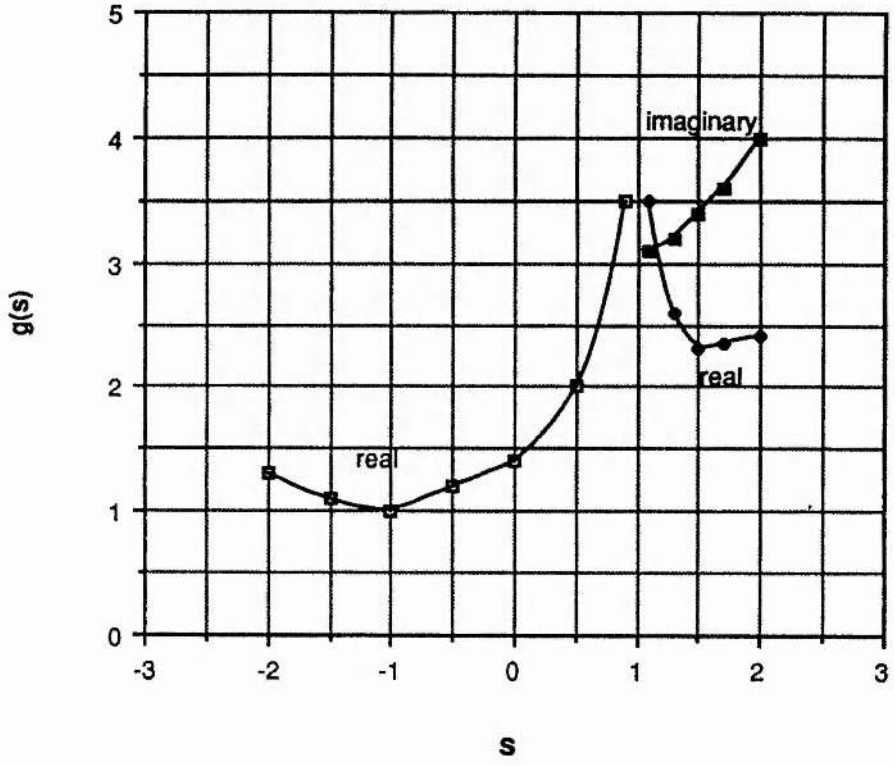

Figure V.4.2: Velocity Modulation across the Brillouin Cloud

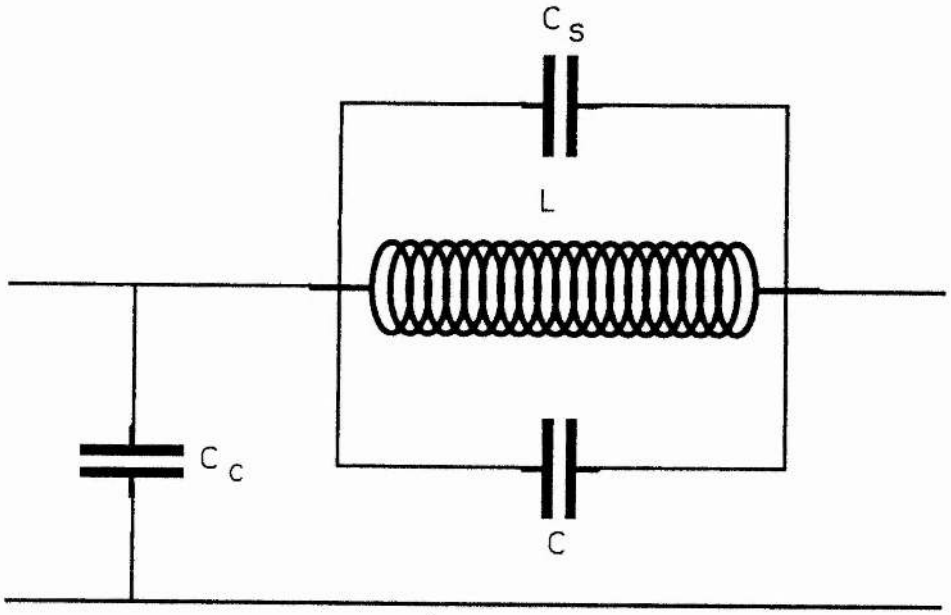

Figure V.5.1: Equivalent Circuit of a Magnetron Resonator

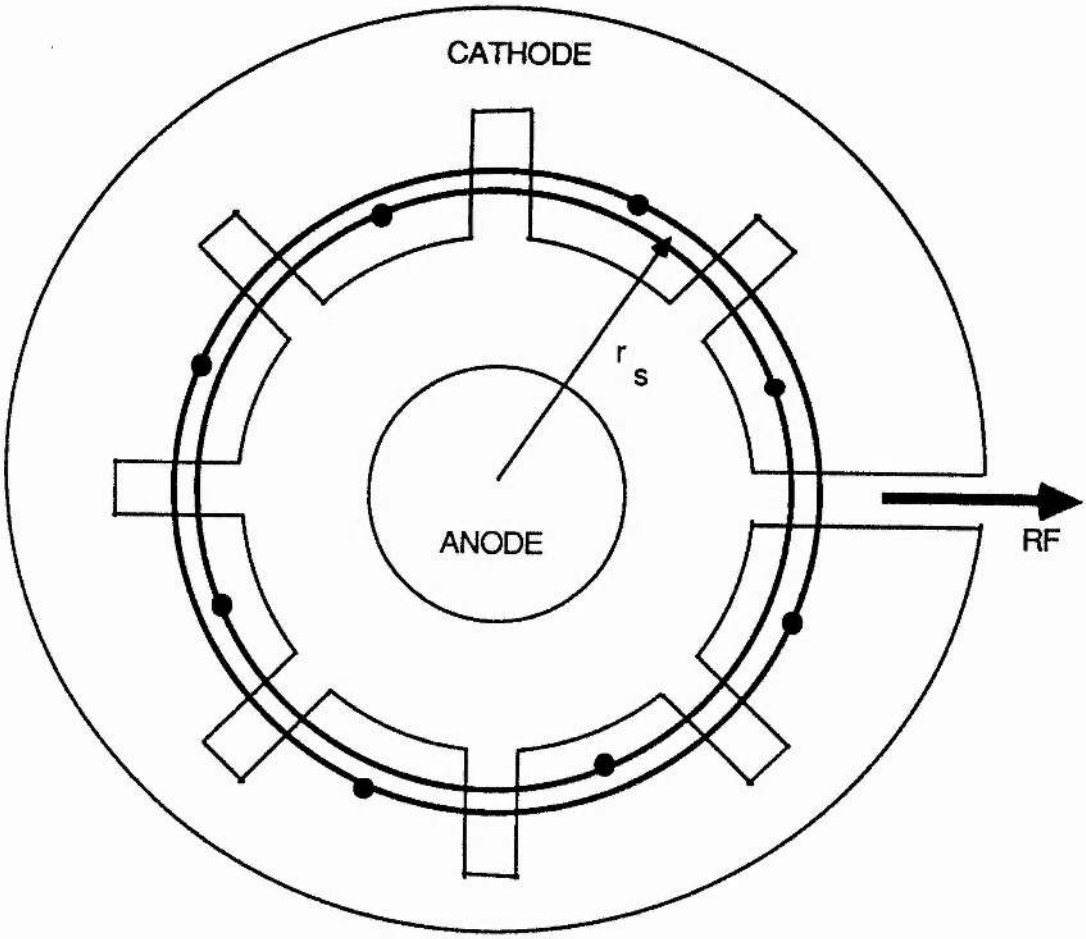

Figure V.5.2: Location of Cavity Straps

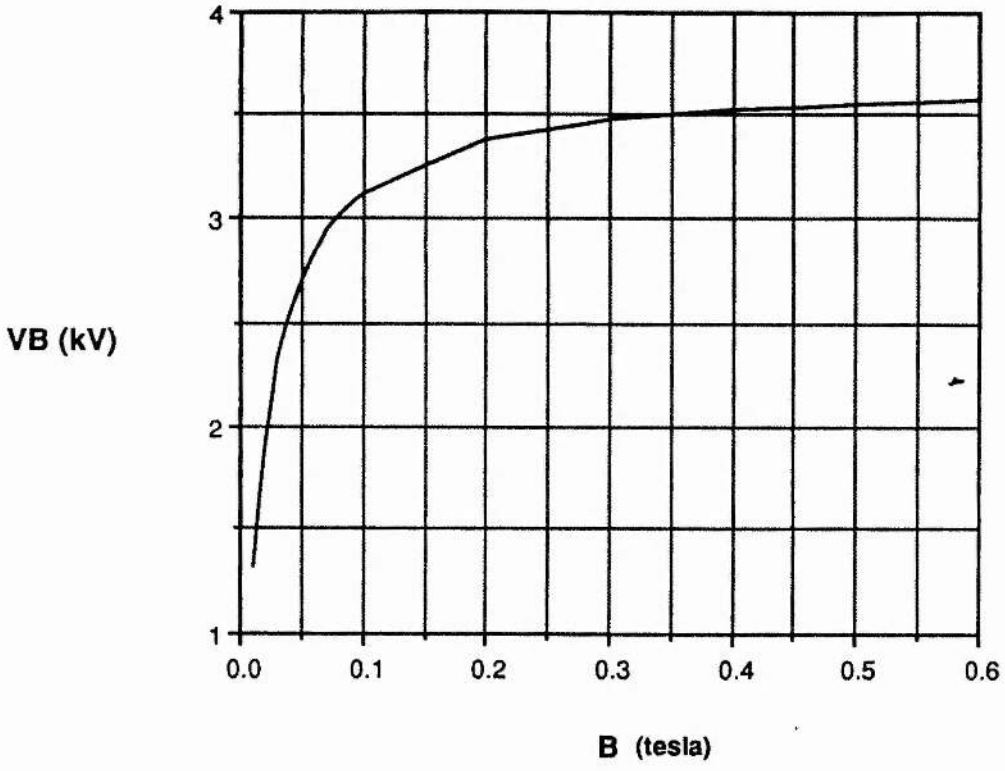

Figure V.5.3: Operating Voltage as a Function of Magnetic Field

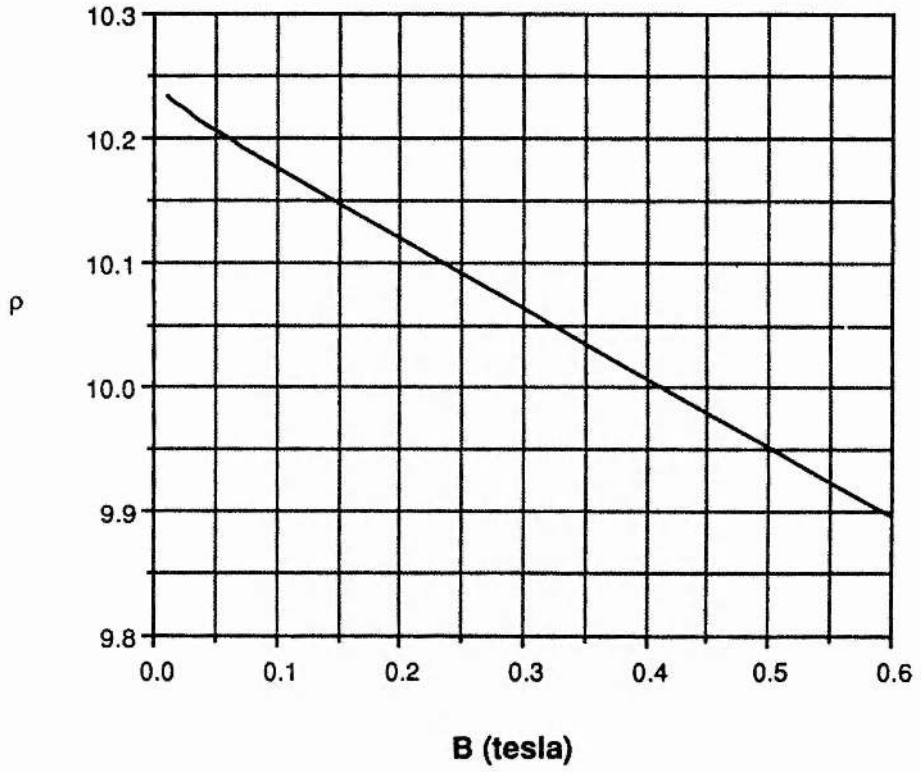

Figure V.5.4: Ratio of Strap Width to Separation as a Functon of Magnetic Field

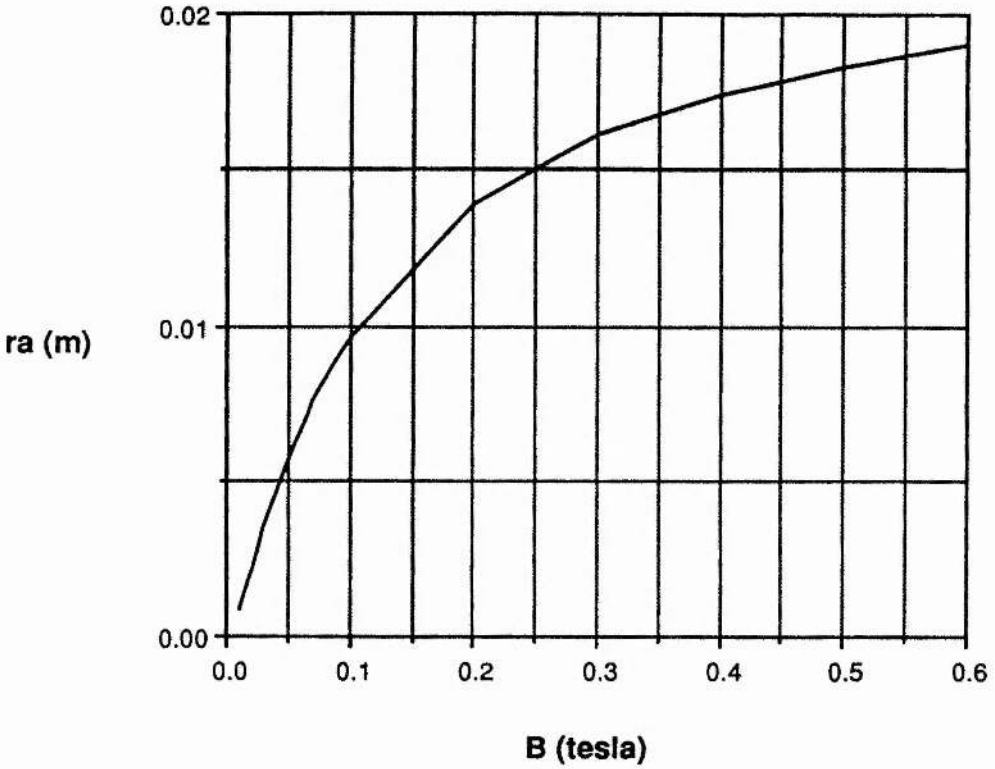

Figure V.5.5: Anode Radius as a Function of Magnetic Field

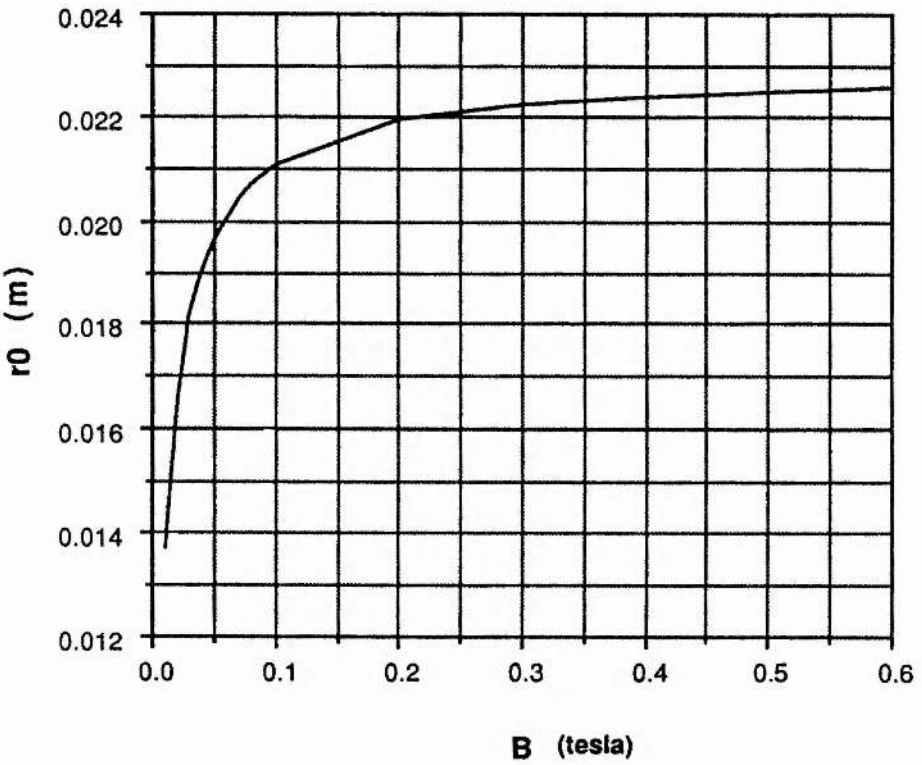

Figure V.5.6: Mean Radius of the Unperturbed Brillouin Cloud as a Function of Magnetic Field

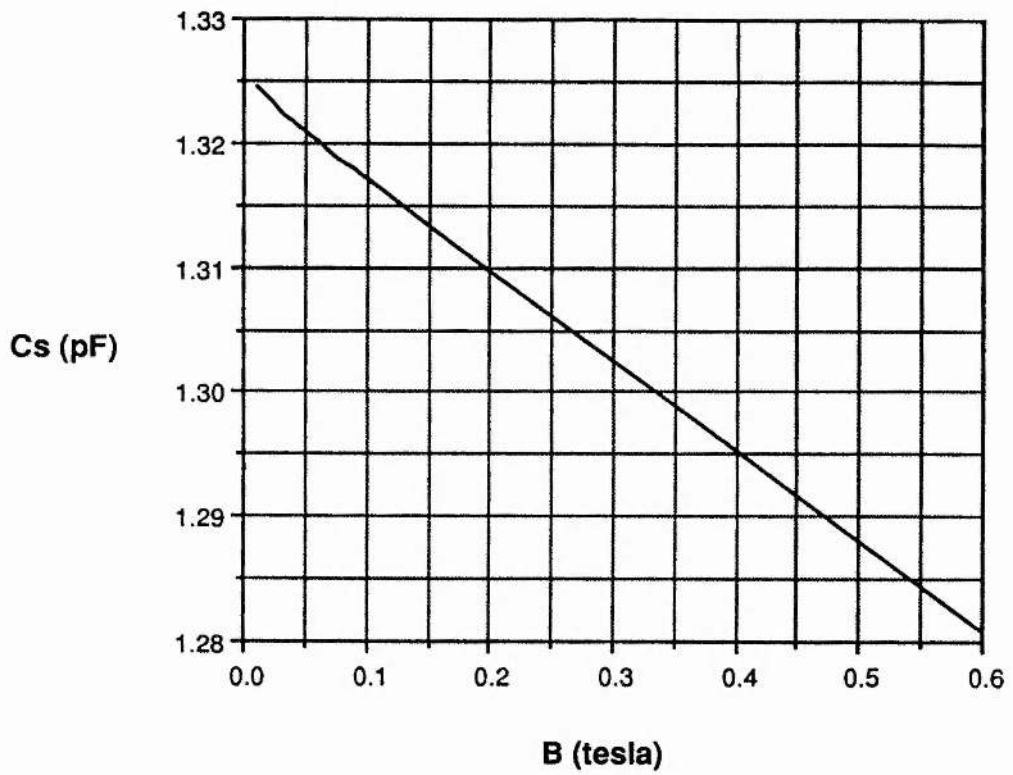

Figure V.5.7: Strap Capacitance as a Function of Magnetic Field

CHAPTER VI

SUMMARY

VI.1 Glow Discharge Electron Guns

The formation of high energy electron beams in a glow discharge with a metal cathode has been investigated. The maximum beam energy is governed by the Paschen breakdown voltage between the anode and the cathode. The generation of high energy electron beams requires the pressure, p, and discharge length, d, to be such that the product (pd) lies on the left-hand branch of the Paschen curve (equation II.2.1). A hydrogen-filled gap with a (pd) of 0.1 mm-mbar, for example, can support a potential difference of the order of 100 kV.

The current density of a glow discharge electron beam is enhanced if the cathode contains a slot (section II.2.4). Beam current densities of the order of 1 A cm^{-2} have been obtained in a DC glow discharge electron gun with a slotted cathode.

The ionisation rate for an electron beam propagating through a gaseous medium has been calculated (equation II.2.4.2) and the equation for the resulting plasma density distribution derived (equation II.2.4.7). If the plasma density is comparable to the electron density in the electron beam (equation II.2.4.10), then space-charge neutralisation occurs and the divergence of the beam is reduced.

Experiments with magnetic focussing of glow discharge electron beams (section II.2.5) show that a longitudinal magnetic field of the order of 100 gauss is sufficient to allow a

20 kV, 1 mA electron beam to propagate 60 cm through helium gas at a pressure of 1 mbar. This distance is limited by the length of the solenoid. The presence of the magnetic field causes an increase in the electron beam current. This is attributed to an increase in the effective pressure due to the gyro-orbital path of the electrons. When the electron gun is aligned at an angle to the magnetic field, the gyroradius of the electron orbit (equation II.2.5.2), together with the magnetic field strength, gives the electron beam energy. The results confirm that the electron beam is accelerated through the entire diode voltage.

A glow discharge electron gun with variable electrode spacing has been characterised. Measurements were made in residual air at 0.4 mbar, with anode-cathode gaps in the range 1 to 8 mm. The electron beam current was found to be proportional to the square of the diode voltage. The departure from the Child-Langmuir "3/2" voltage law occurs because the current is ion-mobility limited rather than space-charge limited. This is evidence of the importance of space-charge neutralisation in glow discharge electron guns. In the mobility-limited regime, the perveance is redefined to be $K=I/V^2$ so that its functional relationship with the electrode separation, d, can be obtained. Simple calculations predict that K should vary as $1/d^3$. The experimental results, however, reveal that K varies as $1/d^{3.3}$ for $d \cong 5$ mm and $1/d^{2.3}$ for $d \cong 2$ mm. This behaviour has been explained in terms of the effects of fringing fields when the electrode structures are of comparable size to the electrode spacing.

A sealed-off glow discharge electron gun operating at 350 kV has been demonstrated. This is believed to be the highest voltage at which a glow discharge electron gun has successfully been operated.

VI.2 The RF Plasma Cathode

A new kind of plasma cathode, the RF plasma cathode, has been proposed (section II.3) in which an electrodeless RF discharge produces a high density plasma cathode. Because the plasma cathode is non-solid, the usual glow discharge problems of cathodic sputtering and damage to the cathode do not occur.

The plasma cathode is controlled by a biased grid electrode. When the grid has a positive bias with respect to the plasma, a negative space-charge sheath forms around the grid. Electrons can be extracted from this sheath, provided that the sheath thickness, s (given by equation II.3.2.1), is greater than the grid thickness. If, on the other hand, the grid has a negative bias relative to the plasma, then a positive ion sheath forms around the grid. Provided that the grid potential is high enough with respect to the electron thermal energy (equation II.3.2.2), the extraction of electrons can be inhibited.

The RF plasma may be generated in a plasma waveguide, by a surface-wave launcher or a helical slow-wave structure. The solutions for the RF fields produced by a slow-wave helix have been obtained (section II.3.7) and used to derive the plasma density. If the discharge is controlled by ambipolar diffusion to the walls (pressure less than 0.5 mbar in H_2), then the plasma fills the container (Figures II.3.7.2-4). When the pressure is sufficiently high, however, (greater than 0.5 mbar in H_2), then recombination becomes important. In this case the plasma occupies an annular region close to the helix (Figure II.3.7.5). The thickness of the annulus is a function of the helix parameters (pitch and radius), microwave power and the gas parameters (species and pressure).

In a proof-of-principle experiment (sections II.3.8 and 9), a plasma cathode has been produced in H_2 at pressures between 0.1 and 2.5 mbar using a microwave-helix discharge. The RF plasma cathode gave currents up to two orders of magnitude greater

than a solid-cathode glow discharge of the same cross-sectional area and gas pressure. The number density in the plasma was calculated to be of the order of 10^{12} cm^{-3} with the plasma generation rate being of the order of 10^{19} cm^{-3} s^{-1}. The existence of a large oscillation of the cathode current which is not present at the anode has not been explained.

Designs for a number of electron devices incorporating an RF plasma cathode have been produced (sections II.3.10-15). The RF plasma cathode offers the capability of instant start, high current operation at high repetition rates with a long lifetime. The cathode processes are, however, very complicated and have not been fully explained. Further research is required to develop a more complete understanding of these devices.

VI.3 Plasma Waveguides

A general formulation of the linearised Maxwell's equations in a cylindrical plasma with uniformity in the longitudinal direction has been given (section III.21). The wave equations for **E** and **H** are, in general, coupled but in some important cases they decouple and can be solved. In particular, plasma-loaded waveguides of circular cross-section have been modelled.

When a waveguide is completely filled with a lossless plasma, the waveguide cut-off frequency is shifted up by an amount equal to the plasma frequency (equation III.2.3.2). No propagation below the cut-off frequency is possible. If, however, the plasma is magnetised or does not completely fill the waveguide cross-section, then propagating modes can exist with frequencies below the empty-waveguide cut-off frequency (sections III.2.4 to 6). These modes are, in general, slow-wave modes having phase velocities smaller than the velocity of light.

Maxwell's equations have been solved for the case of slow-waves in a waveguide containing a longitudinally magnetised plasma, using the quasi-static approximation ("QSA"). The dispersion relations have been obtained and solved for both partially-filled (equation III.3.2.12) and completely-filled (equation III.3.2.16) plasma waveguides. The slow-wave modes have cut-off frequencies which are a function of the geometry and the plasma and cyclotron frequencies. Equations for the magnitudes of the fields as a function of the RF power have been derived (equations III.3.2.25 and III.3.2.28). Near to the cut-off frequencies, the RF fields become very large and the wave can be used to sustain the plasma. Conversely, the RF fields are small for signal frequencies which are far removed from the cut-off frequencies; this defines the condition for efficient power transmission.

VI.4 Plasma Switching and Pulse Compression

The results of the investigation of DC and RF glow discharges and plasma waveguides have been applied to the problem of microwave cavity dumping and RF pulse compression. A simple analysis has been given for the temporal compression of an RF pulse in a dispersive medium (section IV.1.3). A technique for RF pulse compression based on the plasma waveguides discussed in Chapter III has been proposed. The technique relies on the relationship between the group velocity of the plasma-wave and the plasma frequency in a plasma-loaded waveguide. As the leading edge of a pulse propagates along a plasma waveguide having appropriate parameters, some of the energy of the pulse is lost in producing further ionisation of the gas. Thus, the plasma density is higher at the trailing edge of the pulse than at the leading edge. The group velocity is proportional to the plasma frequency (equation IV.1.3.6), so the trailing edge of the pulse catches up with the leading edge, resulting in pulse compression.

A new kind of plasma waveguide closing switch that is the microwave equivalent of an optical saturable absorber has been proposed (section IV.2.2). The plasma waveguide saturable absorber ("WSA") comprises a section of waveguide containing a low pressure gas, together with input and output couplers. The dimensions of the waveguide are such that the incident microwave fields, having a frequency below the waveguide cut-off frequency, are reflected. When, however, the incident power reaches a critical value, the evanescent fields in the waveguide are large enough to ionise the low pressure gas. Propagation below the cut-off frequency is now possible by the plasma waveguide mechanism. Rapid ionisation occurs and the waveguide switches into the transmitting state. After the end of the RF pulse, the switch recovers in a time which is characteristic of the afterglow in the plasma.

A triggered version of the plasma waveguide switch has been proposed, in which the plasma is generated in the waveguide using a microwave helix or a glow discharge electron beam (section IV.2.3). In addition to improving the timing and reproducibility, the triggering mechanism allows the parameters of the plasma to be controlled so that the triggered waveguide switch can operate at higher RF powers than the waveguide saturable absorber.

VI.5 The Glow Discharge Inverted Magnetron

A new kind of magnetron, the "Glow Discharge Inverted Magnetron" (GDIM), has been proposed (Chapter V). The GDIM is an inverted magnetron in which the resonant structure appears on the cathode and glow discharge electron beams are generated in the resonant cavities. Glow discharge electron beams can have current densities of the order of 20 A cm^{-2}, giving the possibility of high power operation without the need for relativistic voltages.

An analysis of the RF signal coupling across the Brillouin cloud of the GDIM has been given (section V.4). This analysis shows that the RF fields in the cavity formed by the anode-cathode gap can couple, across the Brillouin cloud, with the resonant structure on the cathode.

A design study for a 100 MW, S-band GDIM has been completed. The design uses slot resonators, as the optimal slot dimensions for electron beam formation are known from previous work. An analysis of the electron dynamics yields the relationship between the applied fields and the dimensions of the magnetron (equations V.5.1-5). The resonant structure is "strapped" in order to limit operation the the π-mode. The straps also allow some detuning of the resonant structure, to compensate for the effects of space-charge in the cavities.

The GDIM offers the possibility of an instant-start, high repetition-rate source of high power microwaves that can be driven by conventional modulator technology.

VI.6 Concluding Remarks

The application of low pressure plasma technology for the generation of high power microwaves (HPM) is a very rich field. We have examined different aspects of a complete HPM system, including cathode technology, the generation of electron beams, RF power transmission and control and RF sources. In all of these areas, we have found that the use of low pressure plasmas offers the possibility of new kinds of devices with enhanced performance compared with vacuum technology. The physical processes in these devices are very complicated and difficult to model. So much so, in fact, that previous work in this field has been limited. The results of this research prorgamme, however, suggest that the possible benefits of employing low pressure plasmas in HPM systems are sufficient to merit further research.